ANALYSIS ON THE ROBUSTNESS OF FUZZY CONTROL OF A BUILDING TEST-BED UNDER INTERNAL AND EXTERNAL DISTURBANCES

A Thesis

Presented to

the Faculty of the Department of Mechanical Engineering

California State University, Los Angeles

In Partial Fulfillment

of the Requirements for the Degree

Master of Science

in

Mechanical Engineering

By

Anayely M. Saguilan

May 2024

© 2024

Anayely M. Saguilan

ALL RIGHTS RESERVED

The thesis of Anayely M. Saguilan is approved.

Dr. Arturo Pacheco-Vega, Committee Chair

Dr. Mario Medina

Dr. Salvador Rojas

Dr. Mathias Brieu, Department Chair

California State University, Los Angeles

May 2024

ABSTRACT

Analysis on the Robustness of Fuzzy Control of a Building Test-bed Under Internal and External Disturbances

By

Anayely M. Saguilan

This study extends on prior work based on the development of a fuzzy logic controller for the regulation of temperature within a sub-scaled building test-bed. The objective of this analysis, however, was to investigate the robustness of this controller by conducting a series of comprehensive tests. The testing conducted in this study was aimed to evaluate controller response to both internal and external disturbances introduced to the system. A total of five different types of tests were performed; three tests examined controller response to internal disturbances while two examined the response produced due to external disturbances. The internal disturbance tests comprised of including (1) multiple changes in the temperature setpoints, (2) a sudden change and (3) two sudden changes in setpoint temperatures while keeping different temperatures within any given pair of rooms. To test controller adaptability to external disturbances, the cold air delivered by the external air conditioning unit was changed three times during a 90-minute testing period while (1) setting one setpoint temperature for all rooms, and (2) setting different temperature setpoints for each pair of rooms.The test-bed building measures 1.2 m $\times$ 0.92 m $\times$ 1.1 m and it consists of eight rooms distributed among two floors. A cooling unit supplies cool-air to each room, eight 40 W light bulbs serve as heat sources, and type-T thermocouples gather the temperature data. The duct system incorporates eight

dampers, each of which is connected to a servo motor that adjusts the airflow rate supplied to individual rooms based on controller output. The controller uses the difference between a temperature setpoint and actual room temperature, the derivative of this error, and the cumulative integral of the error to form a decision on the output angle of each damper. The fuzzy sets of the controller and if-then rules were built based on experimental data, the Mamdani inference method was used to provide the inputs to the actuators. Results from experimental tests showed that the fuzzy logic based controller was able to maintain the room temperature setpoints while managing the internal and external disturbances introduced to the system.

ACKNOWLEDGMENTS

I would like to thank my advisor, Dr. Arturo Pacheco-Vega, for his invaluable guidance throughout my graduate studies. I greatly appreciate his mentorship and support. I would also like to thank Dr. Mario Medina and Dr. Salvador Rojas for being part of my committee and for their feedback. I would like to extend my gratitude to CREST-CATSUS (NSF HRD-2112554) for their support, as this research would not have been possible without them. I would like to thank all of the CATSUS faculty for being amazing mentors. Thank you Dr. Deborah Won! Thank you Dr. Chris Bachman! Thank you Dr. Jeffrey Santner! Thank you Dr. Curtis Wang! Thank you Dr. Jim Kuo! Thank you Mayra Alonzo!

I would like to express my gratitude to my mom, Estela Beltran, for her encouragement throughout my undergraduate and graduate degrees. Her boundless resiliency and selflessness inspire me to be a better person everyday. I also want to thank my dad, Gabriel Saguilan, whose work ethic has taught me that anything is possible through grit and hard work. My parents are my motivation, I would not be here if it were not for their support. Thank you.

I would like to also thank my uncle Alfredo Beltran, whose optimism is contagious. I would like to thank my siblings, who have always encouraged me to try my best. I would like to extend my thanks to Ruby, the most loyal pup I have ever known. She stood by my side throughout my undergraduate degree, constantly attempting to pull all-nighters with me while I studied. That is something that I will never forget, she is immensely missed.

TABLE OF CONTENTS

ABSTRACT iv

ACKNOWLEDGMENTS vi

LIST OF TABLES xi

LIST OF FIGURES xii

NOMENCLATURE xiv

1 INTRODUCTION 1

1.1 Motivation 1

1.2 System Dynamics and Control 3

1.3 Fuzzy Control and its Applications 8

1.4 Objective of Work 10

1.5 Thesis Overview 11

2 DESCRIPTION OF EXPERIMENTAL TEST-BED 12

2.1 Building Test-bed 12

2.2 Instrumentation and Data Acquisition System 15

2.3 System Variables 19

2.4 System Dynamics 20

3 FUZZY LOGIC 24

3.1 Fuzzy Sets and Membership Functions 24

3.2 Inference Systems and Rule-based Process 29
3.3 Defuzzification Methods 35
3.4 Examples of Modeling With Fuzzy Logic 37

4 FUZZY CONTROL RESPONSE TO DISTURBANCES: TESTS AND RESULTS 38
4.1 Fuzzy Controller Description 39
4.2 Results to Internal Disturbance 43
4.3 Response to External Disturbance 53

5 CONCLUSIONS AND FUTURE WORK 59
5.1 Conclusion 59
5.2 Future Work 60

REFERENCES 62

A Using MATLAB and LabVIEW to Operate the Sub-scaled Building Test-bed Fuzzy Controller 72

B FUZZY LOGIC INFERENCE SYSTEM FOR SINE FUNCTION 79
B.1 Abstract 79
B.2 Problem Introduction 79
B.3 Solution Plan 80
B.4 Fuzzification 80
B.4.1 Membership Function Inference 90
B.4.2 Defuzzification 92

B.5 Results 94
B.6 Appendix 97

C FUZZY LOGIC EXAMPLE OF HEAT EXCHANGER MODELING 98
C.1 Abstract 98
C.2 Problem Introduction 98
C.3 Analytical Solution 99
C.3.1 Mamdani Method 100
C.3.2 Sugeno 106
C.3.3 Tsukamoto 108
C.4 Simulated Results 109
C.5 Conclusion 112

LIST OF TABLES

3.1 Truth table example for single-input single-output fuzzy system 34

4.1 Decision matrix 1 for $\theta_{\Delta T}$. 42

4.2 Decision matrix 2 for $\theta_{\Delta T}$. 42

LIST OF FIGURES

1.1 Schematic of all-air HVAC system, taken from [1]. 5

1.2 Direct Digital Control process. 6

2.1 Building test-bed 13

2.2 Door placement in each room. 14

2.3 Damper and servo motor subsystem. 15

2.4 Thermocouple arrangement in rooms. 16

2.5 Diagram of system instrumentation. 18

2.6 Schematic of building. 20

2.7 Open damper dynamics test result. 22

2.8 Open-close damper dynamics test result. 23

3.1 Common membership functions. 27

3.2 Graphical representation of fuzzy logic operations. 29

3.3 Example of linguistic variables for a range of ages. 31

3.4 Example of linguistic variables for a range of activity levels. 31

3.5 Example of linguistic variables for risk of cardiovascular disease. 32

3.6 Diagram of the fuzzy inference system. 32

3.7 Diagram of the fuzzy inference system for “AND” operator. 33

3.8 Aggregate output for risk of cardiovascular disease example. 36

4.1 Closed-loop fuzzy control. 39

4.2 $E_{\Delta T}$ 40

4.3 $dE_{\Delta T}/dt$ 41

4.4 $\int E_{\Delta T} dt$ 42

4.5 $\theta_{\Delta T}$ 43

4.6 Results for Internal Disturbance Test 1. 46

4.7 Results for Internal Disturbance Test 2. 49

4.8 Results for Internal Disturbance Test 3. 52

4.9 Results for External Disturbance Test 1. 55

4.10 Results for External Disturbance Test 2. 58

NOMENCLATURE

$\underset{\sim}{A}$	Fuzzy set A
$\underset{\sim}{A}_i^k$	Fuzzy set A for ith input of kth rule
$\underset{\sim}{B}$	Fuzzy set B
$\underset{\sim}{B}^k$	Fuzzy set B of kth rule
dE	Energy differential [kJ]
DP	Differential pressure [Pa]
dQ	Differential of energy transferred into a system [kJ]
e	Error
$E_{\Delta T}$	Temperature Error [°C]
k	Conductivity coefficient of the fluid
T	Temperature [°C]
ΔT	Change in temperature [°C]
t	Time [minutes]
V	Voltage [v]
$\dot{V}$	Volumetric airflow [m^3/s]
X	Universe of discourse
x	Element within universe X
y^k	Output variables in rule base
z^i	Intersection of all individual rule consequences
z^*	Defuzzified output value
$\bar{z}$	Centroid of each symmetric membership function

Greek symbols

α^k	Rule change
Δ	Change in
$\theta_{\Delta T}$	Fuzzy controller output
$\mu_{\underset{\sim}{A}}(x)$	Degree of membership of element x in fuzzy set $\underset{\sim}{A}$
σ	Standard deviation
Φ	Viscous dissipation function
ρ	Density

Statistical symbols

$\in$	Belongs in
$\notin$	Does not belong in
$\cup$	Union
$\cap$	Intersection
$\bar{A}$	Complement of A

CHAPTER 1

INTRODUCTION

This chapter establishes the motivation and objective for this work. The first section begins by describing what the repercussions of using fossil fuels as energy sources are and then states the need for robust heating, ventilation, and air conditioning (HVAC) control systems. The second section provides an outline of the governing equations related to convection heat transfer in HVAC systems and introduces the existing control strategy utilized in commercial-grade building HVAC controllers. The third section presents fuzzy logic as a control methodology while giving examples of various practical applications for fuzzy logic controllers. The fourth section states the objective of this work while the concluding section of this chapter provides an overview of the following chapters of this document.

1.1 Motivation

The Industrial Revolution, a period marked by significant technological advancement and economic growth [2], led to the widespread adoption of fossil fuels as the primary source for global energy [3]. Since then, our reliance on fossil fuels has increased significantly and is forecasted to keep on increasing in proportion to economic growth, population growth, and urbanization. The burning of fossil fuels has been linked to the release of greenhouse gases, which contribute to the global warming phenomenon [4]. This phenomenon is a result of air pollutants accumulating in the atmosphere and creating a "shield". This causes the absorption of sunlight and solar radiation, thus heating the Earth [5]. Consequently, this collection of aerial contaminants has been associated with a

variety of health issues among humans, including respiratory and cardiovascular diseases, mental health disorders, and cancer [6]–[9]. Furthermore, the gradual heating of Earth due to the "shield" of pollutants around the atmosphere has been detrimental to the environment. This has given rise to the recession of glaciers, melting ice caps, rising sea levels, coral reef bleaching, and the slowing of agriculture productivity [10]–[14].

In their report, the U.S. Energy Information Administration (EIA), estimated a rapid increase in energy consumption through 2050 in non-OECD (Organization for European Co-operation and Development) Asian countries as a result of an increase in household income [15]. This increase in income would allow more people to have access to electrical power and comforts such as space heating and cooling. Buildings currently account for 40% of energy use worldwide with 38% of this consumption used for HVAC systems [16]. As of 2016, EIA has estimated that the energy consumed by households worldwide would increase by 48% throughout the years of 2012 to 2040 [17]. Therefore, to address this issue and promote sustainability in both commercial and residential buildings, it is imperative to develop robust HVAC control systems [4].

This, however poses a difficult challenge as there exists many uncertainties that have to be taken into account when designing HVAC control systems for buildings. These challenges include nonlinear dynamics, time-varying setpoints and disturbances, complex interactions between temperature and humidity, building operating modes, and occupant schedules. Aside from this, building HVAC systems are composed of multiple subsystems, each of which need to be considered when creating HVAC control algorithms. As such, it is difficult to find a "one-size-fits-all" controller as the dynamics of buildings become complex in relation to building geometries and the multitude of components that make

up an HVAC system.

1.2 System Dynamics and Control

An efficient HVAC controller can help in reducing energy consumption and associated costs by adjusting the amount of energy required to heat or cool a building based on building energy demands. HVAC systems, however, are difficult to model because they consist of various mechanical components that have their own set of dynamics and therefore can become potential points of failure [18]-[20]. Additionally, physical building parameters must be considered when developing mathematical models for HVAC controllers. Things such as windows, building geometry, building materials, doors, and light bulb types must be taken into account to accurately represent the amount of energy needed to be removed or added into a space on account of these items [21]-[23]. Therefore, the HVAC control engineer must consider each of these components when designing an HVAC control system. Understanding the complex thermal dynamics involved with the development of realistic building HVAC models is crucial for creating energy-efficient buildings.

To ensure an effective HVAC mathematical model, it must accurately predict the energy needed to adjust room conditions for human comfort. Achieving this relies on leveraging thermodynamic, heat transfer, and fluid dynamic principles. Expressing the energy transfer from the refrigerant fluid to its surroundings using the continuity equation, Eq. (1.1), Navier Stokes equation, Eq. (1.2), and energy equation, Eq. (1.3), is important as these equations are essential for the analysis of convection heat transfer [24]. Using the following equations along with the appropriate boundary conditions one

can develop a comprehensive model for energy transport within fluid flows,

$$\frac{D\rho}{Dt} + \rho \bigtriangledown \cdot \mathbf{v} = 0 \tag{1.1}$$

$$\rho \frac{D\mathbf{v}}{Dt} = - \bigtriangledown p + \mu \bigtriangledown^2 \mathbf{v} + \mathbf{F} \tag{1.2}$$

$$\rho c_p \frac{DT}{Dt} = k \bigtriangledown^2 T + \mu \Phi \tag{1.3}$$

where $\mathbf{v}$ is the velocity vector, μ is the fluid viscosity, T is the temperature, k is the conductivity coefficient of the fluid, Φ is the viscous dissipation function, $\bigtriangledown$ is the gradient operator $\frac{\partial}{\partial x} i + \frac{\partial}{\partial y} j + \frac{\partial}{\partial z} k$, $\frac{D\rho}{Dt}$ is the substantial derivative of density, $\frac{D\mathbf{v}}{Dt}$ is the substantial derivative of velocity, and $\frac{DT}{Dt}$ is the substantial derivative of temperature.

Aside from heat transfer considerations, mathematical models for building HVACs also need to take into account the various components that make up an HVAC system. Buildings that require individual control conditions are generally equipped with all-air heating and cooling systems [1]. All-air HVAC systems are capable of carrying energy and ventilating air between the furnace and the conditioned space through ducts. The configuration of these HVAC systems makes individual control of air flow conditions possible. As illustrated on Figure 1.1, commercial building HVAC systems are made up of boilers, pumps, temperature sensors, humidity sensors, air flow sensors, dampers, chillers, cooling towers, return air fans, supply fans, filters, heat coils, cooling coils, humidifiers, valves, and various ducts.

In the event of creating a controller to automate the process of cooling or heating a space, commercial HVAC controllers utilize Direct Digital Control (DDC), Figure 1.2

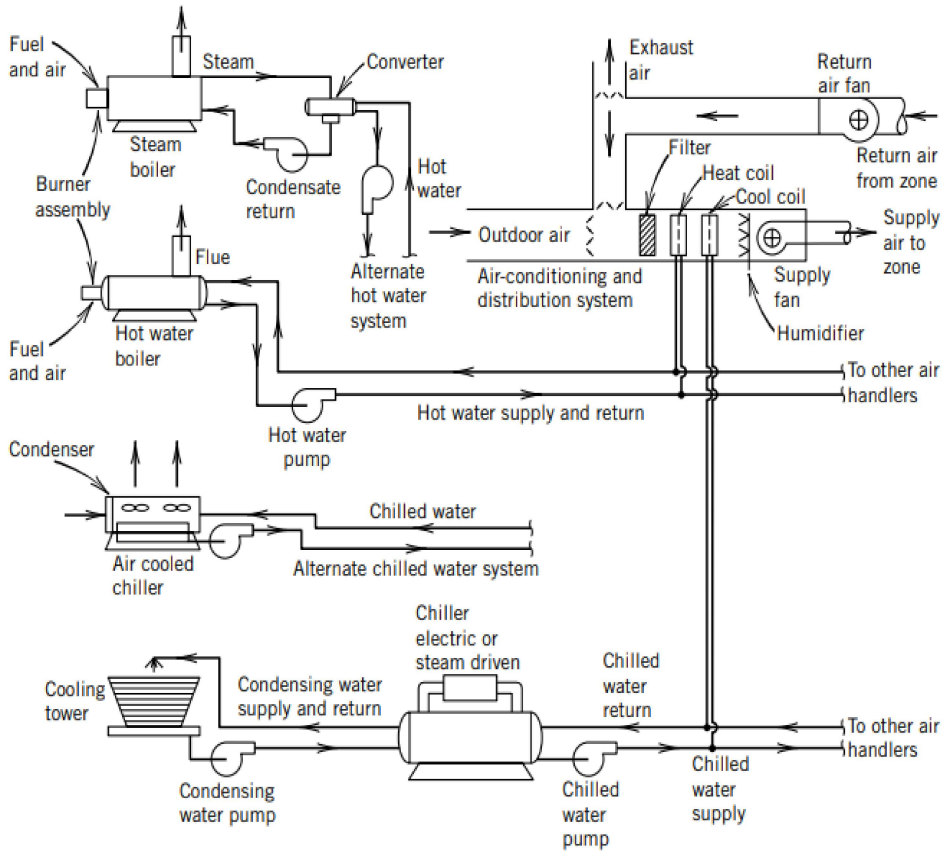


Figure 1.1: Schematic of all-air HVAC system, taken from [1].

shows a general DDC structure. DDC is the process in which control actions are enacted through the use of a digital device such as a microprocessor. Each subsystem in an HVAC is fitted with a DDC system that is in charge of measuring the process output using a set of algorithms to compare sensor input to a prescribed setpoint. All DDC signals from each HVAC subsystem are gathered and transported to a centralized controller. As it is the case with many industrial applications, centralized HVAC DDC systems are mainly regulated using the Proportional-Integral-Derivative (PID) control methodology [25]. The widely used PID control strategy offers a simplistic and easy to understand solution for feedback control as the availability of PID tuning rules is vast, their operation does not require much experience, and they are inexpensive to maintain.

However convenient, PID based controllers also have their draw-backs. For instance, PID controllers can be sensitive to disturbances, unstable if poorly tuned, be slow to respond, and are better suited for single input-single output (SISO) systems [26, 27].

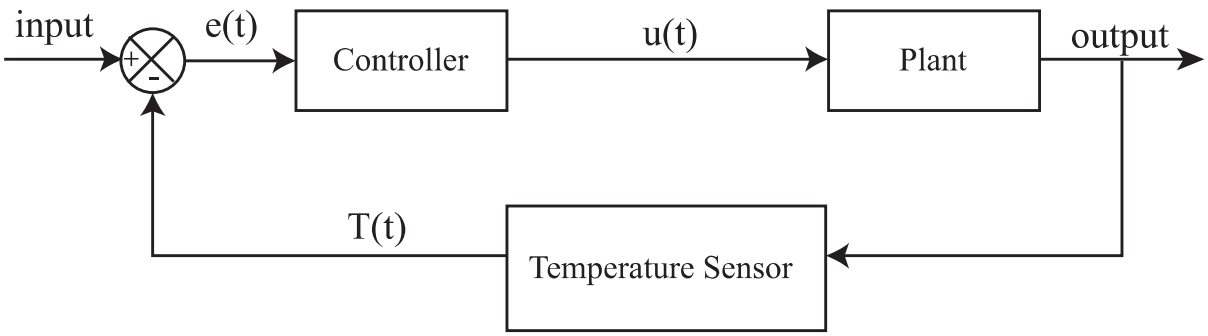


Figure 1.2: Direct Digital Control process.

Building HVAC systems, however, are governed by time-varying dynamics that include time varying set-points. An HVAC control system must take in real-time temperature data to properly adjust its settings, this means that they are bound to time-varying disturbances which results in system non-linearity. Therefore, applying PID control strategies to HVAC control systems may result in an inefficient use of electricity [28]. Thus, using a PID control methodology may prove to be difficult when trying to control complex and non-linear systems such as building HVAC units. As a result, this warrants for alternative HVAC control strategies.

Aside from PID controllers, current literature shows that there is very prominent research being done in the area of HVAC control methodologies. This includes the use of Predictive Mean Vote [29, 30], genetic and artificial neural network algorithms [31] -[33], Model Predictive Control [34] -[36], and fuzzy logic [37] -[40]. Predictive mean vote learning was developed to determine the thermal comfort of occupants within a

building by using a prediction model. This method, however, lacks the ability to account for non-linear dynamics such as occupant behavior and adaptive cooling and/or heating [41]. This gives rise to the need of creating control strategies with the capacity to handle complex and non-linear systems. In their work, Nassif [42] explored the idea of using an artificial neural network (ANN) to model an HVAC system and a genetic algorithm for optimization. The results presented in their paper show that when compared to pre-existing data, their HVAC ANN model was able to give good accuracy and provide a cooling energy savings of 11%. Although ANN networks have a great ability to predict models, they require large amounts of data and therefore can be computationally taxing.

As such, Behrooz et al. [43] outlines the advantages of using MPCs for HVAC management. In their work, they explain that MPC models require a mathematical model of the system in order to predict its future states. In their 2014 paper, Parisio et al. [44] proposed a scenerio-based MPC (SMPC) for HVAC systems that would take into account the uncertainty of the weather and the occupancy of model building. They found that the response of their SMPC was a lot smoother than the response generated from the PI controller that they tested their SMPC model against. They also found that the SMPC was able to keep the indoor temperature closer to the lower bound of 20°C during low occupancy simulations. Although MPCs are an excellent choice for HVAC control, they require accurate models such as black box [28], grey box [45], and white box [46], therefore it could make them a bit difficult to implement as cooling and heating requirements within buildings are difficult to model mathematically.

1.3 Fuzzy Control and its Applications

Lotfi A. Zadeh introduced fuzzy logic in 1965 with the aim to enable computers to manipulate vague and imprecise data. His publication "Fuzzy Sets" [47] was the framework for fuzzy logic and fuzzy set theory, thus significantly impacting the field of artificial intelligence (AI). Unlike binary logic, where something either belongs or does not, fuzzy logic recognizes that truth values may lie somewhere in between belonging and not belonging. This characteristic has proven invaluable in control theory, as it enables the representation of complex systems through the use of linguistic variables. Consequently, the development of a fuzzy logic-based controller (FLC) necessitates a deep understanding of the system in question and it dynamics. As such, fuzzy logic has been implemented in many real-world applications where mathematical simulations would not be possible due to the complexities of the control system.

Since its inception, fuzzy logic has had a role within many present control systems. The Sendai Subway 1000 series in Japan has employed the use of fuzzy logic as a speed controller since 1987. This drew the interest of researchers and thus the research on fuzzy logic speed controllers has increased [48]–[51]. Although the practicality of fuzzy logic as a means of speed control in trains has been proven, the use of fuzzy logic control strategies has trickled on to house hold items. The usefulness of fuzzy controllers extends to household products such as rice cookers [52], electric cookers [53], washing machines [54], heat pumps [55], and HVAC units [56].

Fuzzy logic, which is a form of multi-valued logic, is based on human reasoning and experience, therefore it does not require the use of a mathematical model [57]. In their

paper, Rashidi et al. [58] developed a hybrid fuzzy-PID HVAC controller. Since their model included the use of simulations for testing, they used the multi-input multi-ouput (MIMO) model outlined by [59]. They found that their fuzzy-PID controller was able to reach the set point temperature at a faster speed than their PID based controller. In a separate study, Ahmed et al. [56] proposed a fuzzy logic based controls scheme to maintain the temperature within 20 - 25°C and the humidity within 40 - 70% of two lab rooms within the Universiti Teknologi Malaysia. In this work, the authors were able to successfully implement their proposed controller to the thermostat that controls the central air within the two lab rooms. This was done by representing both inputs (i.e. temperature and humidity) as a set of linguistic variables, as such, their work did not utilize a mathematical model. The application of fuzzy logic for HVAC control is extremely beneficial in that fuzzy logic can be coupled with other control strategies. In their work, Alcalá et al. [60] combined the use of fuzzy logic and genetic algorithms where they prove that coupling the fuzzy logic technique with genetic algorithms can improve the robustness of these controllers. In a separate study Killian et al. [61] used a cooperative fuzzy model predictive control controller (CFMPC) for the heating and cooling of a building. In their study, they use a mathematical model of a building to build the CFMPC where they found that their proposed controller was able to accommodate for both cooling and heating modes. While research in building HVAC control utilizing fuzzy logic strategies primarily centers on developing mathematical models to simulate buildings, the importance to validate these control strategies with physical systems is crucial.

Thus, in preceding work, Joshua Baltazar developed three fuzzy logic controllers to

regulate the temperature within a sub-scaled building test-bed [62]. These controllers were built using experimentation and leveraging user expertise regarding the dynamics of the system. The initial controller was designed to use the difference between the actual room temperatures and a set point temperature. The second controller utilized both the temperature error and its derivative, while the third controller expanded on this by incorporating the temperature error, the derivative of the error, and the integral of the error as inputs. The study found that the fuzzy logic controller equipped with the most information about the building yielded the highest performance.

1.4 Objective of Work

The objective if this work was to conduct robustness testing on a fuzzy logic controller that was developed to control the temperature within a multi-room subscaled building test-bed [63, 64]. This controller was built using the difference between the temperature and its setpoint, the derivative of the error, and the integral of the error to keep room temperatures close to their setpoints. A series of tests were conducted to assess controller robustness by introducing internal and external disturbances. This was done to simulate irregular cooling loads that might be experienced within a real building. The internal disturbance tests were created to mimic residents of a building changing their thermostat to different temperatures throughout a 90 minute period with 30 minute intervals. The external disturbance tests where conducted to simulate a building with changing cooling loads on account to exposure of different weather conditions.

1.5 Thesis Overview

This section will give an overview of the chapters of this paper and their contents. Chapter 1 provides background information about the the need for better HVAC control strategies and the usefulness of fuzzy logic based controllers. Chapter 2 presents a description of the experimental test-bed. This chapter gives an overview of the various components that make up the test-bed such as dampers, instrumentation, and system variables. Chapter 3 gives an overview of fuzzy logic. This chapter examines some of the important aspects of fuzzy logic systems such as fuzzy sets, membership functions, defuzzification, and logic operations. Chapter 4 explains the design of the fuzzy logic controller and the results for the robustness testing. The final chapter, Chapter 5, give the conclusions gathered based off of the test results as well as offering directions for future work. Appendix A gives instructions on how to set-up and operate the LabVIEW and MATLAB codes for testing. Appendix B gives an example on using fuzzy logic to estimate a sine wave, while Appendix C gives a fuzzy logic example for modeling a heat exchanger.

CHAPTER 2

DESCRIPTION OF EXPERIMENTAL TEST-BED

Chapter 1 entailed a brief description behind the incentive to improve upon current building HVAC automation controllers. From the methods covered, it was determined that the fuzzy logic control methodology provided an excellent solution. Thus, the succeeding chapter gives a detailed description of the experimental system. The first section of this chapter discusses the test-building structure and the cooling load delivery system. After which, the data gathering process and associated devices used will be explained. This chapter will conclude with identifying the variables considered through out the experimental process of this work.

2.1 Building Test-bed

Utilizing a sub-scaled building test-bed to test HVAC controller schemes holds many benefits as it is (1) cost-effective, (2) allows for the testing of various "indoor" temperature conditions without disruption of inhabitants, and (3) allows for the controlled simulation of various climate conditions. The experimental test-bed used in this work was designed, constructed, and tested by three mechanical engineering senior design groups at California State University, Los Angeles. The first group designed the building, the second group built the building, and the third group added the duct and damper systems [65]-[68]. The building test-bed (Figure 2.1) has dimensions of 1.2 m $\times$ 0.92 m $\times$ 1.1 m and it is divided among two floors. Each of these floors contains four rooms, each with dimensions of 0.45 m $\times$ 0.42 m $\times$ 0.52 m that are divided by 3.5 cm thick walls. The interior walls of the upper floor are removable and allow for testing of various floor plan configurations.

Each room in the building contains two glass windows measuring 0.20 m $\times$ 0.15 m, they can be opened or closed by sliding them on rails as seen on Figure 2.2(a). The building features staircase openings to thoroughly assess and study the flow interaction between floors; all door, windows, and staircase openings were closed for the analysis presented in this paper. In addition, each room contains a 13.7 cm $\times$ 29 cm door cut-out on the interior walls with each door connecting to adjacent rooms (Figure 2.2(b)). Each room is fitted with a cold air inlet and return air vents.



Figure 2.1: Building test-bed.

To ensure compliance with industry standards, this test-bed was constructed using materials approved by both the California Building and the U.S. Department of Energy Building Codes. Therefore, the building and rooms are insulated with R-19K insulation, the inner walls of the building are drywall while the outer walls are composed of wood. On the other hand, the ceiling and roof of the test-bed are built from underlayment wood



(a) Window placement. (b) Air temperature from HVAC system.

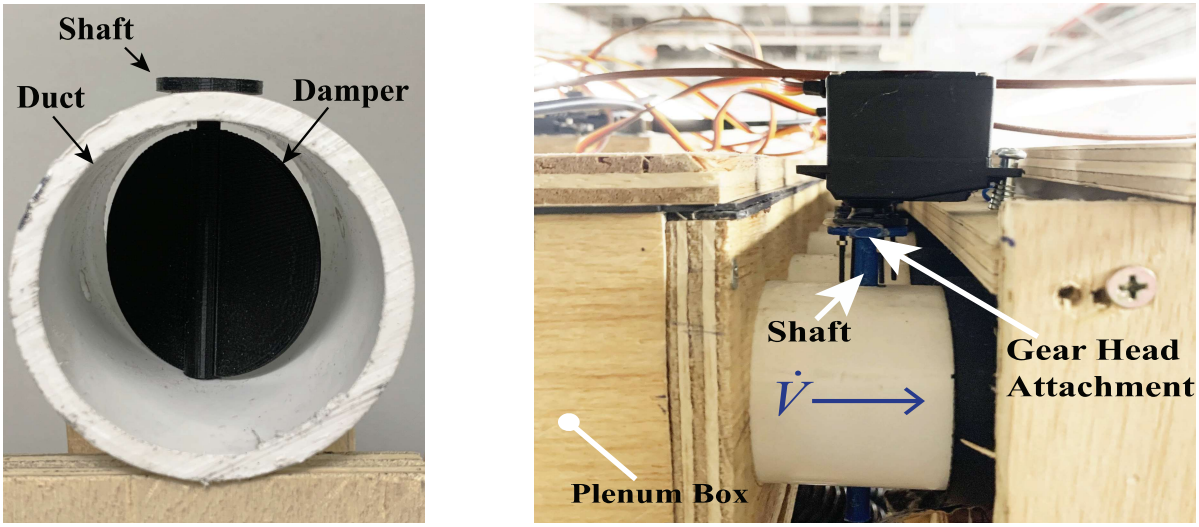
Figure 2.2: Door placement in each room.

planks. The roof system is fitted with latch locks to allow easy access to the second floor.

The initial cooling system design included four Peltier thermoelectric coolers attached to fans as cooling sources, this cooling system was later proven to be inefficient and was replaced by an external HVAC unit [63]. The cooling system for this building test-bed configuration is composed of a network of PVC pipes that guide cold air into each room from an external Air Conditioning unit. The external AC unit chosen is a Haier 115 V ESA410K model with a cooling capacity of 1.06×10^7 J/hr [69]. The external AC unit is fitted with a plenum box to ensure that all the rooms receive an uniform amount of cold air and to reduce the air outflow velocity. The air outlet of the plenum box is divided into eight openings, each of which is attached to a PVC pipe that delivers cold air into its respective room. Every pipe contains a 3D printed ABS damper with a diameter of 2.97 cm. Each damper is attached to a TowerPro SG-5010 Servo motor, which controls the opening and closing of the damper based on controller output. This manipulation of

the damper opening regulates the volumetric airflow rate entering each room.

Figure 2.3 shows the damper and servo motor subsystem. In this configuration, the servo motor is attached to the damper shaft through four small screws placed through the servo gear head attachment and through the damper shaft head. The air delivery pipe system is completely surrounded with R-19K insulation, with the exception of the 2-inch opening shown in Figure 2.3(b). This opening is needed to allow for the servo to fully rotate without interference.



(a) Damper in pipe configuration.

(b) Air temperature from HVAC system.

Figure 2.3: Damper and servo motor subsystem.

2.2 Instrumentation and Data Acquisition System

As previously discussed, the experimental system is composed of a physical building test-bed and an arrangement of data acquisition devices. To collect temperature data, every room in the building is fitted with a pair of type-T thermocouples. Thermocouples are electrical devices that are made from two dissimilar metals. They are joined at a junction (the measuring end) that is kept at a different temperature than the tail end of

these devices. The difference in temperature is read as a voltage difference and turned to temperature by data acquisition (DAQ) devices and computer software.

Various types of thermocouples are available in the market, such as J, K, R, S, T, N, E, and B. What differentiates each of these devices is the type of metal chosen for the wires, the temperature range, and their accuracy levels. In previous work, the teams that built the test-bed used type-K thermocouples which offer a ±2.2°C accuracy when operated within within a range of 0°C to 1250°C and when calibrated using ASTM E230-ANSI MC96.1 standards [70]. This work, however, utilizes type-T thermocouples which offer an accuracy of ±1.0°C within a temperature range of 0°C to 350°C. Since the temperature within each room of the building was not expected to exceed 32.2°C, it was decided that type-T thermocouples were best suited for the following experiments.

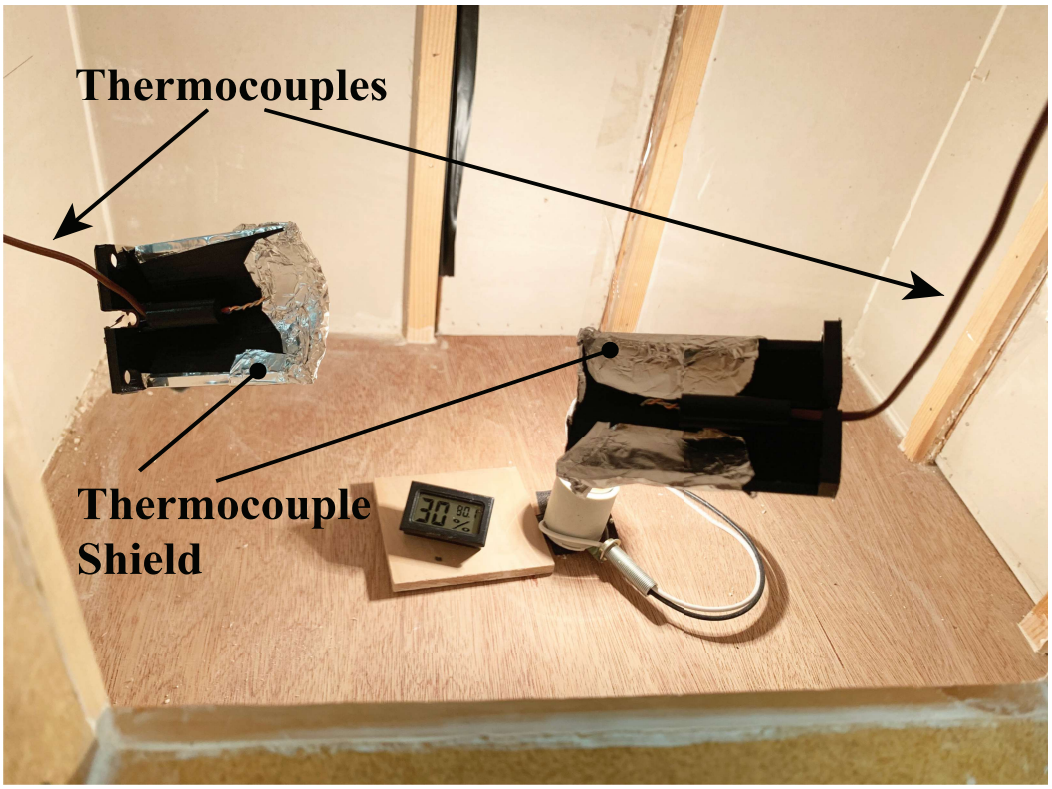


Figure 2.4: Thermocouple arrangement in rooms.

There are a total of 16 thermocouples placed in the building (a pair for each room) divided among two USB-TC DAQ devices. The building contains eight 40 Watt light bulbs, each light bulb is connected to a Measurement Computing (MC) relay box with 24 electromechanical connections. One light bulb is placed in the middle of each room and acts as a heating source, simulating heat generated from building occupants and electrical equipment. The placement of the light bulb and thermocouples is show in Figure 2.4. As seen from Figure 2.4, each thermocouple is fitted with a thermocouple shield to minimize the heat transfer generated through radiation in account of the light bulb. Each shield was blanketed with aluminum foil to help reflect the radiant heat emitted, thus protecting te thermocouples and allowing for only air temperature readings. In addition, the thermocouple shields were designed with a flat bottom to facilitate placement on various surfaces within the room or suspension by the thermocouple wire as depicted on Figure 2.4.

The DAQ devices and the light bulb relay box are connected to a personal computer (PC). The PC is equipped with LabVIEW and MATLAB software that allow for the complete control of this test-bed system. The LabVIEW software uses a graphical programming environment that uses blocks of code (G-code) to allow users to create real-time automated test systems. The LabVIEW algorithm created for testing the test-bed system uses G-code to control the electromechanical pins in the relay to allow users to turn the light bulbs in the building on and off. This LabVIEW algorithm also collects the temperature data gathered from the thermocouples and the DAQ devices and sends it to MATLAB every 1.5 seconds. Once the temperature data is sent to MATLAB, MATLAB enacts the fuzzy controller and generates real-time plots of the air tempera-

ture in each room and the AC air temperature. To enact the control actions of the fuzzy logic controller, MATLAB sends a signal to an Arduino 2560 Mega microcontroller. This microcontroller sends pulses of voltage to the servo motors, which either close or open the damper in relation to the desired control actions (instrumentation illustrated on Figure 2.5). Appendix A contains a step-by-step guide of how to operate the controller that corresponds to this system.

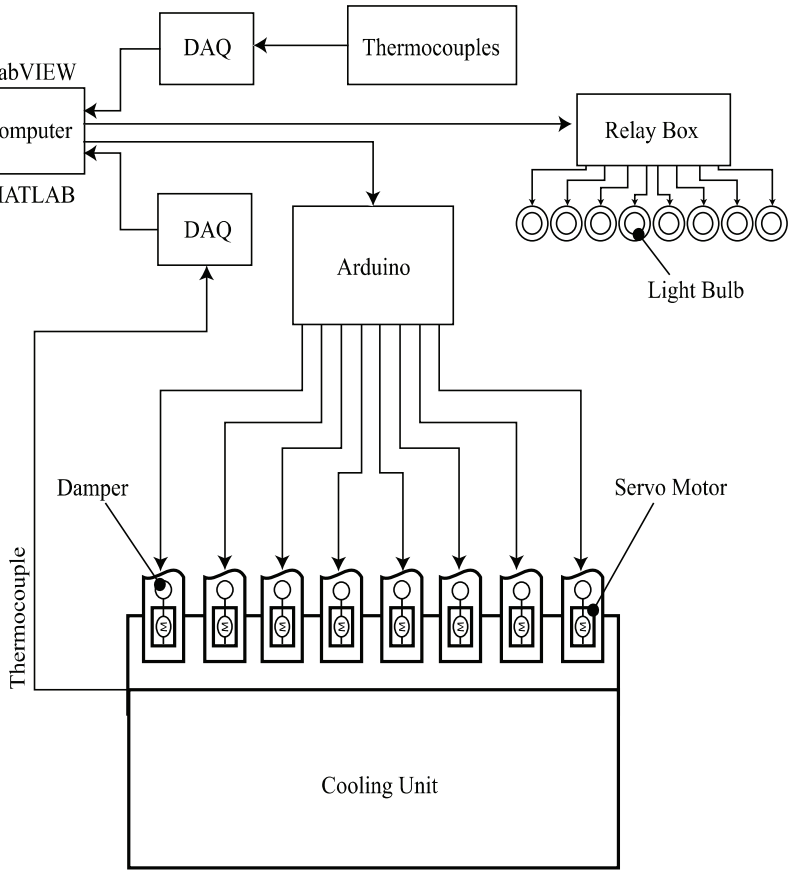


Figure 2.5: Diagram of system instrumentation.

2.3 System Variables

The previous section detailed the type of instrumentation used to collect the temperature data of each room in the test-bed building. However, in order to understand the dynamics of this test-bed it is important to understand what its input and output variables are. As Figure 2.6 shows, the cold air from the AC flows directly into the plenum box. From here, the total air volume is divided into eight individual volumetric air flow rates ($\dot{V}$), each of which is fed into its respective room. Therefore, $\dot{V}$ is denoted as a system input variable. To successfully lower and maintain the temperature in each room, $\dot{V}$ has to successfully remove some of the heat generated by the light bulb. Consequently, the room air temperature, $T(t)$, is referred to as the output variable. It is important to note that since the building is well insulated, the heat loss to the surroundings is not taken into account.

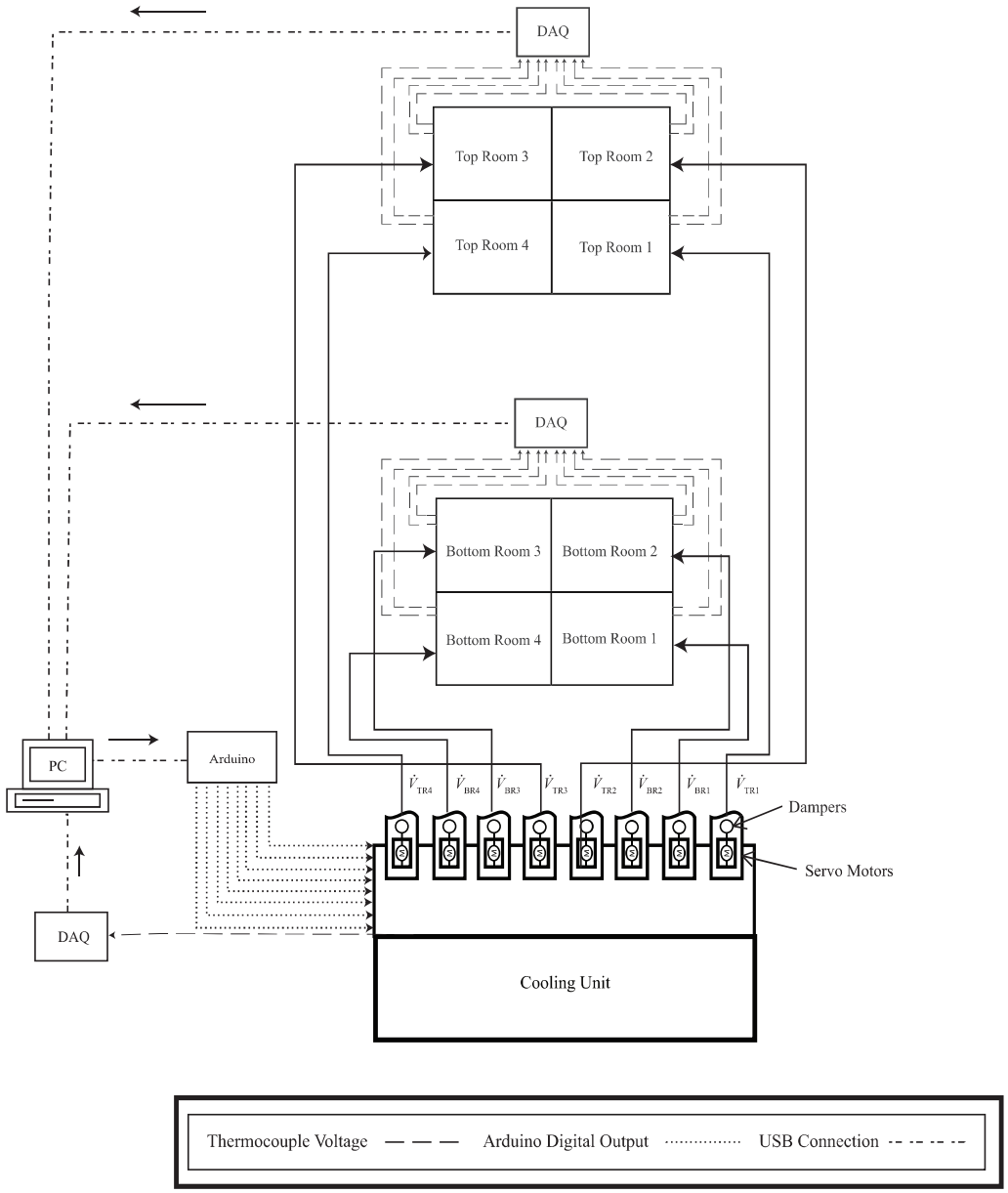


Figure 2.6: Schematic of building.

2.4 System Dynamics

An important aspect within controller development is understanding the dynamics of the system being controlled. Comprehending system behavior in the absence of a controller ensures that the designers develop a controller that operates within the parameters of the system. In the case of this study, it was imperative to document and analyze the

relationship between the amount heating provided by the light bulbs and the rate of cooling of the external AC. Thus, this section will explain the set of tests conducted to study the relationship between the air temperature in the rooms, T_a, and airflow delivered by the external AC unit, $\dot{V}$.

The first test conducted was designed to study way in which the rooms cooled with no controller applied, Figure 2.7. Before running this test, all rooms were heated to 26.7°C. This experiment was then run for a period of 60 minutes, the dampers were fully opened, the external AC unit was operational and set to an air temperature of 18.9°C. When examining Figure 2.7, it is seen that the room temperatures experience an exponential decay within the first 28 minutes. This aligns with Newton's Law of Cooling which states the following:

$$T(t) = T_s + (T_i - T_s)e^{-kt} \tag{2.1}$$

where t is time, $T(t)$ is the temperature at time t, T_s is the surrounding temperature, T_i is the initial temperature, and k is a constant.

An important detail to notice is that the temperatures in the rooms rise and fall from $t \geq 28$ minutes. This is due to the ambient temperature sensor that is placed within the external AC unit. The ambient temperature sensor reads the laboratory temperature and modifies the AC output air temperature to prevent damage to the AC unit. The operating conditions for the Haier ESA 410K listed in the manual [69] state that the nominal indoor state dry-bulb temperature is 26.7°C for an outdoor dry bulb temperature of 35°C. However, at the time of testing, the lab temperature ranged from 17.8°C to 18.6°C. This suggests that the AC was not performing within its cooling

capacity. Forcing its operation within a cooler ambient temperature than what it was rated for caused a decrease in efficiency and a lowered cooling performance.

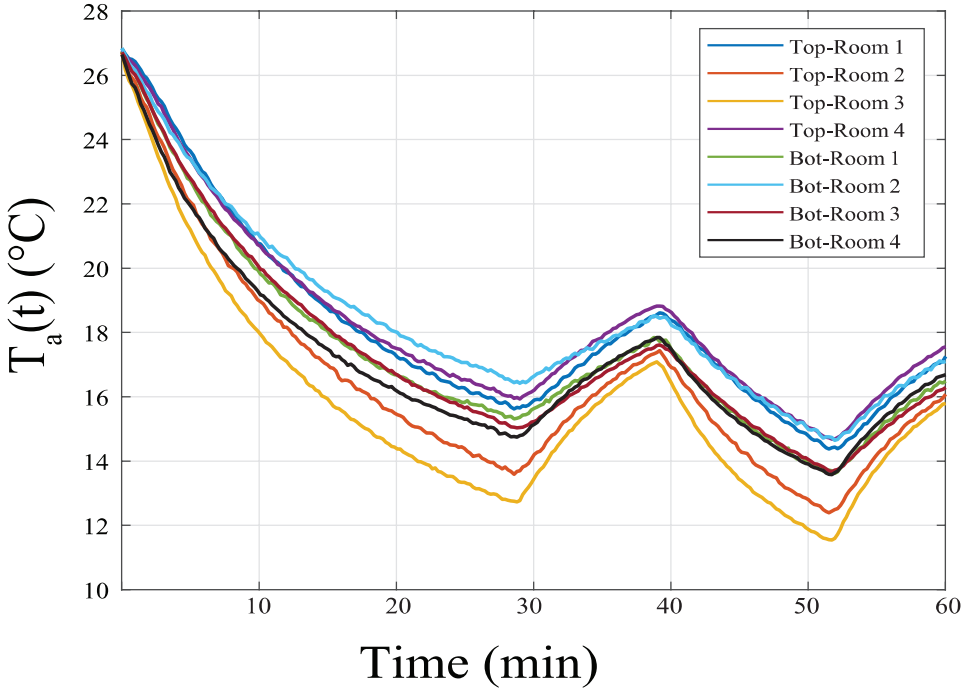


Figure 2.7: Open damper dynamics test result.

As like the first experiment, this test began after all rooms were heated to 26.7°C. This test was conducted over a period of 60 minutes, the dampers where opened and closed at intervals of 3 minutes, the external AC was operational and set to an air temperature of 18.9°C. The results for this test are shown in Figure 2.8. The main objective for this test was to study the rate of heating versus the rate of cooling with an operational AC unit. From the results presented, it is seen that the rooms follow the general exponential decay that was seen in the first dynamics test and that the rate of heating per room is significantly slower than the rate of cooling.

It is important to note that when the dampers are closed, the air stagnates between the AC outlet and the closed damper. When the damper is reopened the trapped cold

air exits and causes the rooms to momentarily experience an excess influx of cold air. As seen from Figure 2.8, the air temperatures in the rooms stop to decrease from t≥40 minutes and instead begin to rise. Like in the previous test, this is due to the internal sensor in the AC unit acting independently and adjusting the AC outflow air temperature to avoid damage to the AC.

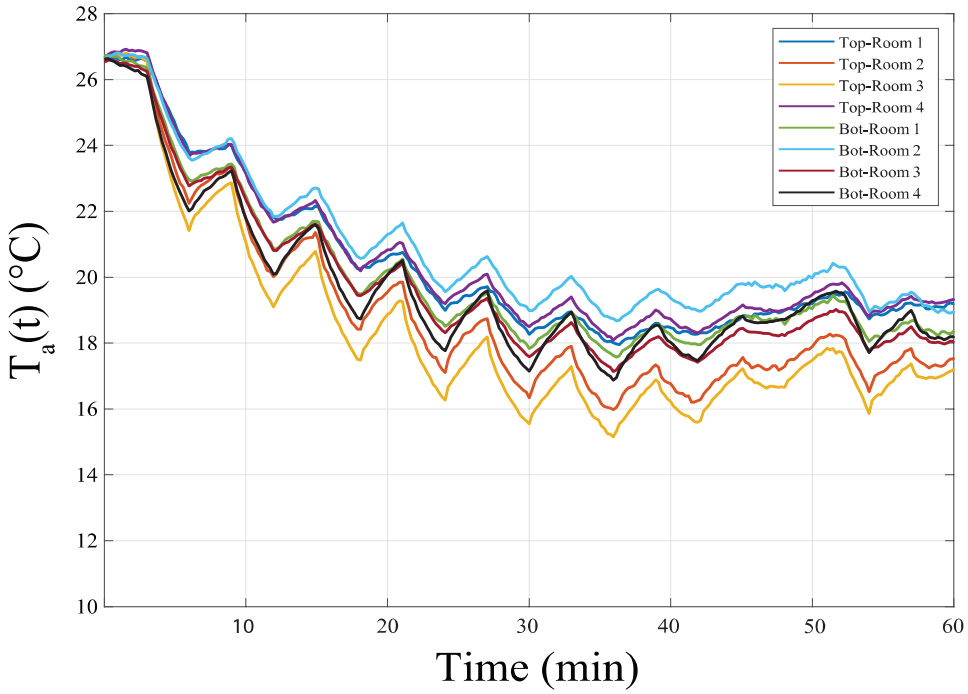


Figure 2.8: Open-close damper dynamics test result.

CHAPTER 3

FUZZY LOGIC

The previous chapters established that fuzzy logic can be used as a means of intelligent control. As such, this chapter will introduce the theory behind fuzzy logic and its convenience when it comes to modeling systems with complex dynamics. The first section of this chapter will go over fuzzy sets and membership functions. The next section will introduce the underlying fuzzy logic inference systems and the importance of the rule-based processes. The third section will give an overview of different types of defuzzification methods and the final section will give a few examples of system modeling using fuzzy logic.

3.1 Fuzzy Sets and Membership Functions

Fuzzy set theory is a branch of set theory that revolves around the study of elements with varying degrees of membership. Before its inception, the study of set theory was limited to what today we know as classical set theory. These sets are said to be "crisp", as there is no allowance for varying degrees of membership within these universes. As follows, let us suppose that there is such a universe X that contains a set defined as A. Each element within set A of universe X is therefore defined as x. In the case of binary (crisp or also referenced as boolean) logic, the membership of each element x within a set A either belongs ($\in$) or does not belong ($\notin$), such that [57]:

$$X_A(x) = \begin{cases} 1, & x \in A \\ 0, & x \notin A \end{cases} \tag{3.1}$$

In contrary, fuzzy theory focuses on the representation of vagueness and ambiguity of elements within any given set. This is mathematically represented as:

$$\mu_{\underset{\sim}{A}}(x) \in [0, 1] \tag{3.2}$$

where $\underset{\sim}{A}$ is defined as any fuzzy set, μ is the membership function used to describe fuzzy set $\underset{\sim}{A}$, and $\mu_{\underset{\sim}{A}}(x)$ is the degree of membership of crisp element x in fuzzy set $\underset{\sim}{A}$.

In the event that the universe of discourse X is discrete and finite, fuzzy set $\underset{\sim}{A}$ can be represented as:

$$\underset{\sim}{A} = \left\{ \frac{\mu_{\underset{\sim}{A}}(x_1)}{x_1} + \frac{\mu_{\underset{\sim}{A}}(x_2)}{x_2} + ... \right\} = \left\{ \sum_i \frac{\mu_{\underset{\sim}{A}}(x_i)}{x_i} \right\} \tag{3.3}$$

where in Equation (3.3), summation signifies the collection of each element.

The first part of any fuzzy logic system is the fuzzification step. In this step, a crisp number is made fuzzy by classifying its degree of membership through the use of membership functions. Graphically speaking, a membership function is a curve that encompasses all possible degrees of a crisp element within a set ranging from 0 (no membership) to 1 (complete membership). There are several types of membership functions, all with their own set of mathematical representations and uses. Some examples include, but are not limited to trapezoidal Figure 3.1(a), triangular Figure 3.1(b), generalized bell Figure 3.1(c), and gaussian Figure 3.1(d).

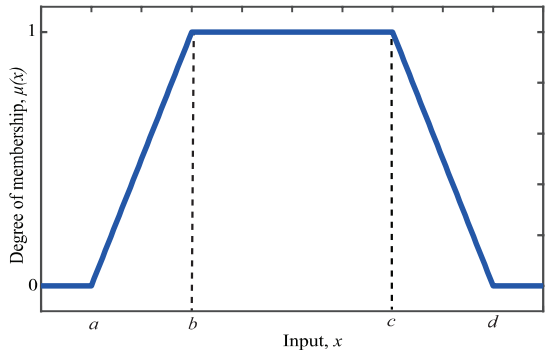
Trapezoidal membership functions are defined by parameters a, d, c, and d. With the highest membership value being represented by the span of b and c. Any crisp input that lies between a and b or c and d can have a membership anywhere between 0 and 1. The notation for these types of membership functions is as follows:

$$\mu_{trapezoidal}(x : a, b, c, d) = \begin{cases} 0, & x \leq a \\ \frac{x-a}{b-a}, & a \leq x \leq b \\ 1, & b \leq x \leq c \\ \frac{d-x}{d-c}, & c \leq x \leq d \\ 0, & d \leq x \end{cases} \tag{3.4}$$

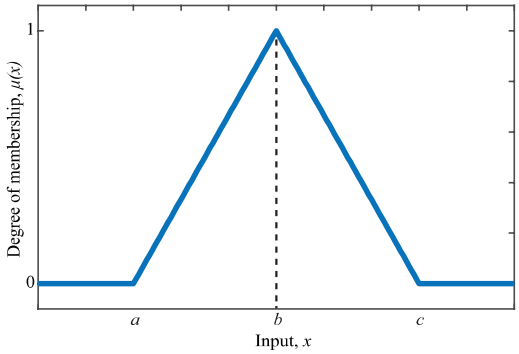
Triangular membership functions are widely accepted as the relationship between their inputs and outputs are easier to understand and define. These types of membership functions are described by the parameters a, b, and c. Parameter b represents the highest point within these types of membership functions, which represent full membership for an input x. In the case of triangular membership functions, inputs that lie within $[a, b]$ and $[b, c]$ have a membership of anywhere between 0 and 1.

$$\mu_{triangular}(x : a, b, c) = \begin{cases} 0, & x \leq a \\ \frac{x-a}{b-a}, & a \leq x \leq b \\ \frac{c-x}{c-b}, & b \leq x \leq c \\ 0, & c \leq x \end{cases} \tag{3.5}$$

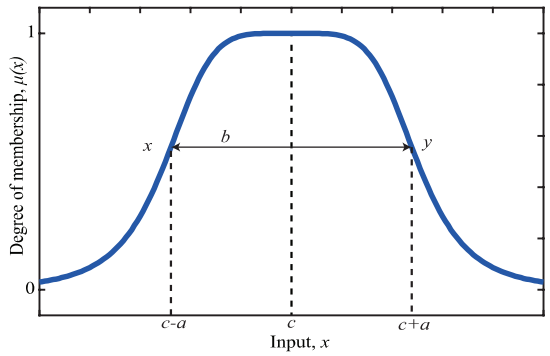
Generalized bell membership functions are represented by parameters a,b, and c. The parameter a determines the width of the curve, b is any positive integer, and c is the



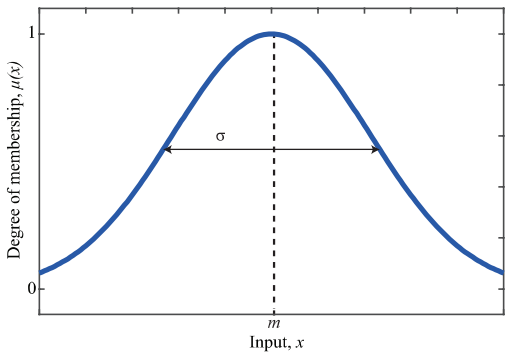
(a) Trapezoidal membership function.



(b) Triangular membership function.



(c) Generalized bell membership function.



(d) Guassian membership function.

Figure 3.1: Common membership functions.

center of the curve.

$$\mu_{bell}(x : a, b, c) = \frac{1}{1 + |\frac{x-c}{a}|^{2b}} \tag{3.6}$$

where the slope at x is taken as:

$$x = \frac{b}{2a} \tag{3.7}$$

and the slope at y is taken as:

$$y = -\frac{b}{2a} \tag{3.8}$$

Gaussian membership functions utilize the parameters m and σ. In this curve, m represents the mean of the gaussian curve and σ is its spread.

$$\mu_{guassian}(x : \sigma, m) = e^{-\frac{1}{2}(\frac{x-m}{\sigma})^2} \tag{3.9}$$

When examining membership functions, it is important to understand a few basic concepts within classical logic operations:union, intersection, and complement. If there is an universe X that contains two sets A and B the the union of these two sets is described as follows:

$$Union: \qquad A \cup B = \{x | x \in A \ or \ x \in B\} \tag{3.10}$$

$$Intersection: \qquad A \cap B = \{x | x \in A \ and \ x \in B\} \tag{3.11}$$

$$Complement: \qquad \bar{A} = \{x | x \notin A, x \in X\} \tag{3.12}$$

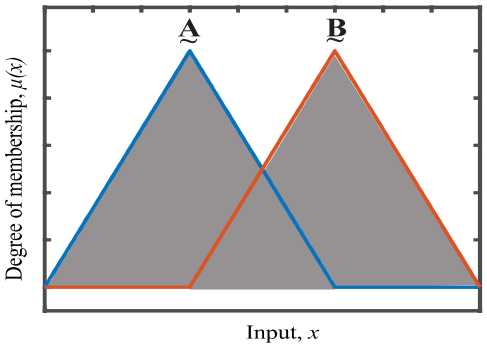
These operations can be expanded to represent fuzzy sets and membership functions. As an example, given that fuzzy sets $\underset{\sim}{A}$ and $\underset{\sim}{B}$ exist within the Cartesian space $X \times Y$:

$$Union: \qquad \mu_{\underset{\sim}{A} \cup \underset{\sim}{B}}(x, y) = max(\mu_{\underset{\sim}{A}}(x, y), \mu_{\underset{\sim}{B}}(x, y)) \tag{3.13}$$

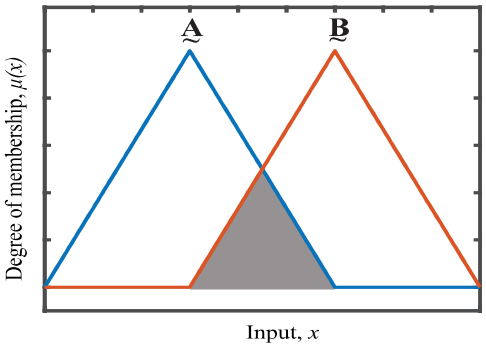
$$Intersection: \qquad \mu_{\underset{\sim}{A} \cap \underset{\sim}{B}}(x, y) = min(\mu_{\underset{\sim}{A}}(x, y), \mu_{\underset{\sim}{B}}(x, y)) \tag{3.14}$$

$$Complement: \qquad \mu_{\bar{A}}(x, y) = 1 - \mu_{\bar{A}}(x, y) \tag{3.15}$$

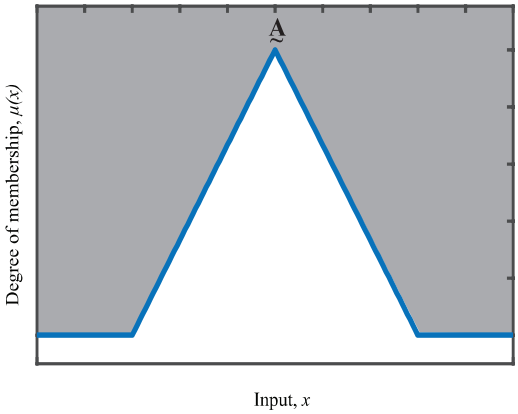
Figure 3.2 is an illustration of the fuzzy logic operations described above.



(a) Union.



(b) Intersection.



(c) Complement.

Figure 3.2: Graphical representation of fuzzy logic operations.

3.2 Inference Systems and Rule-based Process

The inference mechanism of fuzzy logic systems is the process in which fuzzy systems formulate a mapping from an input to an output [57]. There are two main types of fuzzy inference systems that are widely used today: Mamdani and Sugeno. This work, however, uses the Mamdani inference system as it is commonly used and it allows for the output to be represented through membership functions [64]. The Mamdani inference system is an attractive method of procedure for fuzzy systems because of its use of linguistic IF-THEN propositions. This inference system uses the user defined IF-THEN propositions

to find a consequence (output) based on a given antecedent (input). These propositions are of the form:

$$IF\ x_1\ is\ \underset{\sim}{A}_1^k\ and\ \underset{\sim}{A}_2^k\ THEN\ y^k\ is\ \underset{\sim}{B}^k,\ for\ k = 1, 2, ..., r \tag{3.16}$$

where $\underset{\sim}{A}_1^k$ and $\underset{\sim}{A}_2^k$ are fuzzy sets that represent the kth antecedent pairs and $\underset{\sim}{B}^k$ is the fuzzy set representing the kth consequent.

As an example, let us use a single-input and single-output fuzzy system. Refer to Figure 3.3 as a representation of ages for humans within the range of [0, 80]. As seen from the figure, three membership functions map out different stages of the proposed age range. In this case, the linguistic variables represented are *Young*, *Middle-Aged*, and *Old*. with linguistic variable *Young* having a range of [0, 36], *Middle-Aged* $\in$ [36, 54], and *Old* $\in$ [36, 80]. Let us say that we want to use Figure 3.3 to get a fuzzy output for someone who is 30 years old. As seen, this person would fall within the *Young* and *Middle-Aged* membership functions. From here, we can infer that someone who is 30 years of age falls between the *Young* and *Middle-Aged* categories, with more membership within the Middle-Aged group.

Now, let us suppose that we want to map the risk of cardiovascular disease of an individual based on age and activity level. Figure 3.4 demonstrates a set of three membership functions that represent activity levels based on a scale ranging from 0 to 10.

The following figure, Figure 3.5, displays the corresponding output membership functions for this example. In this case, the linguistic variable *Minimal* has a range of [0, 50], *Neutral* $\in$ [30, 70], and *High* $\in$ [50,100].

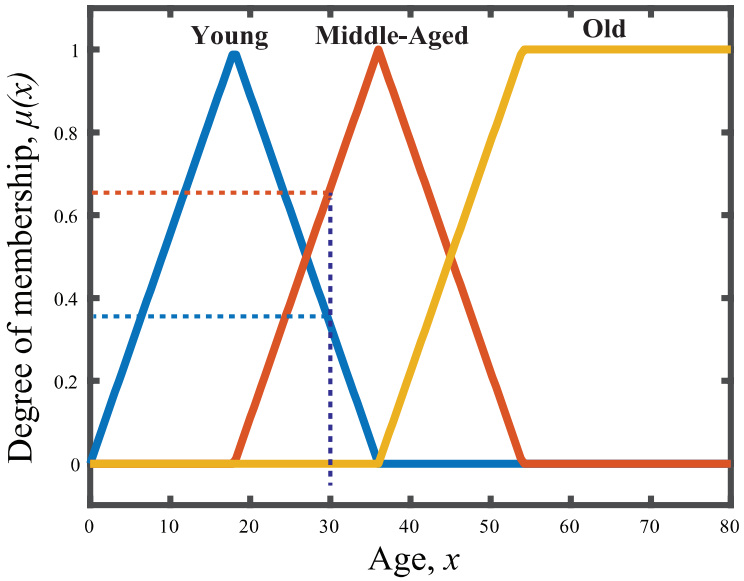


Figure 3.3: Example of linguistic variables for a range of ages.

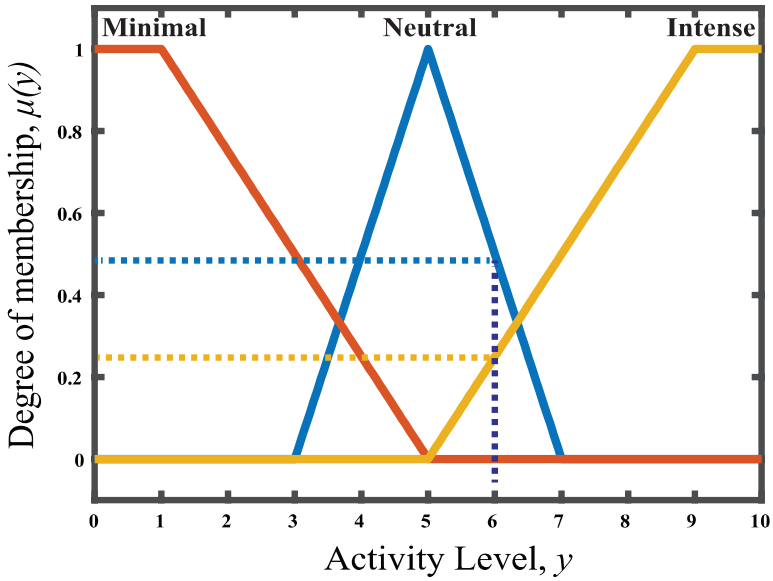


Figure 3.4: Example of linguistic variables for a range of activity levels.

With the inputs and outputs defined, one can proceed to set up the inference system for this example. As previously mentioned, the fuzzy inference engine is an user defined rule-based system that utilizes expert knowledge to make decisions. Using the Mamdani inference method, Eq. (3.16), and intuition [71, 72], we can begin to construct an example of a Mamdani IF-THEN rule.

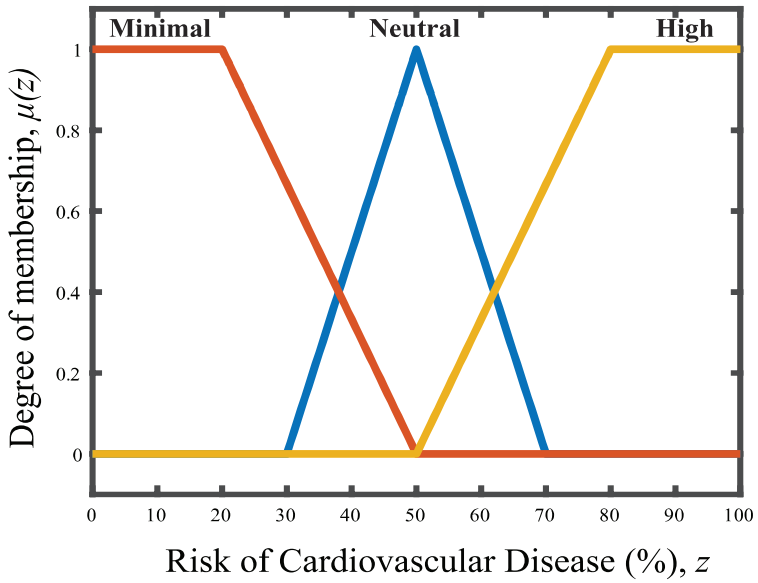


Figure 3.5: Example of linguistic variables for risk of cardiovascular disease.

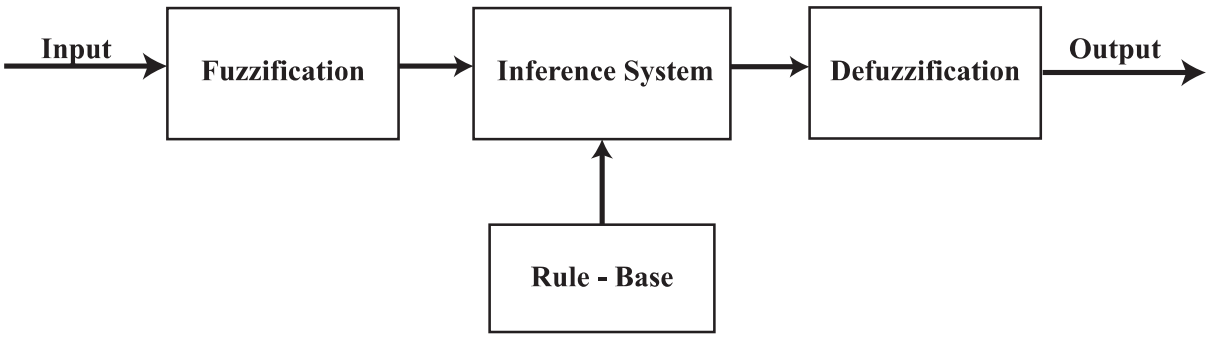


Figure 3.6: Diagram of the fuzzy inference system.

Let us say, that we want to map the risk of cardiovascular disease for a person who is 30 years of age (Figure 3.3) and has an activity level of 6 (Figure 3.4). Based on research, it is safe to assume that a 30-year old individual who maintains a moderate level of physical activity faces minimal risk of heart disease, assuming the absence of external factors such as family history. Therefore, we may have an IF-THEN rule such as the one below:

$$IF\ x\ is\ Young\ AND\ y\ is\ Neutral\ THEN\ z\ is\ Minimal \tag{3.17}$$

where the conjunction *AND* connects the antecedents and the consequent. By using *AND*, the inference system is informed that both antecedents must be satisfied jointly. In any case with an *AND* operator, the aggregate output, z, is found by the intersection of all rule outcomes such that,

$$\mu_z(z) = min(mu_{z^1}(z), mu_{z^2}(z), ..., \mu_{z^r}(z),),\ \ for\ z \in Z \tag{3.18}$$

where z^i is the intersection of all individual rule consequences and 1=1, 2, ..., r.

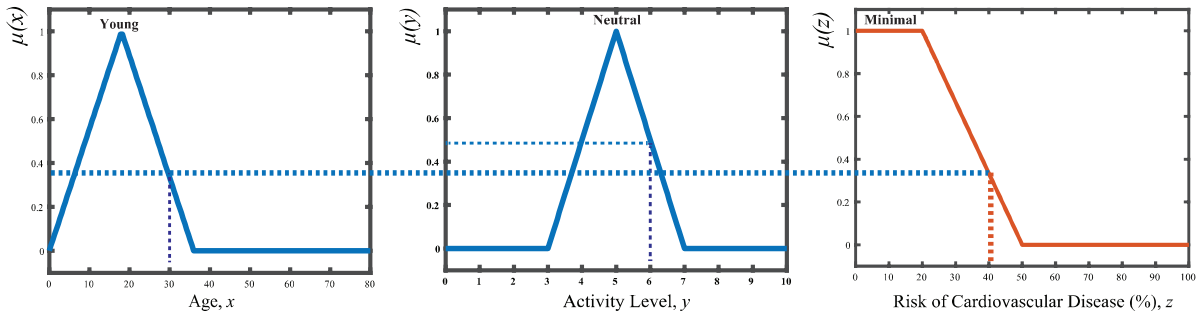


Figure 3.7: Diagram of the fuzzy inference system for "AND" operator.

From Figure 3.7 it is seen that the conjunction *AND* makes it so that we only take the minimum value from both the *Young* and *Neutral* membership functions. This gives a fuzzy input of about 0.38.

On the other hand, suppose that the desired rule aggregation scheme is to be repre-

sented by the disjunction OR. The IF-THEN rule statement would be as follows Eq. (3.19):

$$IF\ x\ is\ Middle - Aged\ OR\ y\ is\ Intense\ THEN\ z\ is\ Neutral \tag{3.19}$$

and the membership function for the consequent would be defined as:

$$\mu_z(z) = max(\mu_{z^1}(z), \mu_{z^2}(z), ..., \mu_{z^r}(z),),\ \ for\ z \in Z \tag{3.20}$$

In this event, the OR operator specifies that the aggregated output is found via the union of the antecedents. Meaning that that specific IF-THEN rule requires that at least one antecedent is satisfied, and therefore the maximum fuzzified input is used by the inference system to map a fuzzy output.

These systems can become quite elaborate as the number of inputs and outputs increases. To present the rules of these fuzzy systems, one often uses what is called a truth table. Generally speaking, a truth table is a way to showcase various fuzzy compound propositions. The truth table for a single-input single-output fuzzy inference system would have the following structure:

Table 3.1: Truth table example for single-input single-output fuzzy system

z	x_1	x_2
y_1	z_1	z_2
y_2	z_3	z_4

where z_i refers to the output based on inputs x_i and y_i.

3.3 Defuzzification Methods

One of the most important steps within any fuzzy system is that of defuzzification. Defuzzification is the process in which fuzzy sets are converted to precise quantities, or scalars. This step is of importance within fuzzy control systems because this operation is responsible for turning fuzzy approximations to tangible/crisp numbers that can be used to manipulate mechanical objects. As described by Timothy J. Ross [57], there are four main defuzzification methods used in practice: (1) Max membership principle, (2) Mean max membership method, (3) Weighted average method, and (4) Centroid.

The Max membership principle defuzzification method Eq. (3.21) is only applicable when the height of membership functions is unique.

$$Max\ membership\ principle: \qquad \mu_{\underset{\sim}{A}}(z^*) \geq \mu_{\underset{\sim}{A}}(z) \tag{3.21}$$

The Mean max method of defuzzification Eq. (3.22) is similar to the Max membership principle, however it differs in that the maximum is not limited to a single point.

$$Mean\ max\ method: \qquad z^* = \frac{a+b}{2} \tag{3.22}$$

The Weighted average method of defuzzification Eq. (3.23) is regarded as the more computationally efficient method. This method, however, is usually restricted to symmetrical output membership functions.

$$Weighted\ average\ method: \qquad z^* = \frac{\sum \mu_{\underset{\sim}{A}}(\bar{z}) \cdot \bar{z} dz}{\int \mu_{\underset{\sim}{A}}}(\bar{z}) dz \tag{3.23}$$

The Centroid method of defuzzification Equation (3.24) is the mostly used defuzzification method. The Centroid method is used as the defuzzification method for the controller used in this study.

$$Centroid\ method: \qquad z^* = \frac{\int \mu_{\underset{\sim}{A}}(z) \cdot z dz}{\int \mu_{\underset{\sim}{A}}}(z)dz \tag{3.24}$$

If graphically mapping IF-THEN rules Equation (3.17) and Equation (3.19), the aggregate output will be as shown in Figure 3.8. Where the centroid method to defuzzify the output for inputs of $Age = 30$ years and $Activity\ Level = 6$ is used and the risk of cardiovascular disease is computed to be 37%.

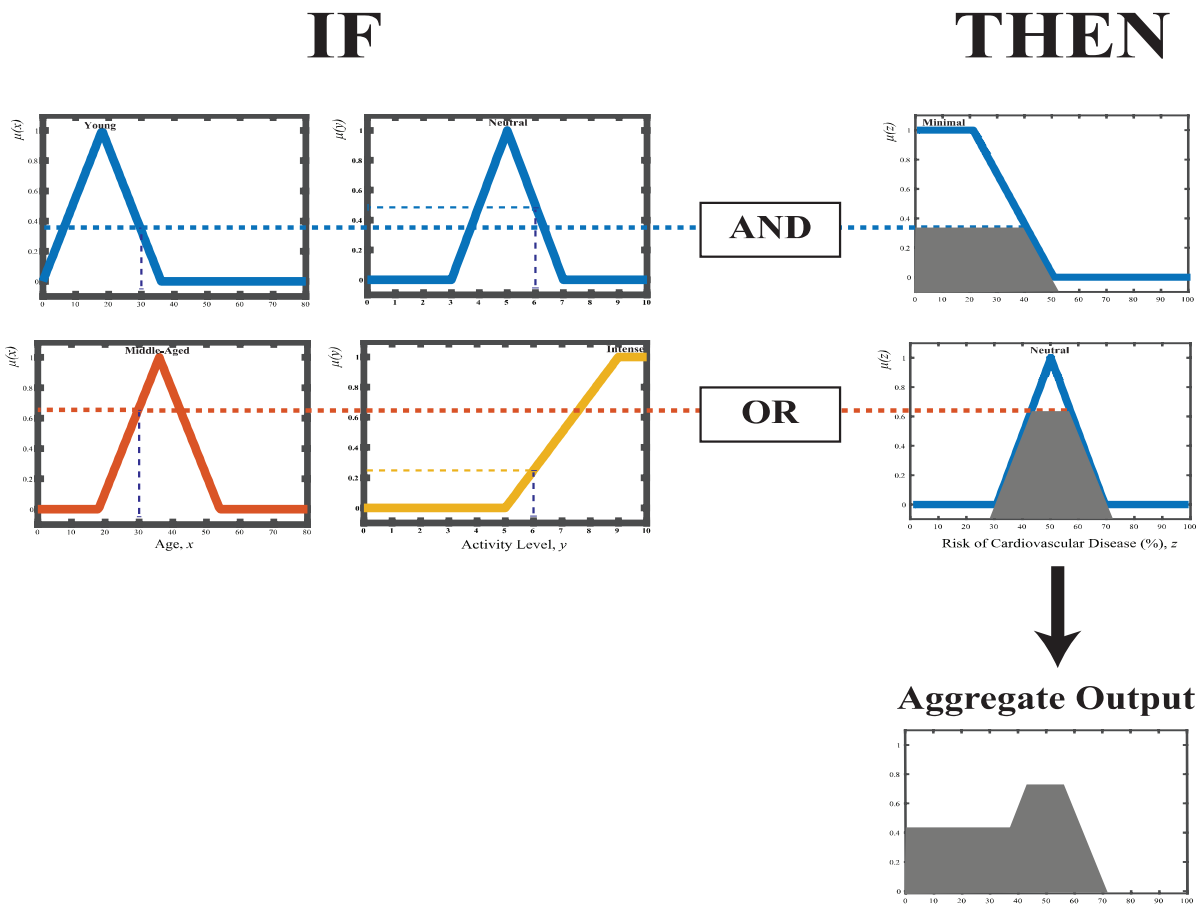


Figure 3.8: Aggregate output for risk of cardiovascular disease example.

Therefore, the following steps must be taken to establish a Mamdani-based fuzzy controller: (1) have a clear understanding of the system and its dynamics, (2) determine input and output variables, (3) create membership functions to represent the inputs and outputs of the system, (4) set up the user defined IF-THEN rules, and (5) decide the method of defuzzification that best suits the needs of the system in question.

3.4 Examples of Modeling With Fuzzy Logic

As mentioned in Chapter 1, fuzzy logic controllers can be found in many household items. These include, but are not limited to, washing machines, toaster ovens, rice cookers, Sony pocket computers, vacuum cleaners, etc. Appendices B and C go over examples to give a better understanding on how fuzzy logic controllers are designed. In addition, Appendix C gives a well-rounded overview on how different defuzzification methods are used. This Appendix gives analytical solutions for the centroid, weighted average, and the mean max methods of defuzzification while comparing them to MATLAB simulated results.

CHAPTER 4

FUZZY CONTROL RESPONSE TO DISTURBANCES: TESTS AND RESULTS

The previous chapter introduced the theory behind fuzzy logic. This chapter will go over the results gathered from the robustness testing of the fuzzy logic controller. The first section of this chapter will give a description of the fuzzy logic controller. The second section will explain the results of the internal disturbance testing. The third and final section of this chapter will discuss the controller response to the external disturbance testing.

As noted on Chapter 1, preceding work on the building by Joshua Baltazar showed that the fuzzy logic controller that included the most information about the building testbed system resulted in a controller that performed the best at keeping room temperatures close to their setpoints [62]–[64]. This work, however, will focus on examining the robustness of the controller by conducting a series of experiments to assess its ability to respond when internal and external disturbances are introduced to the control system. For the purposes of this work, internal disturbances are defined as a perturbation that is introduced into the system (i.e. the test building) whereas an external disturbance is defined as a perturbation that is introduced to the system from outside its boundaries (i.e. the external AC).

Three tests were done to examine the controller response to internal disturbances by (1) two sudden changes in setpoint temperature, (2) a sudden change and (3) two sudden changes in setpoint temperature while keeping different temperatures within each pair of rooms. Similarly, two tests were conducted to test controller response to external

disturbances. This was done by changing the temperature of the cold air delivered by the external AC unit twice during a 90 minute testing period while (1) setting one setpoint temperature for all rooms, and (2) setting individual setpoints for each pair of rooms. The results presented in this chapter have been presented and published in the 9th Thermal and Fluids Engineers Conference (TFEC) [73] and in the 9th European Thermal Sciences Conference [74].

4.1 Fuzzy Controller Description

For the thermal control of the building testbed, the key variables are the air flow rates, $\dot{\mathcal{V}}(t)$, and room temperatures, $T(t)$. Therefore these variables will be used to build membership functions to describe the dynamic state of the building testbed. Following Baltazar et al. [63, 64], the overall control system has eight single-input single-output (SISO) control loops, each illustrated in Figure 4.1. The control input from each fuzzy controller is the air flow rate $\dot{\mathcal{V}}(t)$, while the room air temperature $T(t)$, is the output.

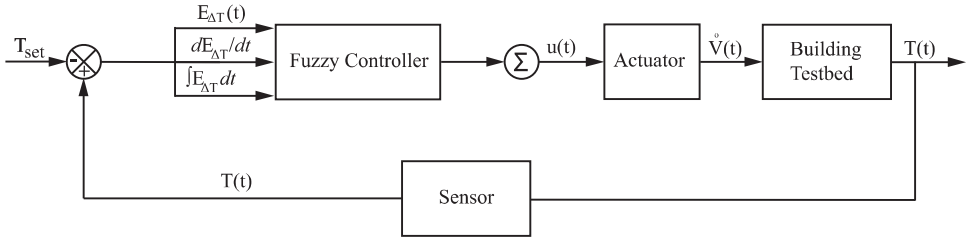


Figure 4.1: Closed-loop fuzzy control.

Following the work of Pacheco-Vega and Ruiz-Mercado et al. [75], all controllers are built with a linear combination of information about the error between an user defined setpoint, T_{set}, and the actual room temperatures, $T_a(t)$; i.e., $E_{\Delta T} = T_{set} - T_a(t)$, its difference over time $dE_{\Delta T}/dt$, and the integral of such error over a specified period of time, $\int E_{\Delta T} dt$.

The corresponding membership function and fuzzy sets for $E_{\Delta T}$ are shown in Figure 4.2. For $E_{\Delta T}$ the fuzzy sets has two trapezoidal and three triangular membership functions in the range [-10, 10]°C. Noting that, to help the reader view the dominant part of $E_{\Delta T}$, Figure 4.2 shows a truncated figure of the membership function range. The corresponding linguistic variables are represented as NL (Negative Large), NS (Negative Small), Z (Zero), PS (Positive Small), and PL (Positive Large).

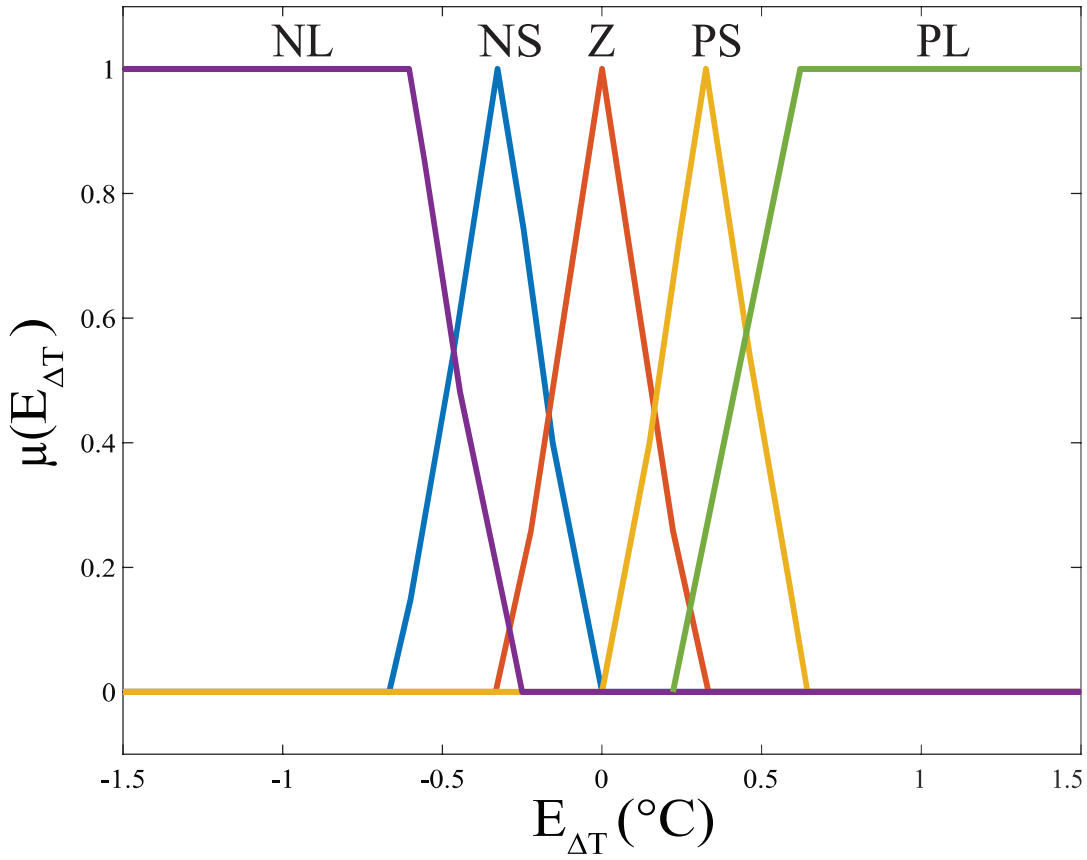


Figure 4.2: $E_{\Delta T}$

The membership function for $dE_{\Delta T}/dt$ is shown on Figure 4.3. In this case, the membership functions for $dE_{\Delta T}/dt$ are composed of 2 trapezoidal and one triangular membership functions in the range [-1.5, 1.5]°C/s. The corresponding linguistic variables are represented as N (Negative), Z (Zero), and P (Positive).

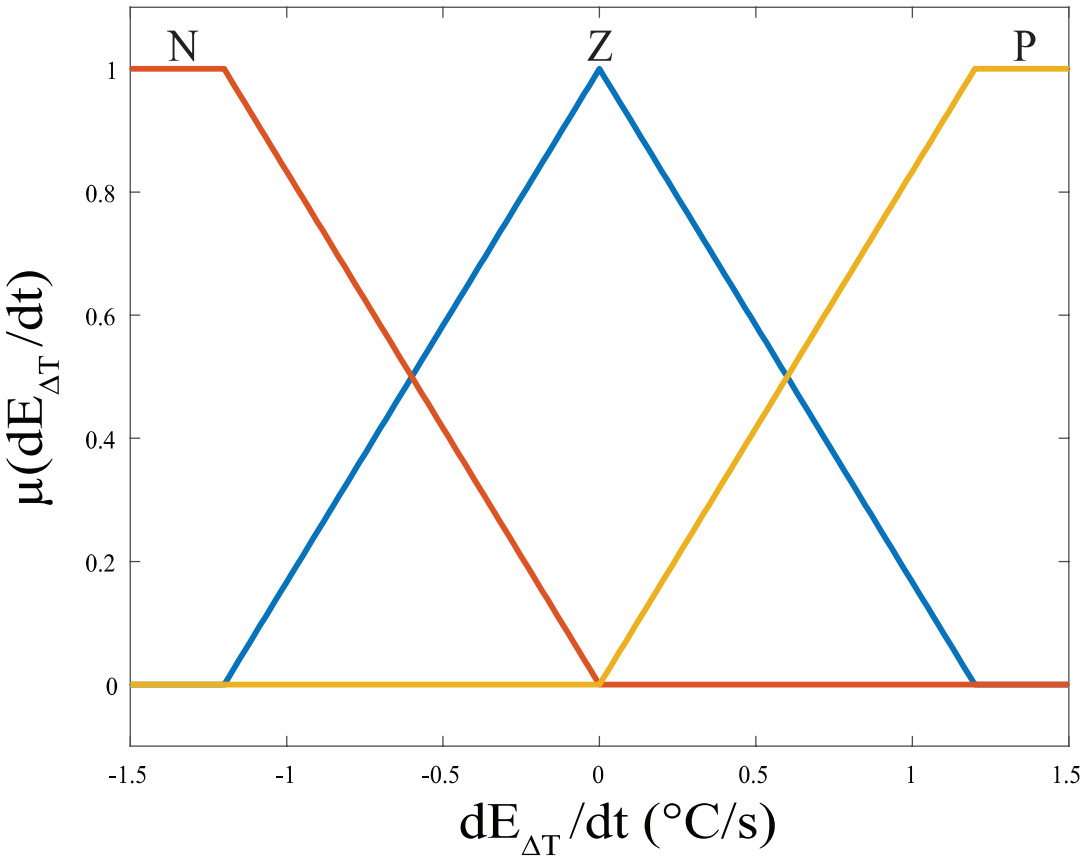


Figure 4.3: $dE_{\Delta T}/dt$

Finally, the fuzzy sets for $\int E_{\Delta T} dt$ are shown on Figure 4.4. The range for these functions was set to [-10,10]°C-s, and the linguistic variables are AN (Always Negative) and AP (Always Positive). The fuzzy sets for the output angle $\theta_{\Delta T}$ has 5 triangular membership functions in the range [0, 1.57] rad (where $\theta_{\Delta T} = 0$ rad defines a fully-closed damper and $\theta_{\Delta T} = 1.57$ rad defines a fully open damper).

The set of inference rules are shown in Tables 4.1 and 4.2 where, in accordance with Figure 4.2 - Figure 4.5, the values for the linguistic variable $E_{\Delta T}$, $dE_{\Delta T}/dt$, and $\int E_{\Delta T} dt$ are also written as 'NL', 'NS', 'Z', 'PS', 'PL', 'N', and 'P', with 'NR' representing a case where a rule was not applied. To defuzzify the outputs and generate a crisp value to the air flow actuators (dampers), the well-known Mamdani inference method [76] was used.

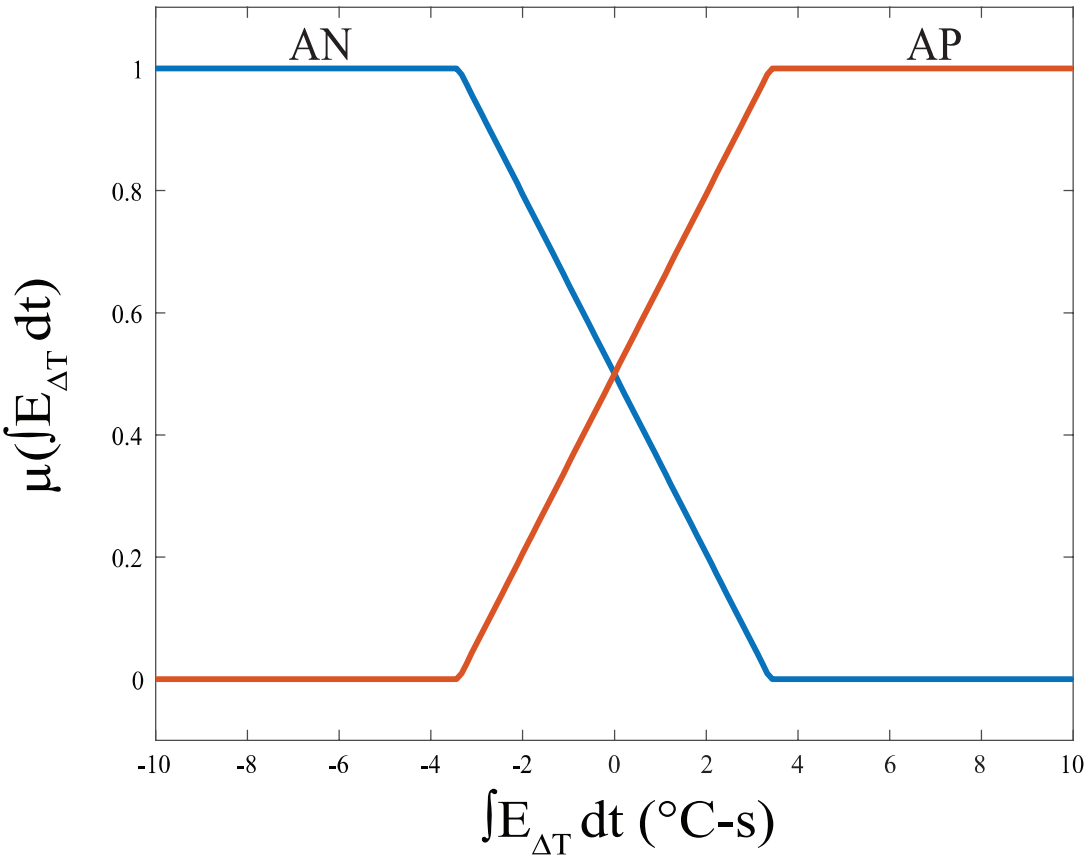


Figure 4.4: $\int E_{\Delta T} dt$

Table 4.1: Decision matrix 1 for $\theta_{\Delta T}$.

$\theta_{\Delta T}$ ↘		$E_{\Delta T}$				
		NL	NS	Z	PS	PL
$dE_{\Delta T}/dt$	N		VL	L		
	Z	VL	VL	L	L	VH
	P		M	H	H	
	NR	VL	L	M	H	VH

Table 4.2: Decision matrix 2 for $\theta_{\Delta T}$.

$\theta_{\Delta T}$ ↘		$\int E_{\Delta T} dt$	
		AN	AP
$dE_{\Delta T}/dt$	N	H	L
	P	L	H
$E_{\Delta T}$	NL	L	
	PS		VL

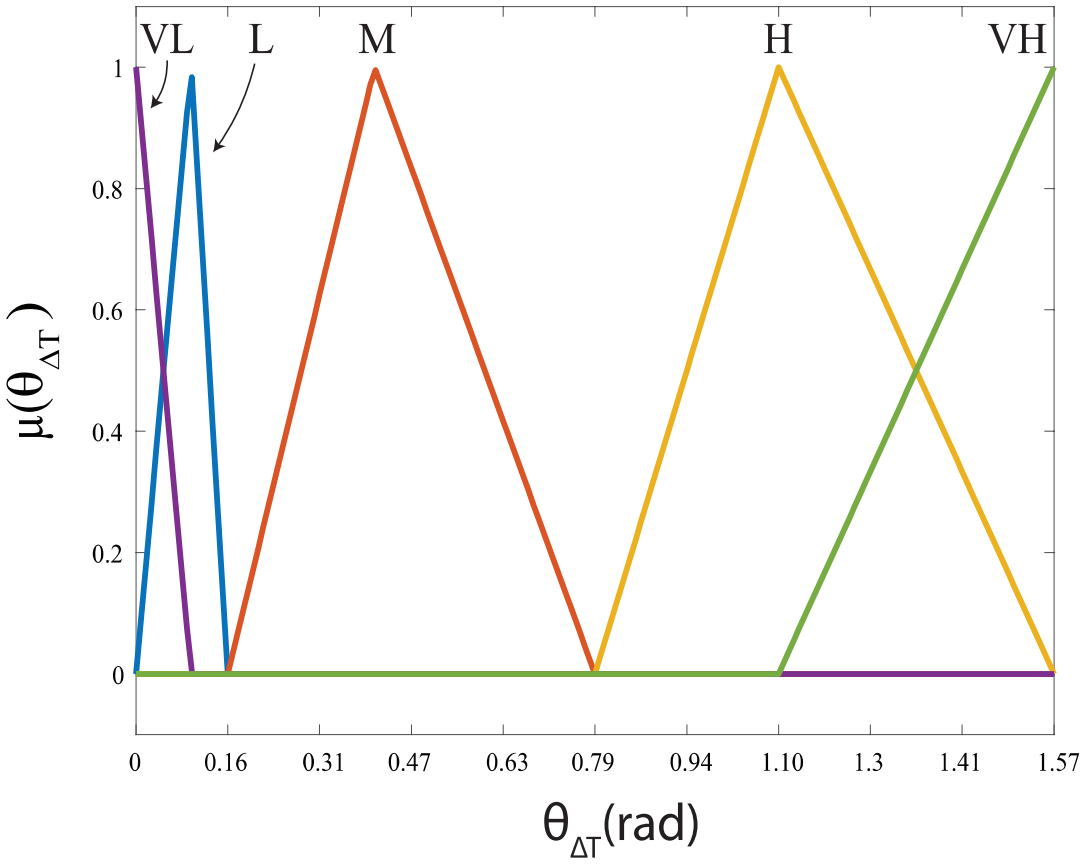


Figure 4.5: $\theta_{\Delta T}$

4.2 Results to Internal Disturbance

As previously mentioned, three comprehensive experiments where performed to assess controller robustness and response to internal disturbances. This included (1) three sudden changes in setpoint temperature, (2) one sudden change in temperature setpoint while keeping different temperature setpoints in any given pair of rooms, and (3) two sudden changes in setpoint temperature while keeping different temperatures within any given pair of rooms. The following tests were repeated five times, all with similar results. The HVAC air temperature shifts were observed throughout all tests and it was seen, through the damper position, that the controller responded appropriately by adjusting the damper angle accordingly.

The first experiment was conducted over a 110 minute time span, in which the controller was subjected to three consecutive sets of temperature setpoints for all rooms in the test-bed. The first set was fixed at $T_{set\ 1} = 23.3°C$ for the first 30 minutes, then changed to $T_{set\ 2} = 21.1°C$ from 30 to 60 minutes, and then changed to $T_{set\ 3} = 22.2°C$ from 60 to 110 minutes. The corresponding results from the experiment are shown in Figure 4.6. Figure 4.6(a) shows the history of room temperatures in response to the fuzzy controller, Figure 4.6(b) is the position of the damper, and Figure 4.6(c) is the temperature of the air supplied by the HVAC.

It is observed from Figure 4.6(a), that the controller was able to bring the temperature of all rooms to 23.3°C within a 6 minute time frame (from an initial value of 26.7°C), and then maintain them within 1°C of the setpoint for about 10 minutes. It is also noted that the temperatures of all the rooms were kept to within ±0.2°C of each other. At $t = 30$ minutes, the setpoint was decreased to $T_{set\ 2} = 21.1°C$, the controller was then able to successfully help the rooms reach temperatures within ±0.2°C of the setpoint and ±0.3°C of each other; this happened for most of the 30 minute period. Finally, at $t = 60$ min, the temperature setpoint was increased to $T_{set\ 3} = 22.2°C$. The response from the controller was to close all dampers an allow the light bulbs to increase the room temperatures, as seen on Figure 4.6(b). This process took 10 minutes due to the relatively-low power of the light bulbs used. It is seen that for the remainder of the test, the fuzzy controller was able to maintain the room temperatures within 0.3°C of the setpoint and roughly within ±0.3°C of each other.

It is to note that, though the fuzzy controller was able to reach and maintain the rooms at different setpoints, there was some variability in the values and trends of room

temperatures. For instance, from Figure 4.6(a), one can see that:

(1) around the 16-minute mark, a small but gradual decline in air temperature below the setpoint, by about 0.3°C for seven rooms, and 0.5°C for Bottom Room 1, occurred;

(2) at $t = 36$ min, a slight temperature increase which was followed by a larger one at $t = 54$ min arose before the controller attempted to reach the new setpoint;

(3) a small decrease in temperature, with maximum temperature change of 0.5°C at $t = 90$ min, followed by a small increase of 0.2°C at $t = 103$ min, were present before the experiment was concluded.

These trends seem to be in line with the changes in the temperature of the cold air supplied by the HVAC, which is shown on Figure 4.6(c). For instance, in agreement with the results above, (1) the downward slope of the cold air in Figure 4.6(c) is proportional to the gradual decline in room temperature during the first 30 minutes of the experiment. This change in cold-air includes a 17°C drop in air temperature, which the fuzzy controller attempted to manage by adjusting the angle of the dampers as seen on Figure 4.6(b). The increases in room temperature at $t = 35$ minutes and $t = 53$ minutes are reflected in the corresponding increase in cold air temperature supplied by the HVAC, which again are much larger (close to 15°C) than those of the room temperatures in the building testbed. From Figure 4.6(b), it is seen that the controller promptly responded to the disturbance by opening the damper for Bottom Room 3; the room most effected by this temperature change.

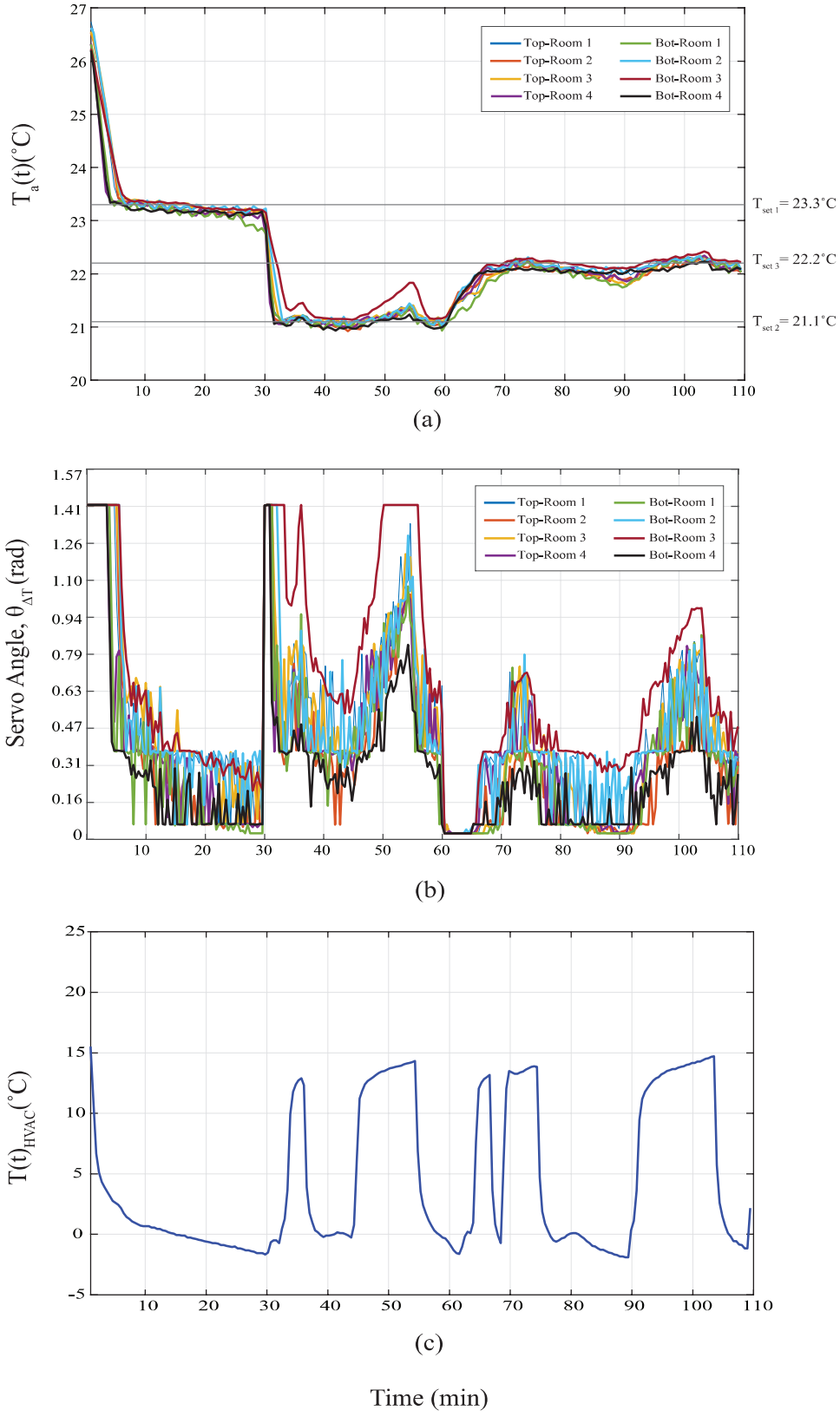


Figure 4.6: Results for Internal Disturbance Test 1.

The second internal disturbance experiment was conducted over a period of 60 minutes, where setpoint temperatures within the range of 22.2°C to 23.9°C were employed. For $t \in [0, 30]$ minutes, Top Room 1 and 2 were set to 23.9°C, Top Room 3 and 4 were set to 23.3°C, Bottom Room 1 and 2 were set to 22.8°C, and both Bottom Room 3 and 4 were set to 22.2°C. The controller was programmed to change the setpoints at $t = 30$ minutes, with Top Room 3 and Bottom Room 1 changed to 23.9°C, Top Room 2 and Bottom Room 3 changed to 23.3°C, Top Room 1 and Bottom Room 4 changed to 22.8°C, and both Top Room 4 and Bottom Room 2 changed to 22.2°C. The corresponding results are presented on Figure 4.7. Figure 4.7(a) illustrates the history of room temperatures in response to the controller, Figure 4.7(b) shows the damper position, and Figure 4.7(c) shows the temperature trend of the cold air supplied by the HVAC. Figure 4.7(a) shows that the controller successfully achieved the desired room temperatures, reaching their respective setpoints within 5 min (from an initial value of 26.7°C) and was able to maintain them within ±0.3°C from their respective setpoints. This figure also shows that each pair of rooms was kept within 0 to 0.2°C of each other.

Once the setpoints changed at $t = 30$ minutes, it took about 2 minutes for the rooms to reach their new temperatures (Bottom Room 1 being the exception as it took 10 min for an increase of 1.1°C). Figure 4.7 shows spikes in temperature for Top Room 4, and Bottom Room 2 of +0.2°C at $t = 40$ min and of +0.3°C at $t = 54$ minutes. These spikes correlate with the changes in temperature from the cold air supply delivered from the HVAC (Figure 4.7(c)). The controller opens the damper in an attempt to bring the temperatures in the rooms back down to their setpoint of 22.2°C, Figure 4.7(b). The air temperature from the AC, however, is not cold enough and it is seen that the

temperatures do not go back down to their setpoints until the air delivered from the AC decreases again.

The similarities between the room and HVAC air temperatures become quite evident when comparing Figures 4.7(a) and 4.7(c). For instance, the temperature decreases in room temperatures at $t = 14$, 33, 45, and 58 min all agree with the dips in temperature presented in Figure 4.7(c). For these cases, the controller took immediate action and either opened or closed the dampers, leading to either an increase or decrease in the air-flow until the setpoint temperatures were met, as seen from Figure 4.7(b).

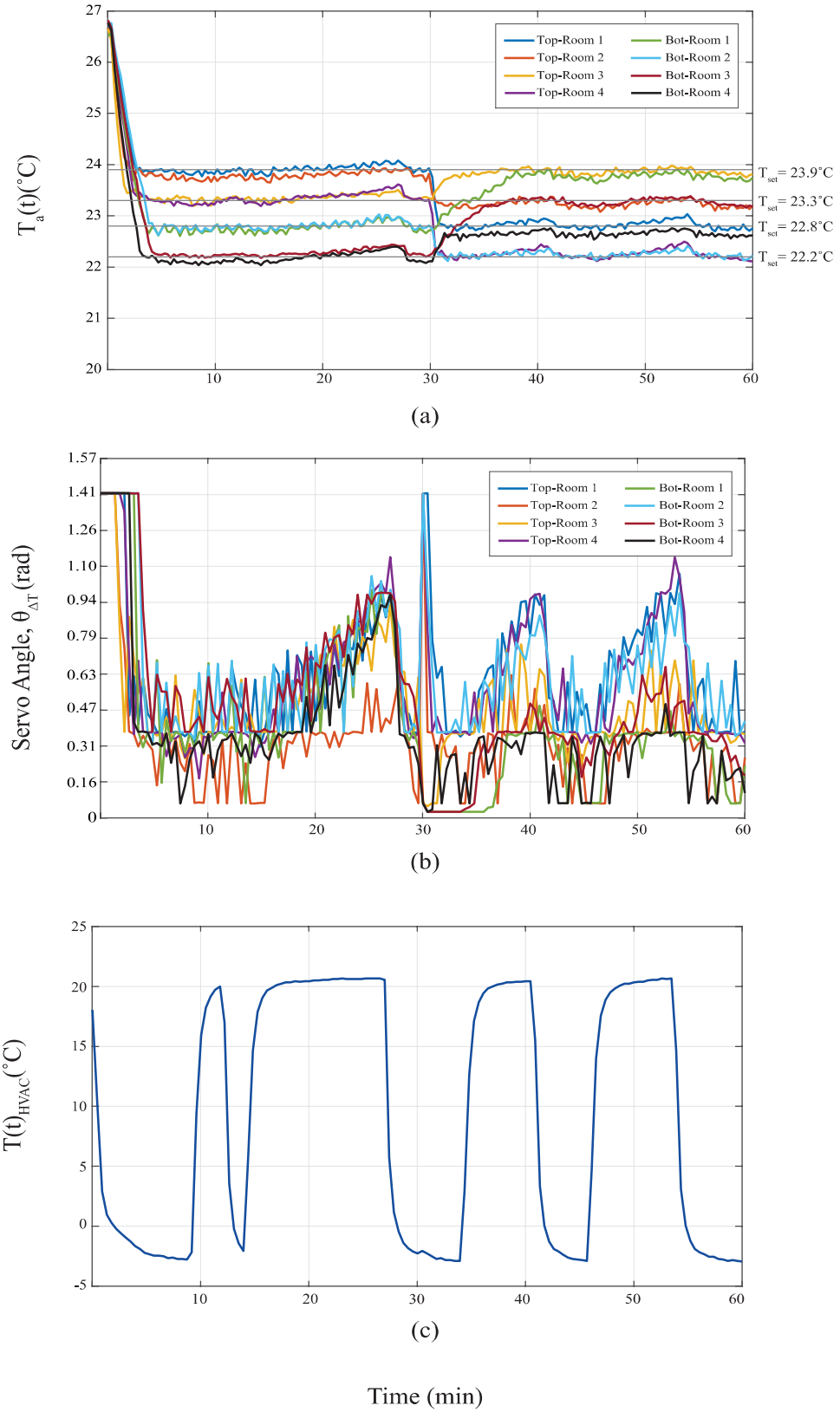


Figure 4.7: Results for Internal Disturbance Test 2.

The third test was conducted over a period of 90 minutes, this time the number of setpoint changes was increased to three. The temperatures utilized in the second test (Figure 4.7(a)) experiment were used for the period of $t \in$[0, 60] minutes. The setpoints for $t \in$[60, 90] minutes were set as follows: Top Room 4 and Bottom Room 2 were set to 23.9°C, Top Room 3 and Bottom Room 4 were set to 23.3°C, Top Room 2 and Bottom Room 1 were set to 22.8°C, and both Top Room 1 and Bottom Room 3 were set to 22.2°C. The corresponding results are shown in Figure 4.8, with the time evolution of room temperatures illustrated in Figure 4.8(a), Figure 4.8(b) shows the damper position, and the temperature of the cold air supply from the HVAC is shown in Figure 4.8(c).

It is seen that it took about 4 minutes for all rooms to reach their setpoints, with the temperatures for each pair of rooms being kept within ±0.2°C of each other. From here it is apparent that the controller was capable of keeping the room temperatures close to the setpoints, the exception being the two major drops of -0.4°C for Top Room 2 at $t = 47.7$ min and of -0.5°C for Bottom Room 1 at $T_{set} = 22.9$°C. During that time period, the controller had no trouble in keeping the temperatures of Bottom Room 1 and Top Room 4 close to their $T_{set} = 22.2$°C, indicating that the light bulbs struggled to provide enough heat to keep the corresponding rooms at $T_{set} = 23.9$°C. As shown in Figure 4.8(b), the controller corrected for this by shutting the dampers in those rooms, which allowed the rooms to increase in temperature and reach 23.9°C.

During the time interval of $t \in$[60, 90] minutes, it is observed that the controller managed to keep the temperatures close to their respective setpoints. As expected, it took longer for Top Room 4 and Bottom Room 2 to reach $T_{set} = 23.9$°C from a temperature of 22.2°C. Likewise, a temperature undershoot is seen for both Top Room 2 and Bottom

Room 1 at $t = 70$ minutes (which parallels the drop in temperature of the HVAC air supply Figure 4.8(c)). The controller acted accordingly by slightly closing the dampers to these rooms, thus allowing their temperatures to increase and reach $T_{set} = 22.8°C$. As previously discussed, from Figures 4.8(a) and 4.8(c) it is easy to see that there is a link between the temperatures in the rooms and the cold air delivered by the HVAC. The temperature decreases in the room temperatures on Figure 4.8(a) agree with the sudden drops seen on Figure 4.8(c) at $t = 17$, 47, 70, and at 90 minutes. When comparing Figure 4.8(a), Figure 4.8(b), and Figure 4.8(c), it is clear that the controller opens and closes the dampers in respect to the HVAC air temperature and the temperature setpoint. The damper angle mirrors the HVAC air temperature trend. The controller opens the dampers when the HVAC air temperature rises, and begins to close them as the air temperature decreases.

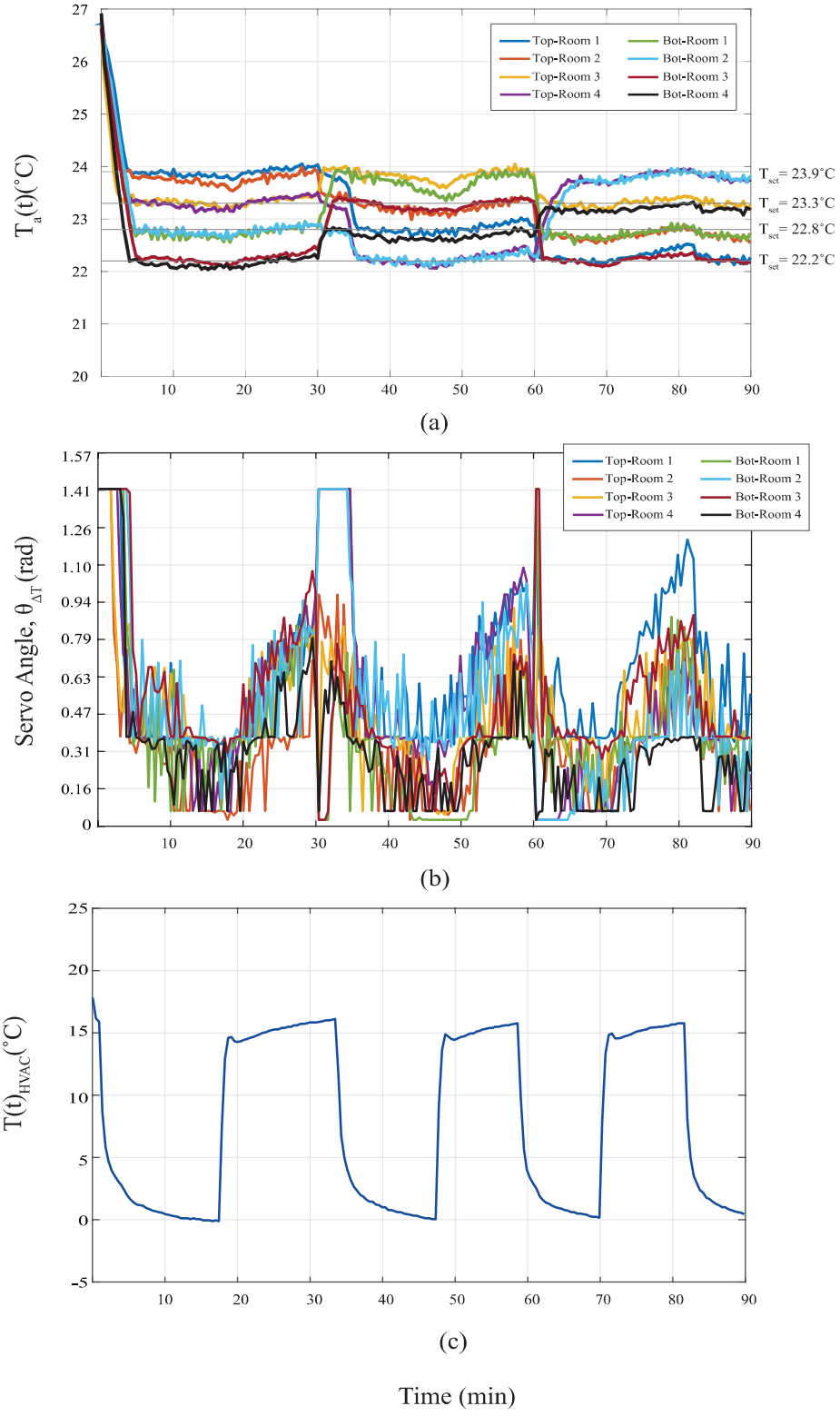


Figure 4.8: Results for Internal Disturbance Test 3.

4.3 Response to External Disturbance

Aside from assessing the ability of the controller to reject internal disturbances, it is just as important to determine its handle of external disturbances. In such case, when examining full-scaled buildings, this may take the form of climate changes, unforeseen thermal loading changes due to an influx or outflow of visitors, and changes in inhabitant area temperatures due to an increase in use of electrical appliances. Therefore, two tests where done to simulate the increase and decrease of temperature variances due to external disturbances. The first of these tests involved multiple changes in HVAC temperature setpoints while keeping (1) an uniform setpoint temperature across all rooms, and (2) differentiating temperatures across any pair of rooms in the building. As it was the case with the internal disturbance tests, the following tests were conducted numerous times. All of the tests gave similar results and the HVAC air temperature fluctuations where observed throughout all tests.

The first of the external disturbance tests was conducted over a period of 90 minutes. Figure 4.9 shows the results for the first external test, with Figure 4.9(a) presenting the room temperatures, Figure 4.9(b) shows the damper position, and Figure 4.9(c) shows the temperature of the air delivered by the HVAC. During this time frame, the setpoint temperatures in all eight rooms were kept at $T_{set} = 23.3°C$. The outflow HVAC temperature was set to 18.9°C for the first 30 minutes of testing, it was then changed to 18.3°C within the period of $t \in [30, 60]$ minutes, and finally it was changed to 19.4°C for the remainder of the test. It took about 3 minutes for all the rooms to reach the setpoint temperature. The rooms experienced a slight under-damping at t= 3.5 minutes, which

was followed by a small increase in temperature until the rooms reached the setpoint. As seen from Figure 4.9(b), the controller immediately corrected for this by briefly closing the dampers. At t = 15.8 minutes, the temperatures in the rooms dropped by 0.3 degrees uniformly before rising again from $t \in$[15.8, 30] minutes.

From times $t \in$[30, 60] minutes, it is seen that the temperatures across all rooms experienced significant decreases in response to the manual decrease in AC temperature. It is seen that the controller attempted to correct for this by closing the dampers. The exception being that of Bottom Room 2, where it is seen that the damper for this room opens and closes. This may be an indication that both Bottom Room 2 receives a lower amount of airflow than what Top Room 2 and Bottom Room 1 receive. As expected, it took Top Room 2 and Top Room 3 considerably longer to increase in temperature and reach T_{set} = 23.3°C. From here, we see that the controller was able to keep the temperatures within the rooms about ±0.1°C from the set point.

It is seen that from 60 to 90 minutes, the rooms in the building heat in accordance with the deliberate AC temperature change. Figure 4.9(b) shows that the dampers open accordingly. The air temperature delivered by the HVAC is heating, therefore the controller opened the dampers to allow more air into the rooms to bring their temperature to the setpoint. However, since the being delivered by the HVAC was warm, the controller continued to open the dampers wider. The test only lasted for 90 minutes, therefore it is speculated that the controller would have of continued to open the dampers in an attempt to decrease the temperature in the rooms.

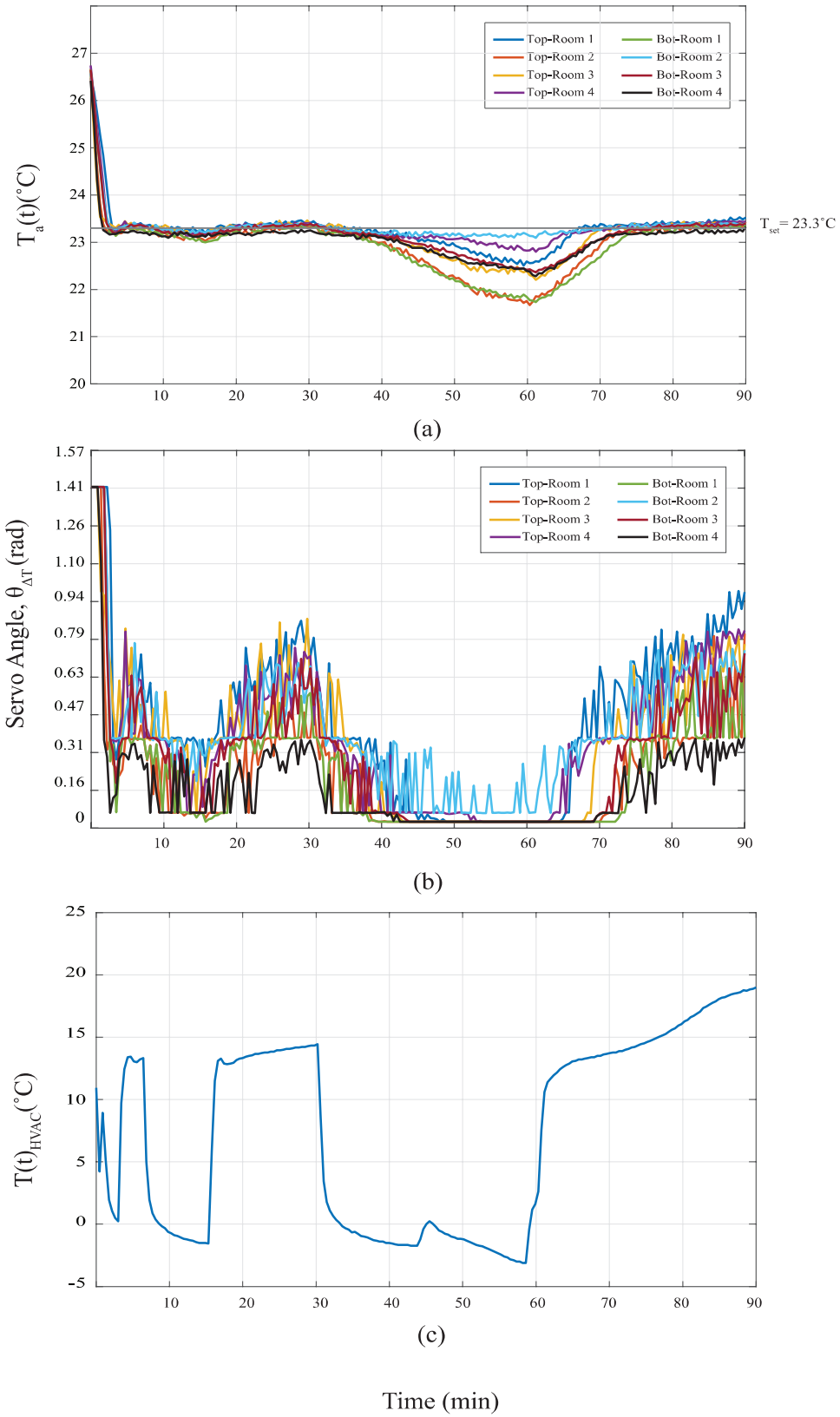


Figure 4.9: Results for External Disturbance Test 1.

The second external disturbance test was run for a period of 90 minutes. The setpoint temperatures were set within the range of 22.2°C to 23.9°C. With Top Room 1 and 2 set to 23.9°C, Top Room 3 and 4 were set to 23.3°C, Bottom Room 1 and 2 set to 22.8°C, and both Bottom Room 3 and 4 set to 22.2°C. As with external disturbance Test 1, the HVAC air temperature was set to 18.9°C for the first 30 minutes, it was then changed to 18.3°C for $t \in$[30, 60] minutes, and then set to 19.4°C for the remainder of the test. Figure 4.10 shows the results for this test, with Figure 4.10(a) displaying the temperatures in the rooms, Figure 4.10(b) presents the damper position, and Figure 4.10(c) shows the air temperature delivered by the external HVAC.

From Figure 4.10(a) it is seen that the rooms in the building were able to reach their setpoint temperatures within 5 minutes of the test start time. The room temperatures begin to drop when the HVAC air temperature is set to 18.3°C, this is especially evident for Top Rooms 1 - 4 and for Bottom Rooms 1 and 3. As with the first external disturbance test, the temperature drop in Bottom Room 2 was not as severe. This, again, may be due to an uneven air distribution across the rooms. Figure 4.10(b) shows that the damper corresponding to Bottom Room 2 was was being opened and closed by the controller. This means that the air temperature within that room was close enough to its setpoint that the controller was trying to maintain that temperature. Bottom Rooms 3 and 4 did not experience an extreme drop in temperature like the rest of the rooms. This suggests that T_{set} = 22.2°C is within the control limits of FLC3 at an HVAC air temperature of 18.83°C.

From Figure 4.10 we see the temperatures in the rooms increased once the HVAC air outflow temperature was increased to 19.4°C. It is apparent that it took Top Room

2 twice as long than Top Room 1 to heat up enough to reach its setpoint and when examined closely it is noted that at t = 60 minutes, Top Room 2 was -1.7 degrees away from T_{set} = 23.9°C whereas Top Room 1 was -1.0°C away. In addition, it is observed that from $t \in$[60, 90] minutes the temperatures across all rooms rose linearly, and thus it is hypothesized that the temperatures would have kept increasing if the test would have been allowed to run longer. As with the previous tests, the HVAC air temperature shown in Figure 4.10(c) agrees with that of the room temperature plot illustrated on Figure 4.10(a). The external disturbance of the HVAC unit, however, does not impede this controller from correcting for the temperature variances experienced in each room.

As with the previous tests, the damper angle follows the same trend as the air temperature delivered by the HVAC. At the start of the test, the dampers are opened momentarily before the controller partially closes the dampers for the rooms with the higher setpoint temperatures. Looking at Figure 4.10(b), it is important to note that for the paired rooms Bottom Room 3 and Bottom Room 4, the controller opens the damper wider for Bottom Room 3 than it does for Bottom Room 4. This may indicate that Bottom Room 3 and Bottom Room 4 do not receive the same amount of airflow. This behavior is also reflected on both the damper positions for Top Room 1 and Top Room 2. It is seen that for these pair of rooms, the controller opens the damper wider for Bottom Room 2 than for Top Room 3.

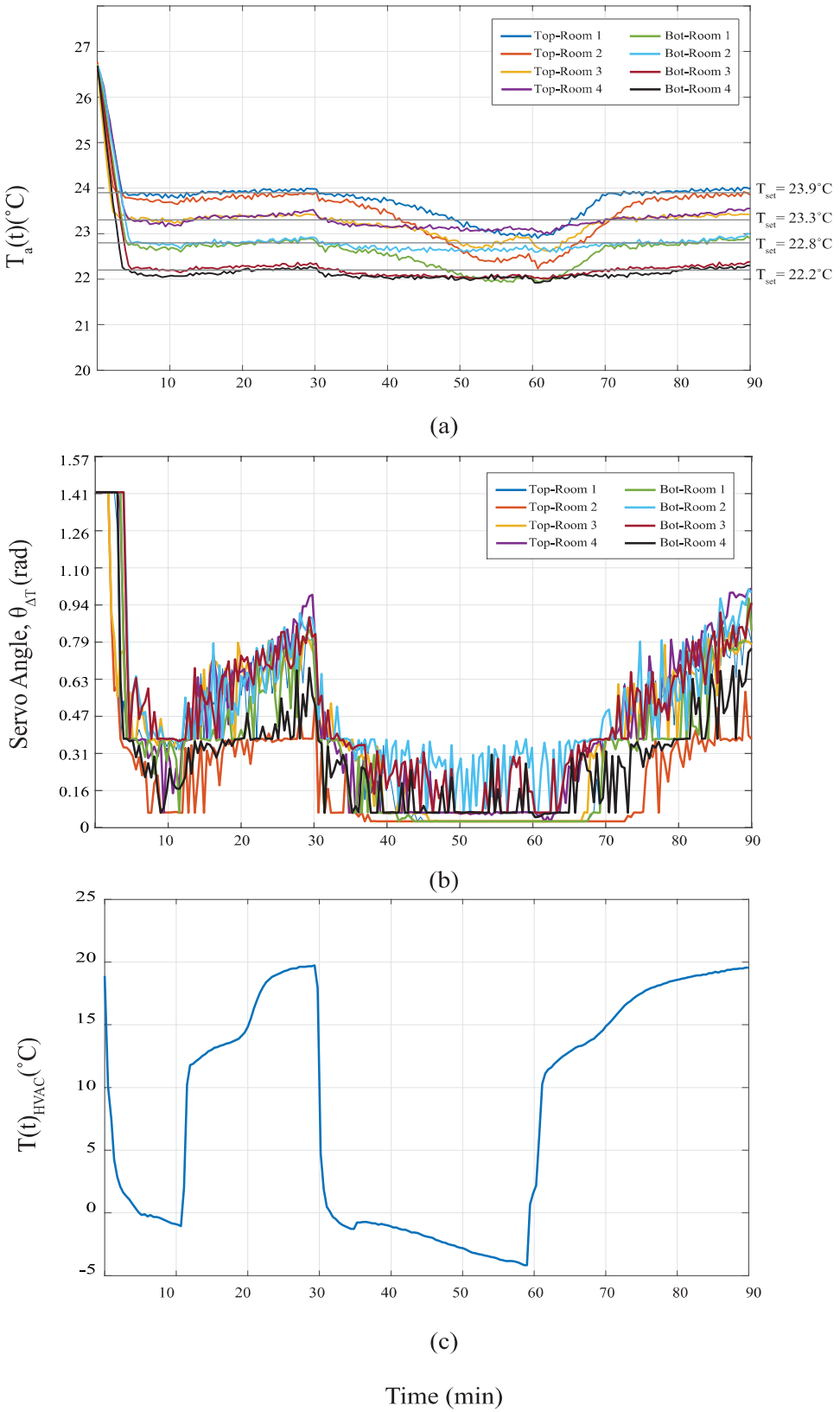


Figure 4.10: Results for External Disturbance Test 2.

CHAPTER 5

CONCLUSIONS AND FUTURE WORK

5.1 Conclusion

Temperature control of multi-room commercial and residential buildings is essential to ensure thermal comfort of occupants and to reduce energy usage. However, control laws commonly used lack robustness and therefore may not be suitable strategies for thermal control in buildings. In previous work [63, 64], it has been demonstrated that controllers based on fuzzy logic are a viable alternative because of their reliance on information from human experience and knowledge of system operation. In this work, the idea has been expanded to test the robustness of a fuzzy controller that is built with information about room temperature error, its derivative and its integral, and assessed its ability to deal with internal and external disturbances.

The results from these tests showed that the fuzzy controller is very robust as it was able to maintain the temperatures in the rooms very close to the corresponding setpoints, despite changes in the setpoints and changes in the temperature of the air supply. However, details in the trends in room temperature clearly show that the external HVAC unit places a crucial role in the control process of the building testbed. These tests show that the HVAC supply air temperature to be oscillatory in nature and provides additional external disturbances to both test types listed on this document. The HVAC air temperature behavior was unaccounted for during the development of this controller. However, even under these extreme conditions, the results demonstrate that the fuzzy controller is able to regulate the temperature of all rooms.

5.2 Future Work

Although these results have proven that the fuzzy logic controller is able to respond accordingly to internal and external disturbances, there are a few important aspects of this system that have yet to be explored.

(1) It has been proven in this work and in [63, 64] that this fuzzy logic controller is robust and able to maintain temperature setpoints within the multi-room building test-bed while being subjected to internal and external disturbances. Now that this has been established, it is important to compare electrical energy consumption of this fuzzy controller with that of a controller that uses an industry "approved" control methodology, such as PID. By performing an energy consumption analysis we can get a better idea of the potential energy savings that fuzzy controllers have when utilized in building HVAC systems.

(2) As is, the building is subjected to additional external instabilities, such as the temperature within the laboratory. The temperature within the laboratory changes with the season and therefore adds an additional challenge when running tests. This makes it so that the external HVAC unit acts on its own, as it has its own internal thermocouple, and either increases or decreases the output air temperature without prompt. In this case, the building and external HVAC system would need to be enclosed to isolate them from the surrounding environment. By doing this, the building surroundings can be controlled and therefore can be made to depict different climates; such as sunny and windy.

(3) As mentioned in the results section, the air delivered to these rooms is not evenly

distributed among the whole building. To begin, it has to be confirmed whether the pressure sensors are calibrated correctly. The pressure sensors used in this system were purchased through the Sensirion website and are named Sensirion SDP816-500Pa Analog. They have a linear configuration with a voltage to differential pressure relationship of [77]:

$$DP = \frac{750 \times A_{out}}{V} - 150$$

where DP refers to the differential pressure, A_{out} is the AC Arduino voltage, and V is the Arduino pin voltage.

(4) Implement an on-off controller to release some of the stagnated air out. The current duct design allows for air to stagnate between the AC outlet and the closed dampers, it would be beneficial to implement valves that would open when the dampers are closed, thus allowing some of that trapped cold air to escape.

REFERENCES

[1] F.C. McQuiston, J.D. Parker, and J.D. Spitler. *Heating, Ventilation, and Air Conditioning Analysis and Design, 6th Ed.* Wiley and Sons, Danvers, MA, 2005.

[2] R.U.Ayres. *Technological transformations and long waves.* International Institue for Applied Systems Analysis, Vienna, Austria, 1989.

[3] G. Clark and D. Jacks. Coal and the industrial revolution, 1700-1869. *European Review of Economic History*, 11:39–72, 2007.

[4] M.R. Allena, D.J. Frame, C. Hintingford, C.D. Joneas, J.A. Lowe, M. Meinshausen, and N. Meinshausen. Warming caused bu cumulative carbon emissions towards the trilionth tonne. *Nature*, 458:1163–1166, 2009.

[5] R. Sathre. Comparing the heat of combustion of fossil fuels to the heat accumulated by their lifecycle greenhouse gases. *Fuel*, 115:674–677, 2014.

[6] K.H. Kim, E. Kabir, and S.A. Jahan. A review of the consequences of global climate change on human health. *Journal of Environmental Science and Health, Part C: Environmental Carcinogenesis and Ecotoxicology Reviews*, 32:299–318, 2014.

[7] A.J. McMichael. Globalization, climate change, and human health. *The New England Journal of Medicine*, 368:1335–1343, 2013.

[8] F. Perera and K. Nadeau. Climate change, fossil-fuel pollution, and Children's health. *The New England Journal of Medicine*, 386:2303–2314, 2022.

[9] G. Naumann, S. Russo, G. Formetta, D. Ibarreta, G. Forzieri, M. Girardello, and L. Feyen. Global warming and human impacts of heat and cold extremes in the eu, 2020.

[10] M. Pawan. Impact of global warming on environment. *International Research Journal of Environment Sciences*, 3:72–78, 2014.

[11] J.M. Pandolfi, S.R. Connolly, D.J. Marshall, and A.L. Cohen. Projecting coral reef futures under global warming and ocean acidification. *Science*, 333:418–422, 2011.

[12] T.P. Hughes, J.T. Kerry, Andrew H. Baird, S.R. Connolly, A. Dietzel, C.M. Eakin, S.F. Heron, S.F. Heron, A.S. Hoey, M.O. Hoogenboom, G. Liu, M.J. McWilliam, R. J. Pears, M.S. Pratchett, W.J. Skirving, J.S. Stella, G. Torda, and G. Torda. Global warming transforms coral reef assemblages. *Nature*, 556:492–496, 2018.

[13] N.P. Singh, B. Anand, and S. Singh. Impact of climate change on agriculture in India: Assessment for agro-climatic zones, 2020.

[14] D.De Wrachien and M.B. Goli. Global warming effects on irrigation development and crop production:A world-wide view. *SciRes*, 6:734–747, 2015.

[15] U.S. Energy Information Administration. International energy outlook 2016, 2016.

[16] M. Gonzalez Torres, L. Perez-Lombard, J.F. Coronel, and I. Rodriguez Maestre. A review on buildings energy information: Trends, end-uses, fuels and drivers. *Energy Reports*, 8:626–637, 2022.

[17] U.S. Energy Information Administration. International energy outlook 2016. `https://www.eia.gov/outlooks/ieo/pdf/0484(2016).pdf`, 2016.

[18] Y. Li and Z. O'Neill. A critical review of fault modeling of HVAC systems in buildings. *Building Simulation*, 11:953–975, 2018.

[19] A. Vedavarz, S. Kumar, and M.I. Hussain. *Handbook of heating, ventilation and air conditioning for design and implementation.* Industrial Press Inc., New York, NY, USA, 2007.

[20] Z. Afroz, G.M. Shafiullah, T. Urmee, and G. Higgins. Modeling techniques used in building HVAC control systems: A review. *Renewable and Sustainable Energy Reviews*, 83:64–84, 2018.

[21] I. De Jaeger, G. Reynders, Y. Ma, and D. Saelens. Impact of building geometry description within district energy simulations. *Energy*, 158:1060–1069, 2018.

[22] K.W. Roth, D. Westphalen, P. Llana, and M. Feng. The energy impact of faults in U.S. commercial buildings. In *International Refrigeration and Air Conditioning Conference*, West Lafayette, IN, USA, 2004.

[23] K. Wan, D. Li, W. Pan, and J. Lam. Impact of climate change on building energy use in different climate zones and mitigation and adaptation implications. *Applied Energy*, 97:274–282, 2012.

[24] A. Bejan. *Conduction Heat Transfer, 4th Ed.* Wiley and Sons, Hoboken, New Jersey, 2013.

[25] Y.G.Wang, Z.G. Shi, and W.J. Cai. PID autotuner and its application in HVAC systems. In *2001 American Control Conference*, pages 2192–2196, Arlington, VA, USA, 2001.

[26] D.P. Atherton and S. Majhi. Limitations of PID controllers. In *1999 American Control Conference*, pages 3843–3847, San Diego, CA, USA, 1999.

[27] S.W. Sung and I.B. Lee. Limitations and countermeasures of PID controllers. *Industrial & Engineering Chemistry R esearch*, 35(8):2596–2610, 1996.

[28] A. Afram and F. Janabi-Sharifi. Theory and applications of HVAC control systems– A review of model predictive control (MPC). *Building and Environment*, 72:343–355, 2014.

[29] J. Wu, X. Li, Y. Lin, Y. Yan, and J. Tu. A PMV-based HVAC control strategy for office rooms subjected to solar radiation. *Building and Environment*, 177:106863, 2020.

[30] T. Wei, Y. Wang, and Q. Zhu. Deep reinforcement learning for building hvac control. In *54th IEEE Annual Design Automation Conference 2017*, pages 1–6, Austin, TX, USA, 2017.

[31] D.F. Espejel-Blanco, J.A. Hoyo-Montano, J. Arau, G. Valencia-Palomo, A. Garcia-Barrientos, H.R. Hernandez-De-Leon, and J.L. Camas-Anzueto. HVAC control system using predicted mean vote index for energy savings in buildings. *Buildings*, 12(1):38, 2022.

[32] M. Palonen, A. Hasan, and K. Siren. A genetic algorithm for optimization of building envelope and HVAC system parameters. pages 159–166, Glascow, Scotland, 2009.

[33] H. Pombeiro, M.J. Machado, and C. Silva. Dynamic programming and genetic algorithms to control an HVAC system: Maximizing thermal comfort and minimizing cost with PV production and storage. *Sustainable Cities and Society*, 34:228–238, 2017.

[34] Y. Ma, F. Borrelli, B. Hencey, B.E. Coffey, S. Bengea, and P. Haves. Model predictive control for the operation of building cooling systems. *IEEE Transactions on Control Systems Technology*, (3):796–803, 2012.

[35] H. Agharazy, M.D. Pricia, and K.A. Loparo. A Two-Level model predictive Control-Based approach for building energy management including photovoltaics, energy storage, solar forecasting and building loads. *Energies*, 15:3521, 2022.

[36] J. Arroyo, C. Manna, F. Spessens, and L. Helsen. Reinforced model predictive control (RL-MPC) for building energy management. *Applied Energy*, 309:118346, 2022.

[37] J. Singh, N. Singh, and J.K. Sharma. Fuzzy modeling and control of HVAC systema - A review. *Journal of Scientific & Industrial Research*, 65:470–476, 2006.

[38] A.H. Attia, S.F. Rezeka, and A.M. Saleh. Fuzzy logic control of air-conditioning system in residential buildings. *Alexandria Engineering Journal*, 36:1–9, 2015.

[39] M. Killian, B. Mayer, and M. Kozek. Hierachical fuzzy MPC concept for building heating control. *IFAC Proceedings Volumes*, 47(3):12048–12055, 2014.

[40] N.U. Ahamed, Z.B. Taha, I.B.M. Khairuddin, M.F. Rabbi, S.A.M.M. Rahaman, and K. Sundaraj. Fuzzy logic controller design for intelligent Air-Conditioning system. In *2nd IEEE International Conference on Control Science and Systems Engineering*, Singapore.

[41] Y.H. Yau and B.T. Chew. A review on predicted mean vote and adaptive thermal comfort models. *Building Services Engineering Research and Technology*, 35(1):23–35, 2012.

[42] N. Nassif. Modeling and optimization of HVAC systems using artificial neural network and genetic algorithm. *Building Simulation*, 7:237–245, 2014.

[43] M.H. Marhaban M.A.M. Radzi F. Behrooz, N. Mariun and A.R. Ramli. Review of control techniques for HVAC sytems-nonlinearity approaches based on cognitive maps. *Energies*, 11:495, 2018.

[44] M. Molinari G. Pattarello L. Fabietti A. Parisio, D. Varagnolo and K. H. Johansson. Implementation of a scenerio-based MPC for HVAC systems: An experimental case study. In *The International Federation of Automatic Control*, pages 599–605, Cape Town, South Africa, 2014.

[45] Y. Li, Z. O'Neil, L. Zhang, J. Chen, P. Im, and J. DeGraw. *Renewable and Sustainable Energy Review*, 146:111174, 2021.

[46] H.I. Tol and H.B. Madessa. *Journal of Building Engineering*, 65:106038, 2023.

[47] L.A. Zadeh. Fuzzy sets. *Information and Control*, 8:338–353, 1965.

[48] A.K. Sinha and A.K. Jha. Speed control of a train using fuzzy logic. *International Journal of Science and Research*, 6:781–784, 2015.

[49] H. Dong, S. Gao, and B. Ning. Extended fuzzy logic controller for high speed train. *Neural Computing and Applications*, 22:321–328, 2013.

[50] W.Y. Liu, J.G. Han, and X.N. Lu. A high speed railway control system based on the fuzzy control method.

[51] X. Wang and T. Tang. Optimal operation of high-speed train based on fuzzy model predictive control.

[52] M.C. Pradhan. An intelligent fuzzy based technique of making food using rice cooker.

[53] A. Ghelli, H. Hagras, and G. Aldabbagh. A fuzzy logic-based retrofit system for enabling smart energy-efficient electric cookers.

[54] K. Raja. Python-based fuzzy logic in automatic washer control system.

[55] C.P. Underwood. Fuzzy multivariable control of domestic heat pumps.

[56] S.S. Ahmed, M.S. Majid, H. Novia, and H.A. Rahman. Fuzzy logic based energy saving technique for a central air conditioning system.

[57] T.J. Ross. *Fuzzy Logic with Engineering Applications, 4th Ed.* Wiley and Sons, West Sussex, UK, 2017.

[58] F. Rashidi, M. Rashidi, and A. Rahmati. A hybrid fuzzy logic and PID controller for control of nonlinear HVAC systems. In *2003 IEEE International Conference on Systems, Man and Cybernetics*, volume 3, pages 2249–2254, 2003.

[59] B. Arguello-Serrano and M. Velez-Reyes. Nonlinear control of a heating, ventilating, and air conditioning system with thermal load estimation. *IEEE Transactions on Control Systems Technology*, 7:56–63, 1999.

[60] R. Alcalá, J. Benitez, J. Casillas, O. Cordon, and R. Perez. Fuzzy control of HVAC systems optimized by genetic algorithms. *Applied Intelligence*, 18:155–177, 2003.

[61] M. Killian, B. Mayer, and M. Kozek. Cooperative fuzzy model predictive control for heating and cooling of buildings. *Energy and Buildings*, 112:130–140, 2016.

[62] J. Baltazar. Toward the intelligent control of multi-room buildings: A fuzzy-logic approach. Master's thesis, California State University, Los Angeles, 2018.

[63] J. Baltazar, A. Yarian, and A. Pacheco-Vega. Development of P- PD- and PID-fuzzy SISO controllers of a sub-scaled multi-room building test-bed. In *Proceedings of the 3rd Thermal and Fluids Engineering Conference (TFEC)*, pages 785–795, Fort Lauderdale, FL, 2018. TFEC-2018-21805.

[64] J. Baltazar, D. Clemons A. Yarian, and A. Pacheco-Vega. On-line fuzzy control of multi-room building facility. In *Proceedings of the 4th Thermal and Fluids Engineering Conference (TFEC)*, Las Vegas, NV, 2019. TFEC-2019-27663.

[65] A. Baghdasarian, O. Ramos, J. Ruvalcaba, S. Talome, and F. Wang. Energy efficient building tes-bed, 2015.

[66] D. Brown, F. Barrios, E. Palma, and T. Huang. Design of an efficient heating and cooling system: Final design report, 2019.

[67] A. Kam, D. Hernandez B. Gaytan, E. Conde, and E. Luu. Second generation building testbed, 2019.

[68] A. Bagdasarian, O. Ramos, J. Ruvalcaba, S. Talome, and F. Wang. Energy efficient building test-bed, 2015.

[69] LTD Haier Air Conditioner General Corp. *Service Manual: Model No. ESA410K*. Haier Air Conditioner General Corp., LTD.

[70] Joseph Wu. *Application Note: A Basic Guide to Thermocouple Measurements*. Texas Instruments Incorporated.

[71] S.Y. Goo, M.K. Lee, D.H. Lee, D.H. Park, and et al. Comparing domain- and intensity-specifc physical activity in coronary heart disease and non-chd individuals. *Scientific Reports*, 14(2622), 2024.

[72] E.B. Winzer, F. Woitek, and A. Linke. Physical activity in the prevention and treatment of coronary artery disease. *Journal of the American Heart Association*, 7(4), 2018.

[73] A. Saguilan and A. Pacheco-Vega. Fuzzy controller response to internal and external disturbances in a multi-room building testbed. In *Proceedings of the 9th Thermal and Fluids Engineering Conference (TFEC)*, Corvallis, OR, 2024. TFEC-2024-50484.

[74] A. Saguilan and A. Pacheco-Vega. Assessment of internal and external disturbances on a fuzzy-based thermal control of a sub-scaled building testbed. In *Proceedings of the 9th Thermal and Fluids Engineering Conference (TFEC)*, Bled, Slovenia, 2024.

[75] A. Pacheco-Vega, C. Ruiz-Mercado, K. Peters, and L. Vilchiz-Bravo. On-line fuzzy-logic-based temperature control of a concentric-tube heat exchanger facility. *Heat Transfer Eng*, 30(14):1208–1215, 2009.

[76] E.H. Mamdani. Application of fuzzy algorithms for control of simple dynamic plant. *IEEE Proc.*, 121(12), 1974.

[77] ANB. *Sensirion: Datasheet SDP8xx-Analog.* Sensirion.

Appendix A

Using MATLAB and LabVIEW to Operate the Sub-scaled Building Test-bed Fuzzy Controller

(1) First open the InstaCal software (a) Figure A.1.

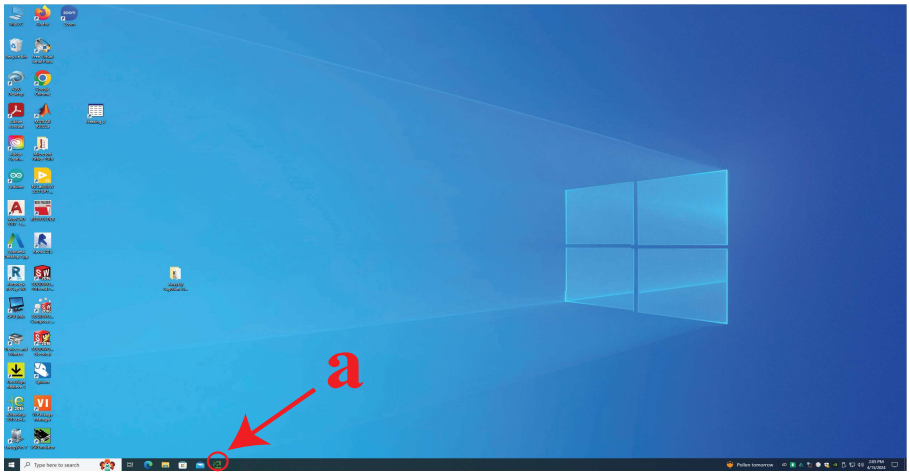


Figure A.1: Step 1.

(2) Upon opening the InstaCal software, a pop-up box titled "System Modifications Required" will prompt you to update utility for USB devices. Select "No", Figure A.2.

(3) Select the "Calibrate" button and calibrate boards 1 - 5, Figure A.3.

(4) Open the VPSEmulator software (b), Figure A.4.

(5) Open the VPSEmulator software window. Select "Device" and "Create", Figure A.5.

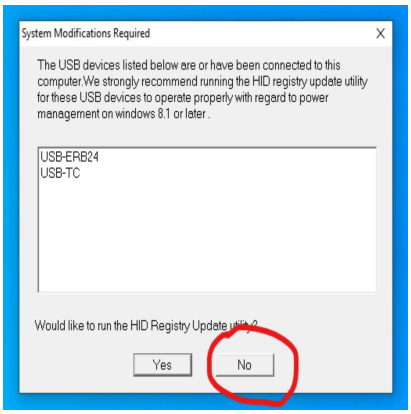


Figure A.2: Step 2.

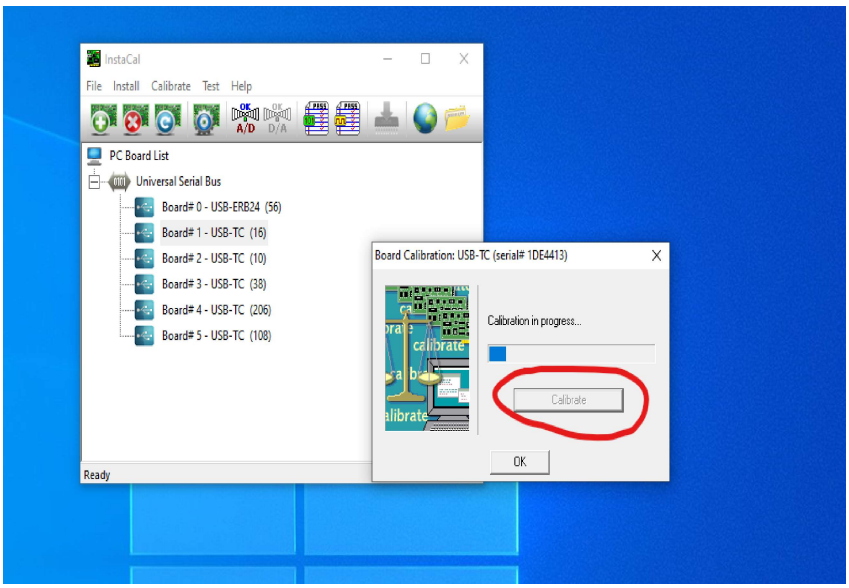


Figure A.3: Step 3.

(6) The "Specify device type" window will prompt you to select a device. Select "Connector", Figure A.6.

(7) Open the MATLAB file that contains the controller. At the time of writing this document, the name of this file is "FLC3_Controller_velocity.m" and can be found in Anayely Saguilan-Files → FLC3, Figure A.7.

(8) Once the .m file is open, find the name of the serial port listed. In VPSEmulator,

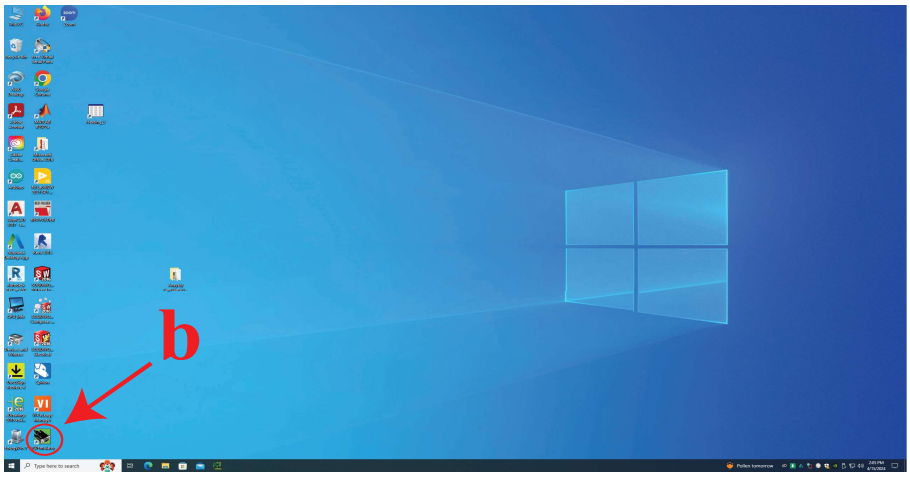


Figure A.4: Step 4.

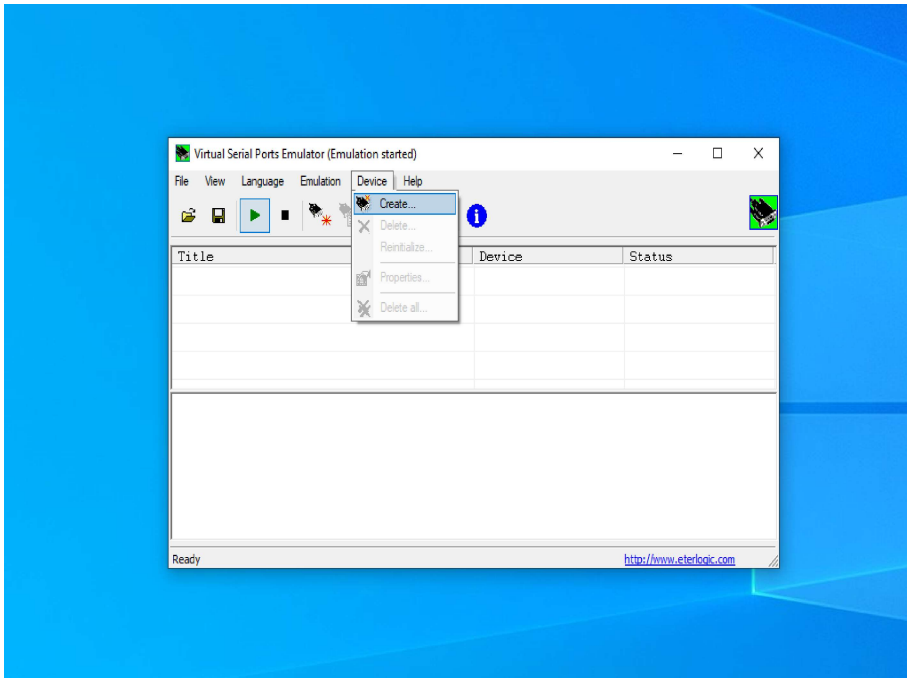


Figure A.5: Step 5.

select the virtual serial port that matches the MATLAB serial port. In this case, the serial port listed in the file is "COM5", Figure A.8.

(9) VPSEmulator can now be minimized Figure A.9.

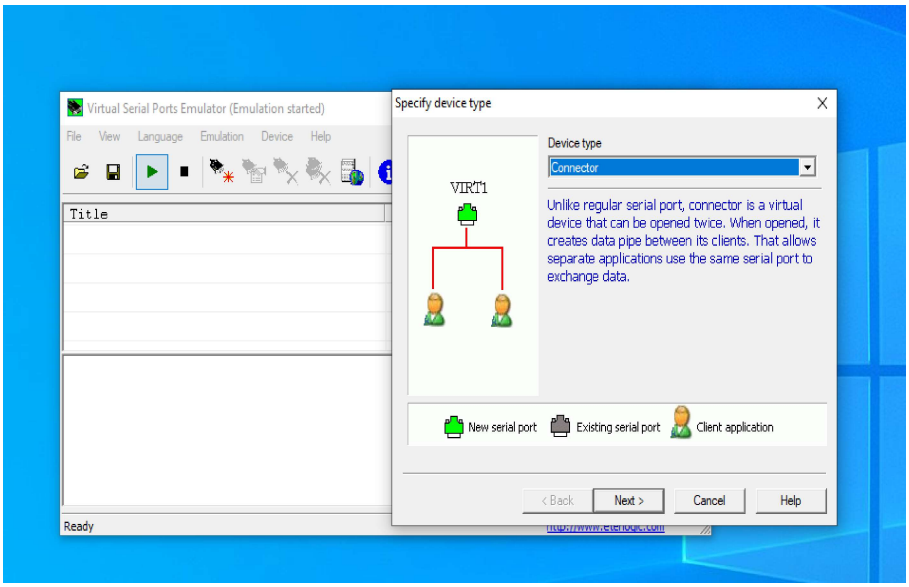


Figure A.6: Step 6.

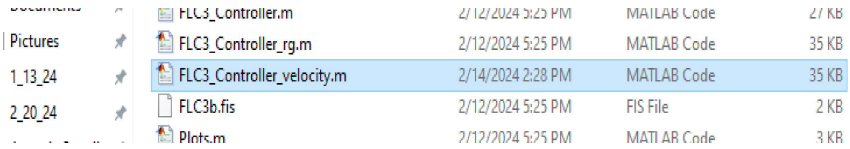


Figure A.7: Step 7.

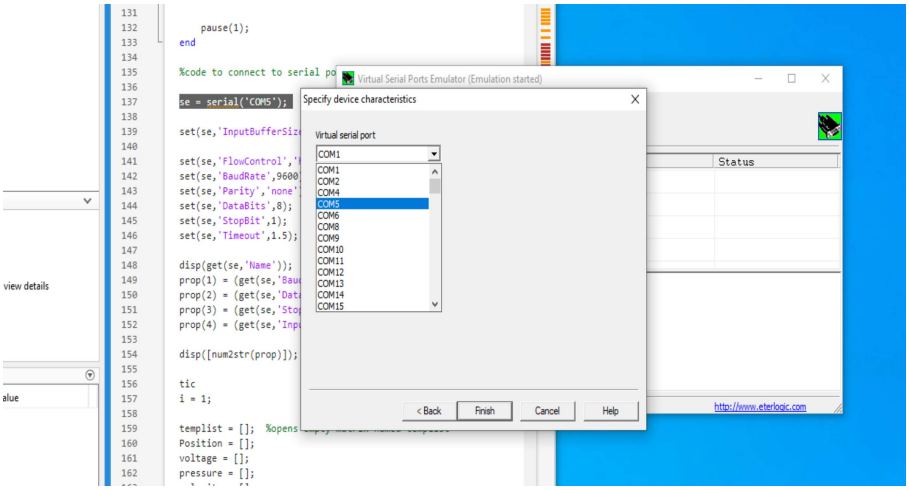


Figure A.8: Step 8.

(10) The following message will appear once VPSEmulator has been minimized, Figure A.10.

(11) Open "Labview2matlab_multi-room_ANA.vi". This vi is responsible for turning

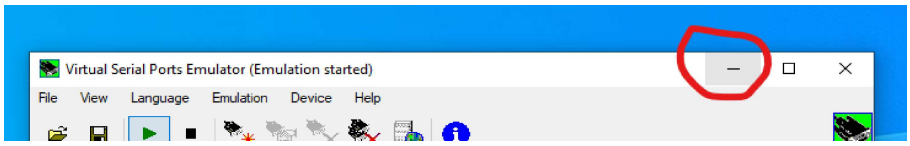


Figure A.9: Step 9.

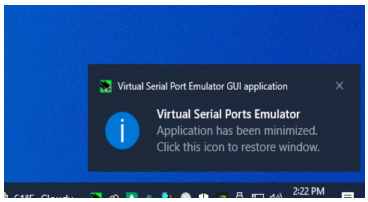


Figure A.10: Step 10.

the light bulbs in the building on and off and for gathering the temperature data from each room, Figure A.11.

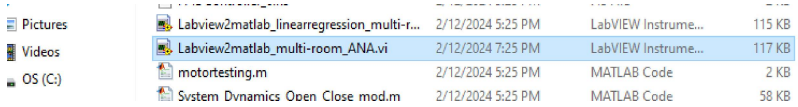


Figure A.11: Step 11.

(12) Open the virtual serial port that was created in step (6), Figure A.12.

(13) Click the white arrow on the top left corner to run the vi, Figure A.13.

(14) Click on the buttons to turn the light bulbs on (or off). Notice that the button will turn green if that light bulb is in operation, Figure A.14.

(15) I use the "Heating_Dynamics.m" (found under Anayely Saguilan-Files → Tests for Dynamics_ana → Heating) to keep track of how much each room is heated. The MATLAB program containing the fuzzy controller ("FLC3_Controller_velocity.m") can be run once all rooms are heated to the temperature needed. Once the rooms have been heated, the controller "FLC3_Controller_velocity.m" can be run. The external AC will have to be manually turned on, Figure A.15.

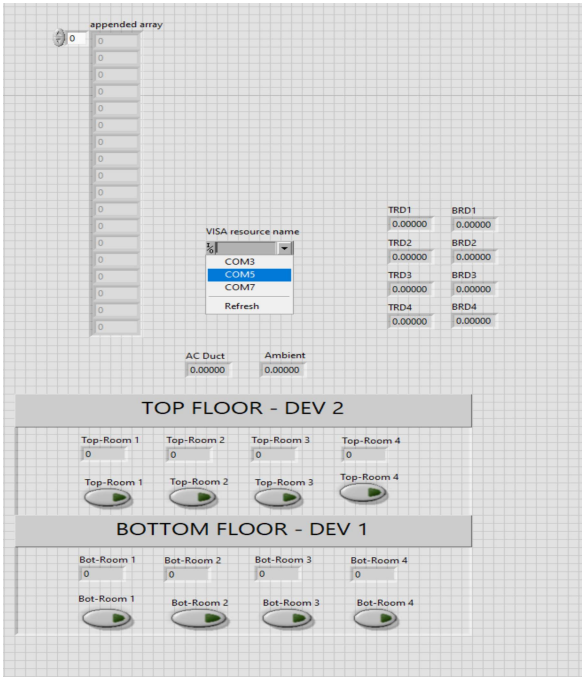


Figure A.12: Step 12.

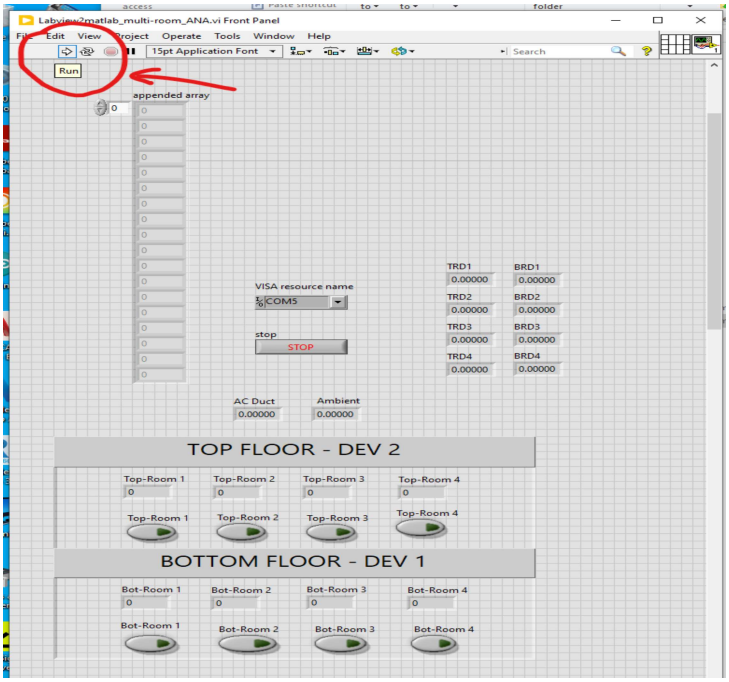


Figure A.13: Step 13.

(16) Once testing is complete for the day: Make sure to **ALWAYS** turn off the power supply to the computer, AC, DAQ boards, and Arduinos. Do this by switching the

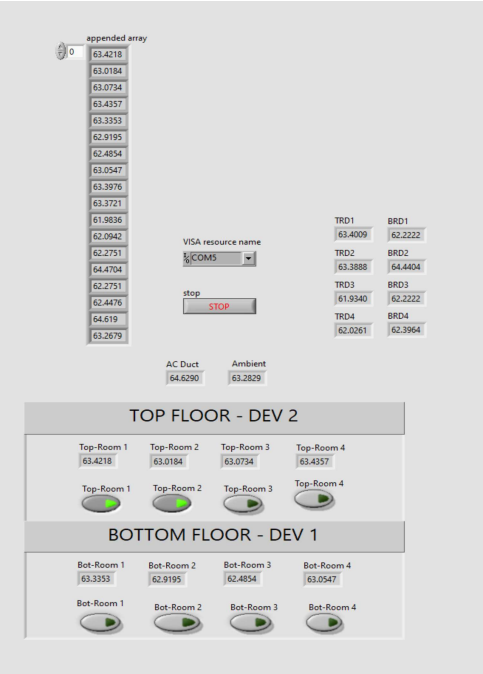


Figure A.14: Step 14.

Heating_Dynamics.asv	2/12/2024 5:25 PM	ASV File	7 KB
Heating_Dynamics.m	2/13/2024 2:03 PM	MATLAB Code	5 KB

Figure A.15: Step 15.

extension cords to “OFF”.

Appendix B

FUZZY LOGIC INFERENCE SYSTEM FOR SINE FUNCTION

B.1 Abstract

The objective of this example was to develop a fuzzy rule-based system by using four simple fuzzy rules to approximate the output y of the function $y = 10 \sin x_1$. The model for this function was built using the Fuzzy Logic Toolbox (found in the MATLAB software) with the Mamdani inference method and the centroid method of defuzzification. A set of five membership functions where used to describe the input variables whereas one triangular and two trapezoidal membership functions were used for the outputs for y. The model created produced a set of outputs, y , that resembled a sine wave.

B.2 Problem Introduction

Unlike classical logic, Fuzzy Logic was created as a way to model vagueness through the graded approach, or in other words, the use of membership between an object and its property. This approach in solving for ambiguity lends itself to be useful in that it mimics human rational through the use of linguistic variables to approximate solutions for models without the use of mathematical modeling.

As such, for this example we used the fuzzy logic approach to create a model that approximates the $y = 10 \sin x_1$ plot. The variable x_1 will be set within the interval of [-190°, 190°] while the output variable y is set within the range [-15, 15]. The input variable is to be divided into five membership functions that indicate the scale in which input x_1 belongs to that respective linguistic variable (Table B.1).

B.3 Solution Plan

There are three imperative steps that need to be taken to solve any fuzzy logic system:

(1) Fuzzify crisp inputs through the use of membership functions and rule based sets

(2) Identify the max or min inference of each membership function

(3) Deffuzify the membership functions' inference through the use of the max membership principle, centroid method, or the weighted average method to produce crisp outputs

B.4 Fuzzification

This model uses triangular membership functions to fuzzify the crisp inputs for x_1. For this, the input variable x_1 was set within the interval of $[-190°, 190°]$. For the output variable y, it was decided that one triangular membership function and two trapezoidal membership functions were to be used. The output variable y was set within the range of [-15, 15]. Following the solution given in the text book *Fuzzy Logic with Engineering Applications* [57] , the range x_1 was divided into 5 membership functions whereas y was divided into 3.

Table B.1 shows the names given to the membership functions for x_1. NB (Negative Big) was created so that all the crisp angles -223.4 to -90 have some membership within the Negative Big set. It follows that NS (Negative Small) encompasses all angles from -180 to 0, Z (zero) encompasses angles from -90 to 90, PS (Positive Big) encompasses angles from 0 to 180, and PC (Positive Big) encompasses angles from 90 to 236 (Table B.2).

Table B.1: Membership function name designation for inputs.

Abbreviation	**Linguistic Variable**
NB	Negative Big
NS	Negative Small
Z	Zero
PS	Positive Small
PB	Positive Big

Table B.2: Membership function name designation for outputs.

Abbreviation	**Linguistic Variable**
Neg	Negative
Zero	Zero
Pos	Positive

Table B.3: Membership of x_1 in sets NB, NS, Z, PS, and PB.

Membership Function	**Degree of Membership**
NB	$\mu_{\underset{\sim}{NB}^k}(x_1)$ ∈[-223.4 -90]
NS	$\mu_{\underset{\sim}{NS}^k}(x_1)$ ∈[-180 0]
Z	$\mu_{\underset{\sim}{Z}^k}(x_1)$ ∈[-90 90]
PS	$\mu_{\underset{\sim}{PS}^k}(x_1)$ ∈[0 180]
PB	$\mu_{\underset{\sim}{PB}^k}(x_1)$ ∈[90 236]

These rules where input into Matlab's Fuzzy Logic Designer (Figures B.1 - B.5):

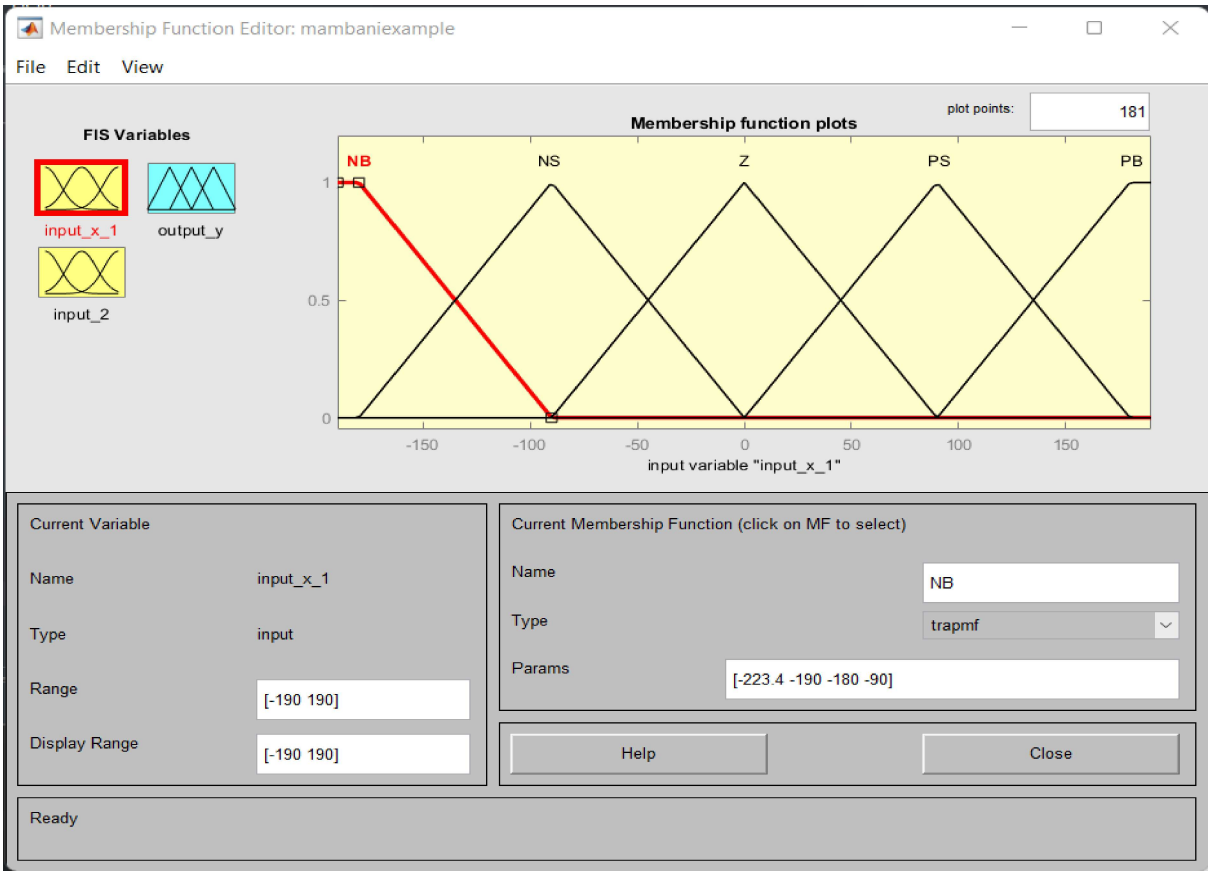


Figure B.1: Parameters for membership function NB.

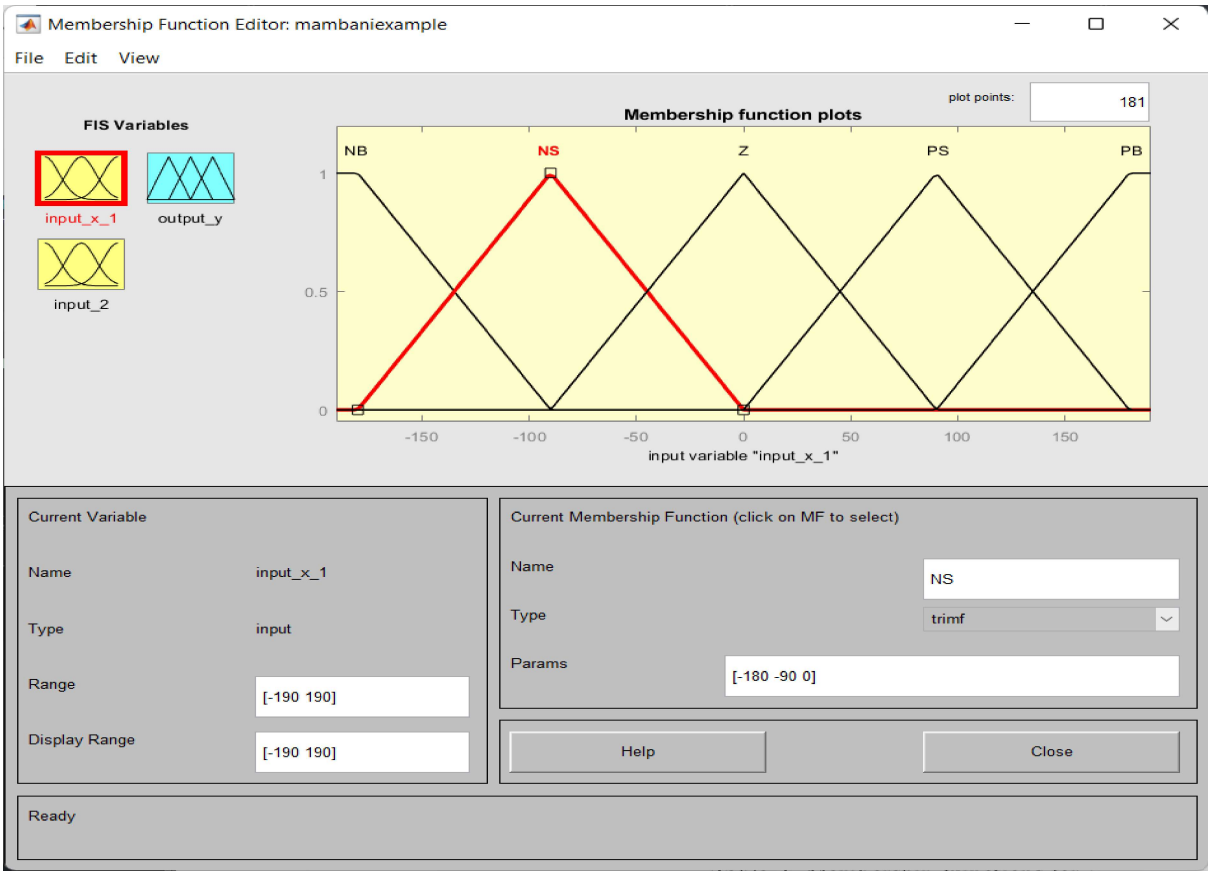


Figure B.2: Parameters for membership function NS.

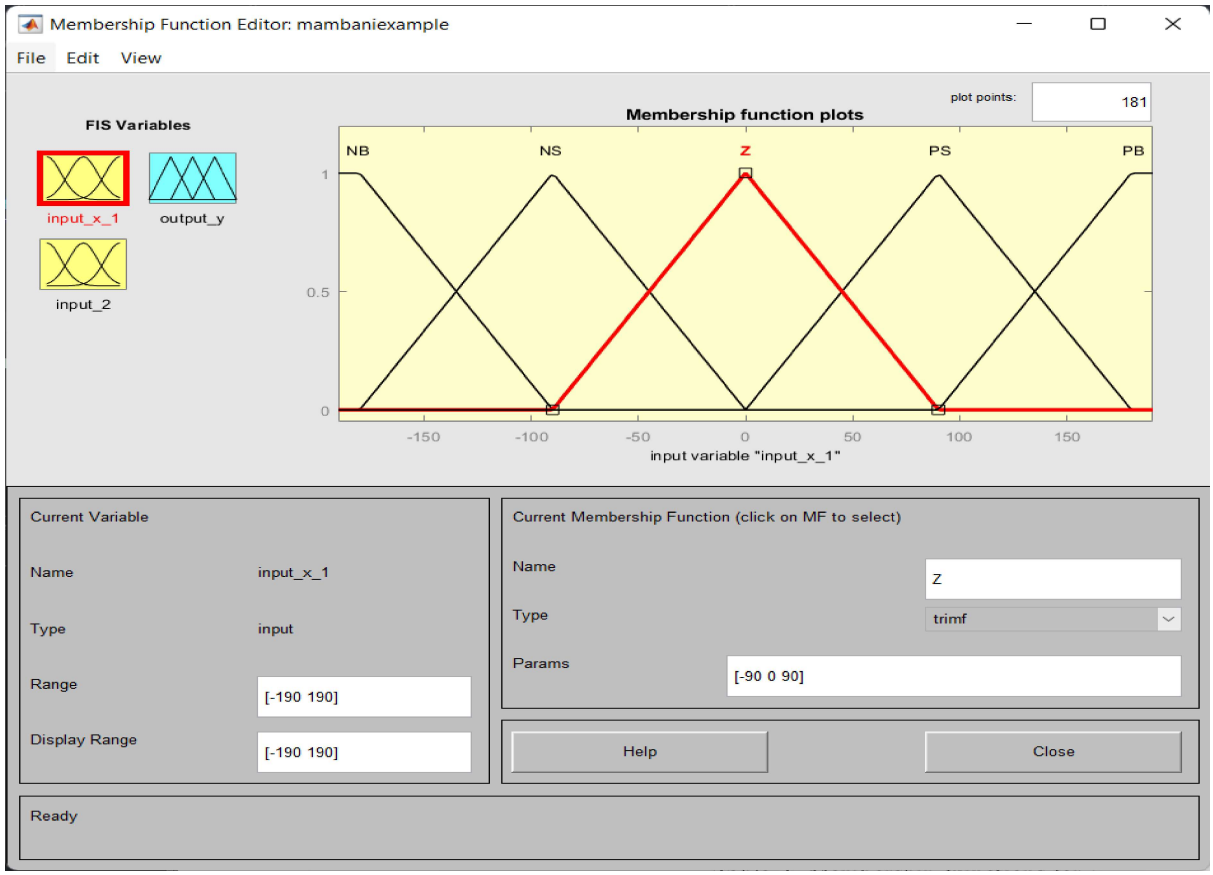


Figure B.3: Parameters for membership function Z.

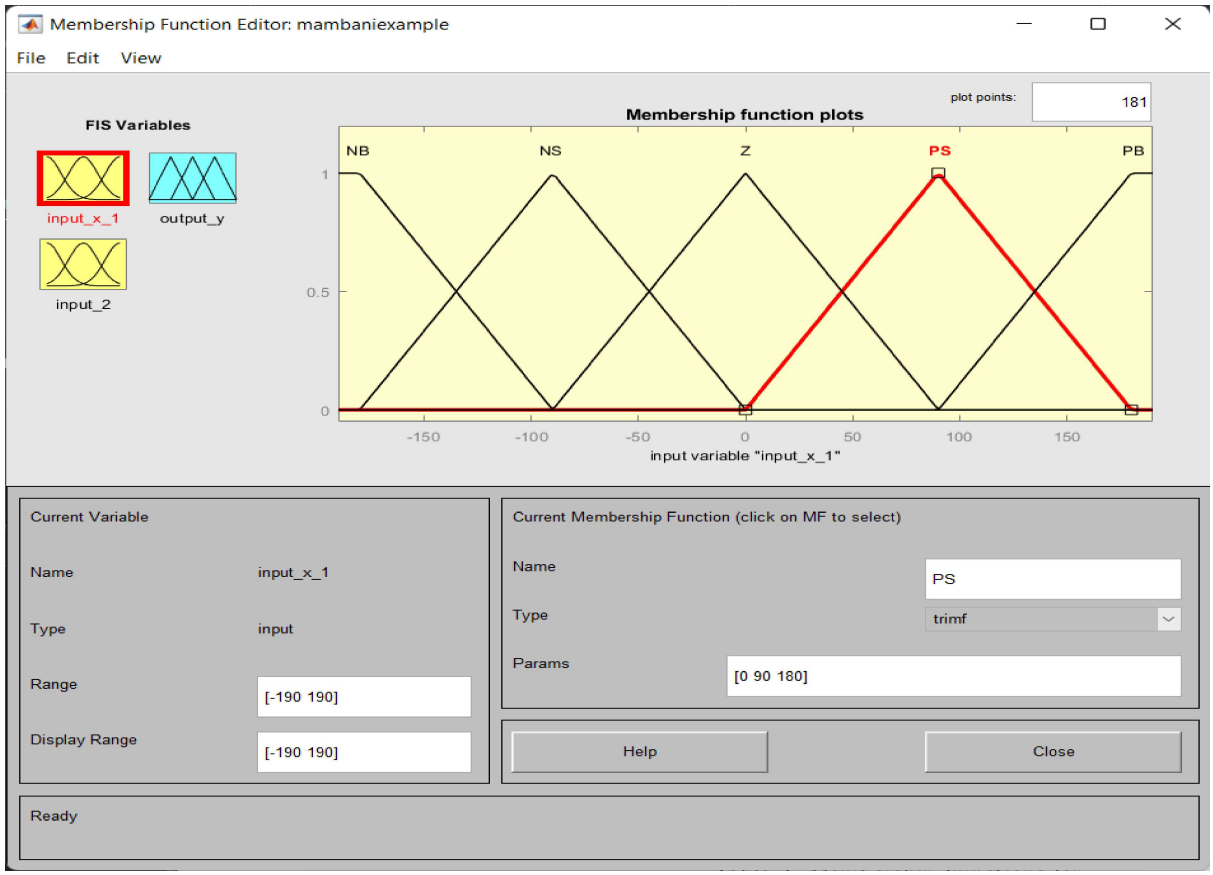


Figure B.4: Parameters for membership function PS.

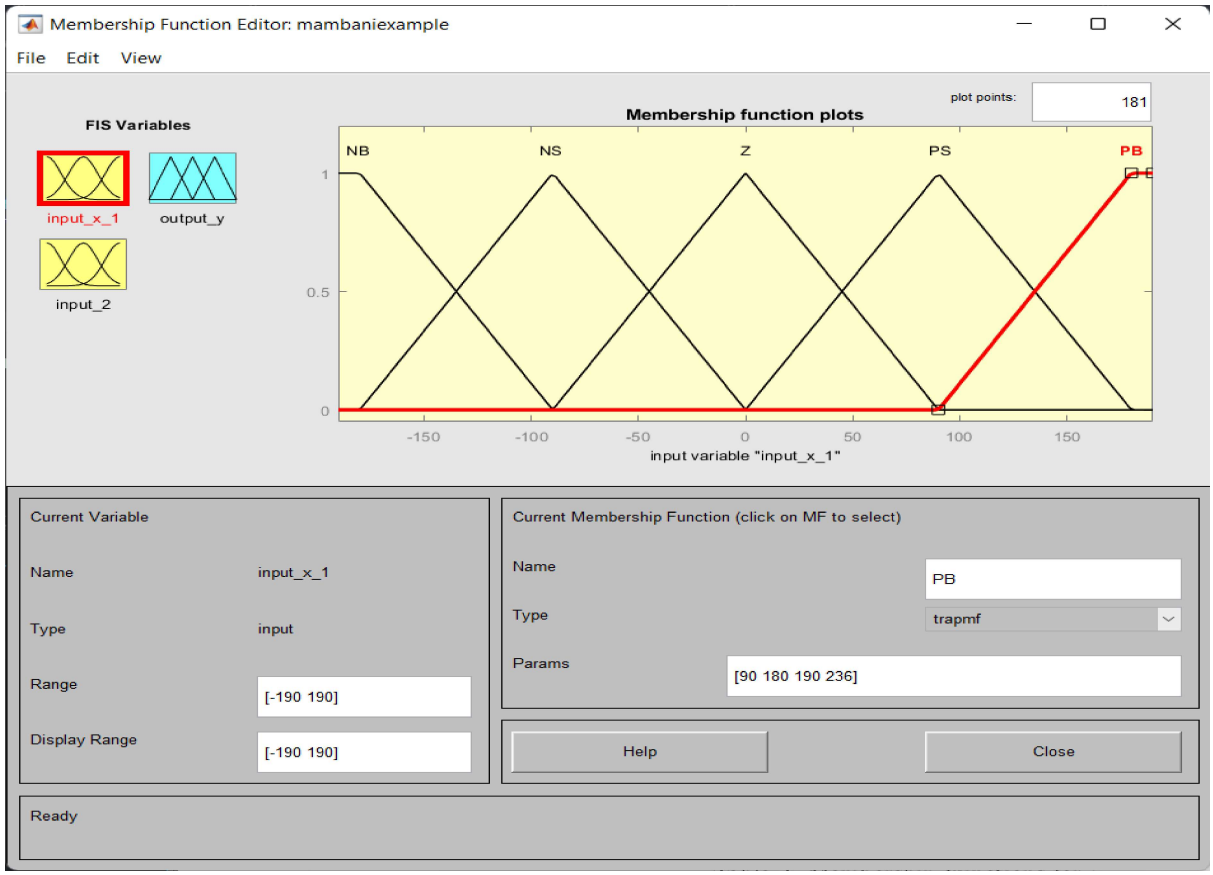


Figure B.5: Parameters for membership function PB.

The degree of membership for the outputs y within the membership functions listed on Table B.2 are listed on Table B.4.

Table B.4: Membership of y in sets Neg, Zero, and Pos.

Neg	$\mu^k_{\underset{\sim}{Neg}}(x_1) \in$[-19 0]
Zero	$\mu^k_{\underset{\sim}{Zero}}(x_1) \in$[-10 10]
Pos	$\mu^k_{\underset{\sim}{Pos}}(x_1) \in$[0 19]

These membership functions for y where input into Matlab's Fuzzy Logic Designer (Figures B.6 - B.8):

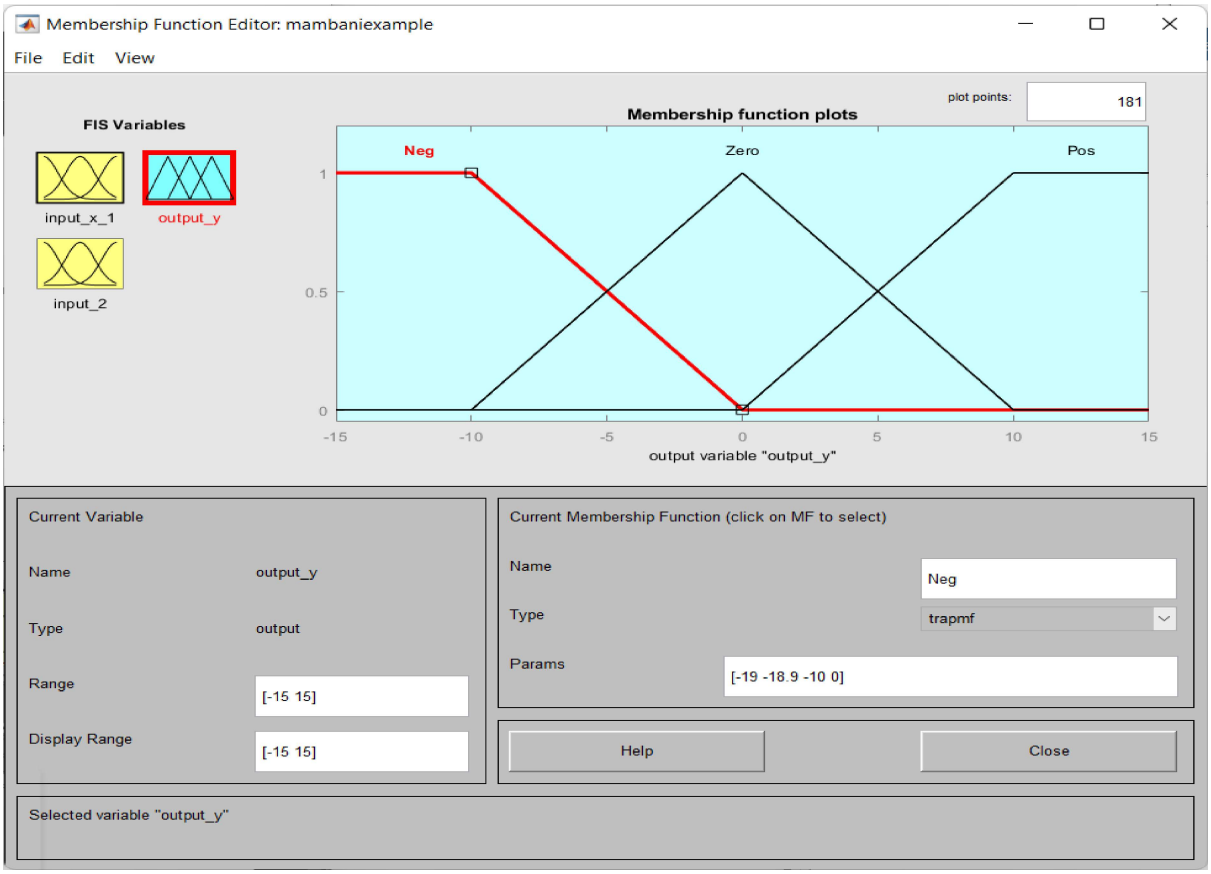


Figure B.6: Parameters for membership function Neg for the outputs of y.

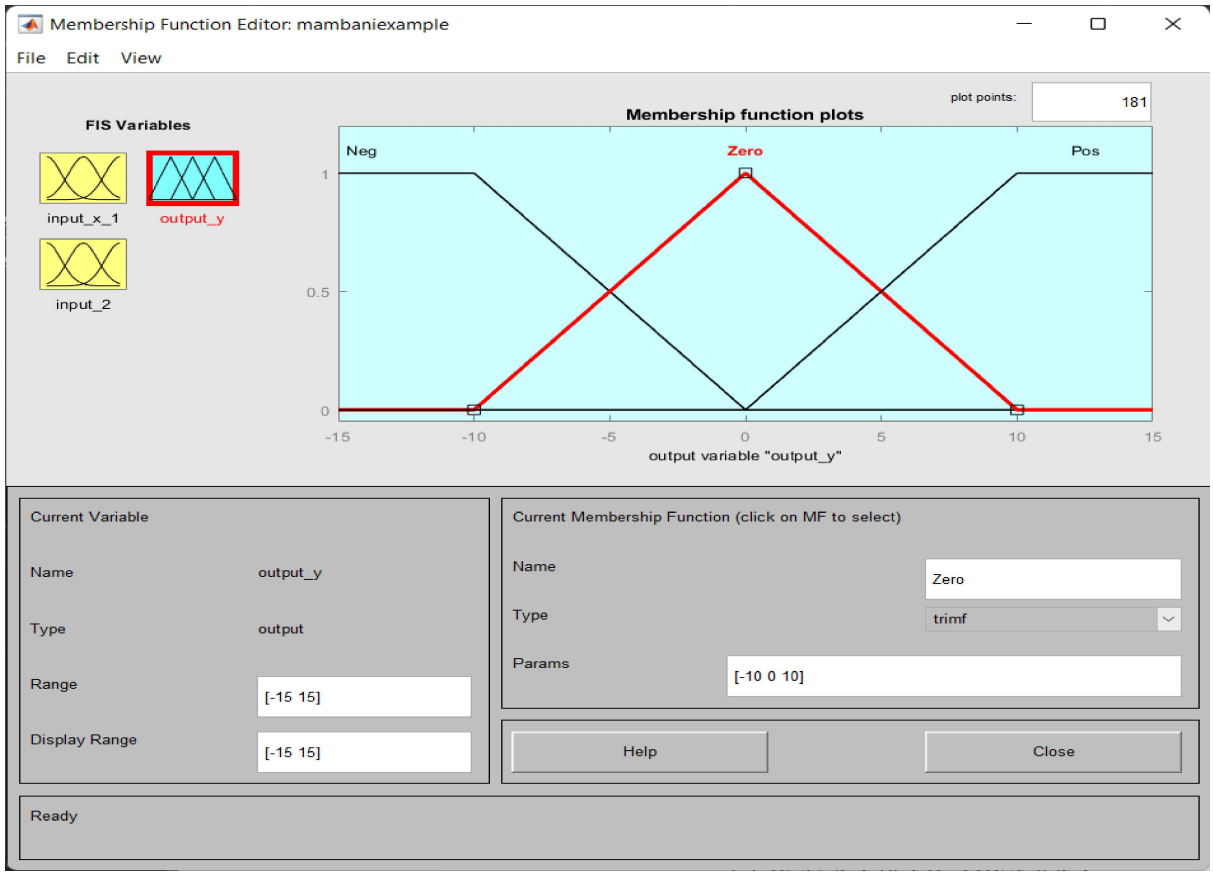


Figure B.7: Parameters for membership function Z for the outputs of y.

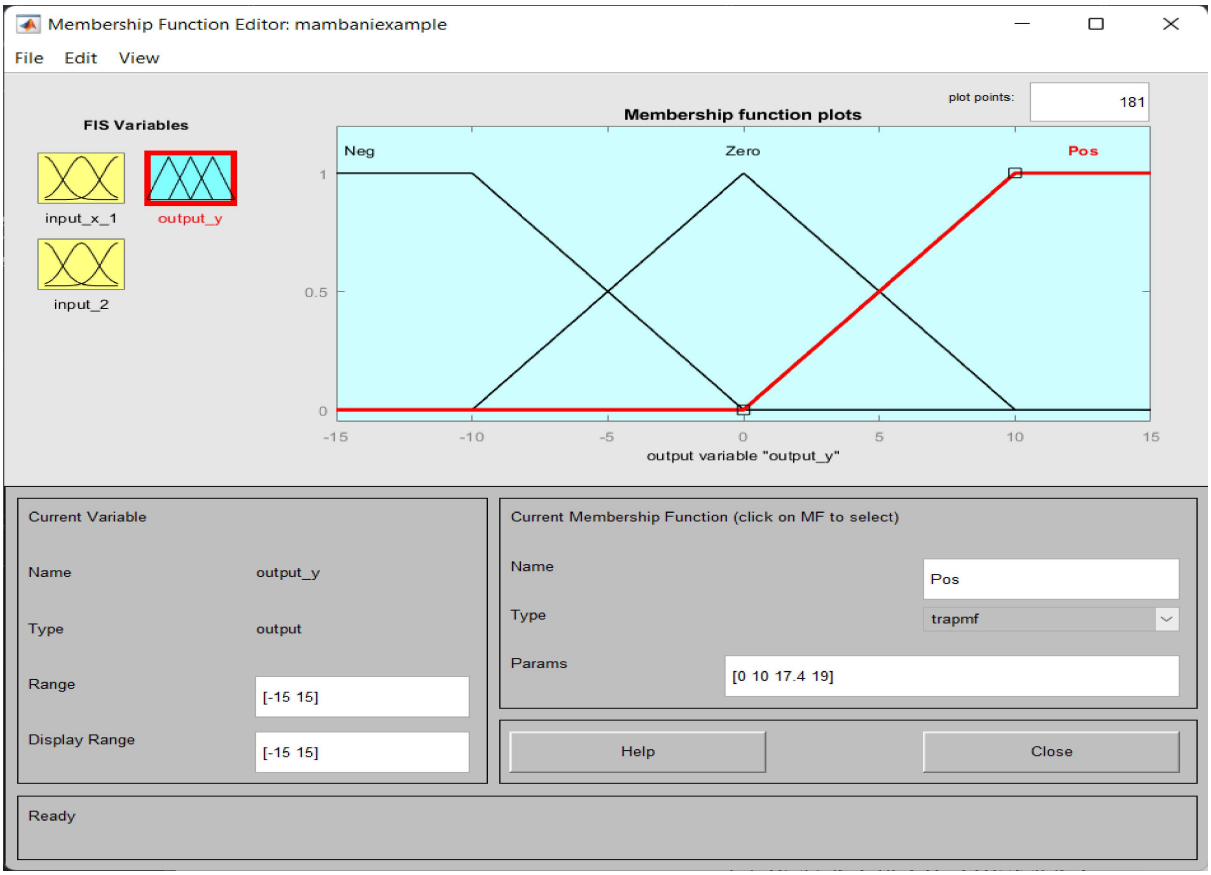


Figure B.8: Parameters for membership function Pos for the outputs of y.

Since this problem requires two sets of inputs, the second set of membership functions, $input_2$ will be defined in the same manner as the membership functions of $input_{x1}$.

Next, the Rule table was defined for the inputs x_1 and the outputs y.

Table B.5: Rule Table

1	IF x_1 is Z or PB, THEN y is Z
2	IF x_1 is PS, THEN y is PB
3	IF x_1 is Z or NB, THEN y is Z
4	IF x_1 is NS, THEN y is NB

Which looks like Figure B.9 when represented in Matlab's Fuzzy Designer.

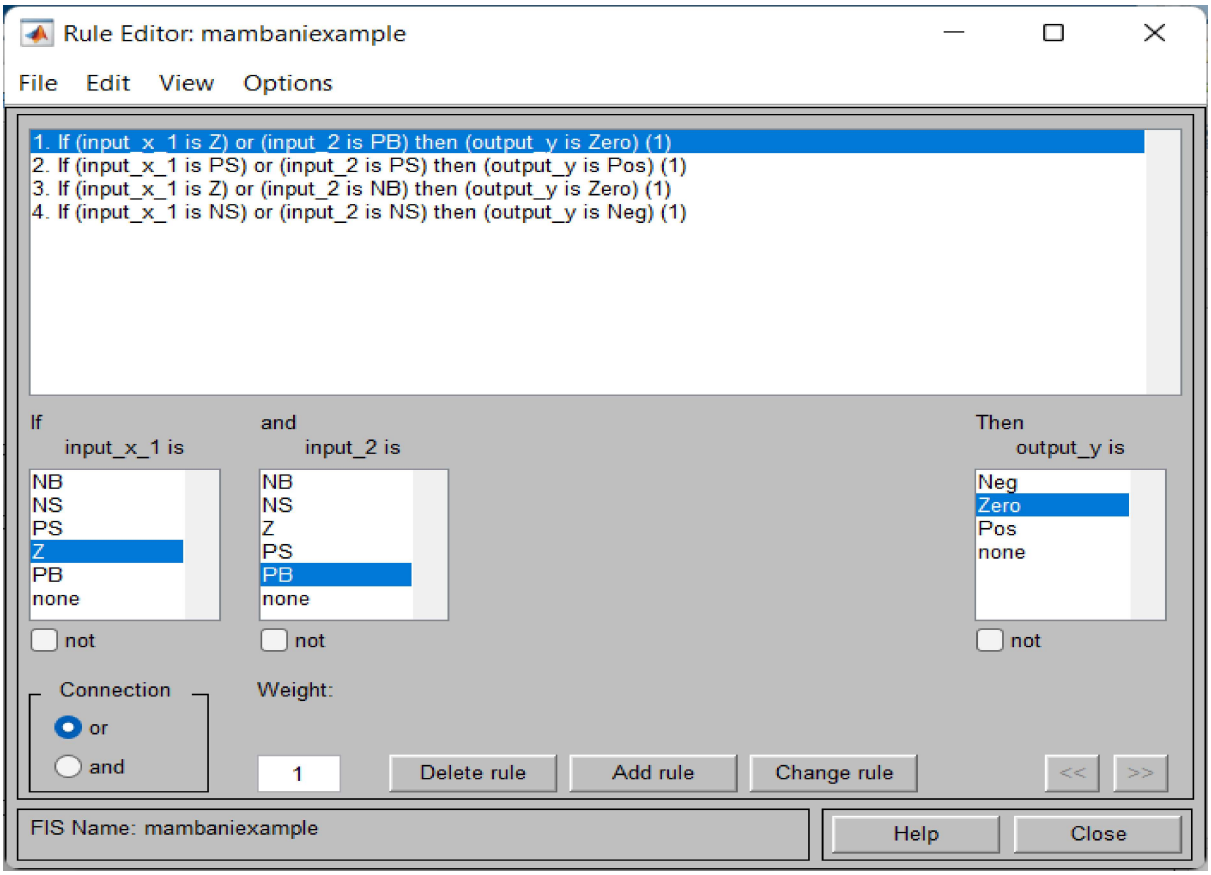


Figure B.9: Fuzzy Rules for Defuzzification

B.4.1 Membership Function Inference

In order to identify the inference of each membership function, one has to first determine whether the rules that govern the fuzzy system define a conjunction or a disjunction of inputs and outputs. To further analyze this system, the graphical rule base section within the Fuzzy Logic Designer will be explained.

Figure B.10 shows a graphical representation of the rule sets and defuzzification, where the first two columns represent the graphical inference for the rule base used for this solution. The last column shows the maximum fuzzy consequents of the rules.

The filled-in yellow triangles for the shown inputs [45 , 180] in the *Input* window

show that the rules 1 - 3 were activated. Meaning that since the input 45 falls under the membership functions that encompass *Zero* and *Positive* Small, then rules 1 and 3 satisfy this input. For the second input, 180, falls under membership function *Positive Big*, therefore rule 1 applies to this input (notice that rule 1 was the only rule activated in Figure 4 for an input of 180).

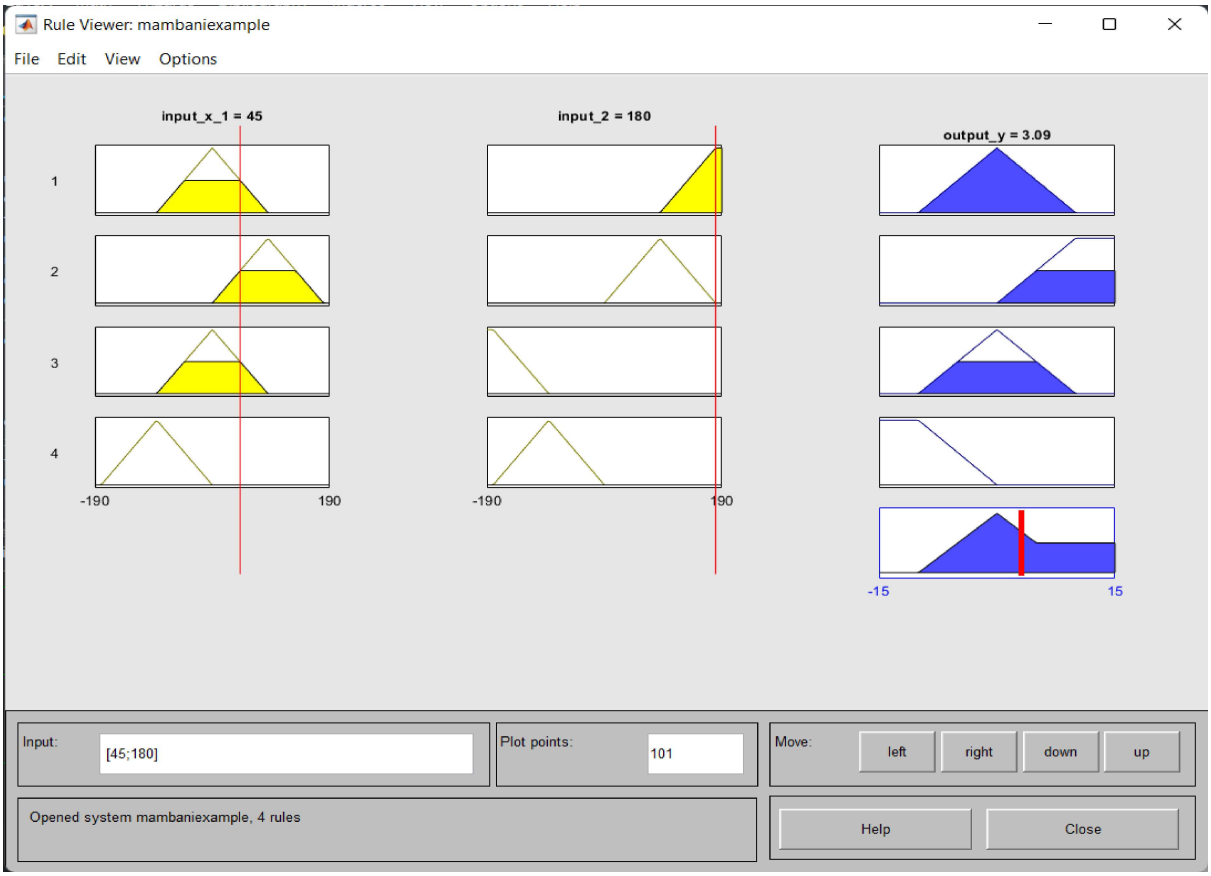


Figure B.10: Membership Propagation and Defuzzification.

As an example lets take Rule 1, which is defined in Figure B.11. Lets assume that $inputx_1$ is equal to 80 and $input_2$ is equal to 135. Referring back to Table B.5, where it states that for Rule 1:

IF x_1 is Z or PB, THEN y is Z

paying extra attention to the disjunction "OR". In this case, we use the max-min Mamdani implication method of inference which in this case is defined as,

$$\mu_{\underset{\sim}{B}^k}(y) = \max_k(min[\mu_{A_1^k}(inputx1), \mu_{A_2^k}(input2)])$$

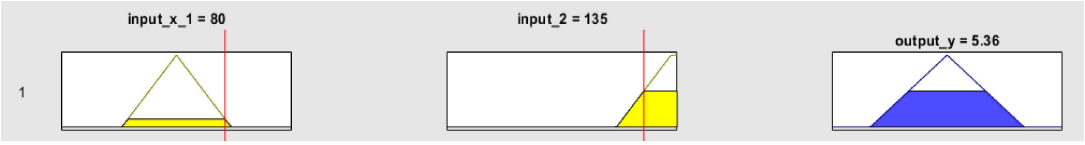


Figure B.11: Rule 1

Since Rule 1 is governed by "OR", the maximum of each triangular inference with crisp inputs are taken to be $inputx_1 = 80$ and $input_2 = 135$. The maximums of μ_B are shown by the red lines. The triangle in the last column is the consequent of the inputs according to Rule 1.

B.4.2 Defuzzification

For this solution, the method of defuzzification chosen was the centroid method. The centroid method for defuzzification is defined as follows:

$$y^* = \frac{\int \mu_{\underset{\sim}{C}}(y) \cdot ydy}{\int \mu_{\underset{\sim}{C}}}(y)dy$$

Where:

$\int \mu_{\underset{\sim}{C}}(y) \cdot ydy \rightarrow$ The aggregated consequents of rules 1 - 4

$\int \mu_{\underset{\sim}{C}} \rightarrow$ The maximum each triangular membership function

$y^* \rightarrow$ The crisp output y

The following figure shows the deffuzified results. Noticing that the red line in the figure shows the centroid of the aggregated outputs for the four rules. The centroid demonstrated in Figure B.12 corresponds to the crisp output shown in Figure B.11; $output_y = 5.36$

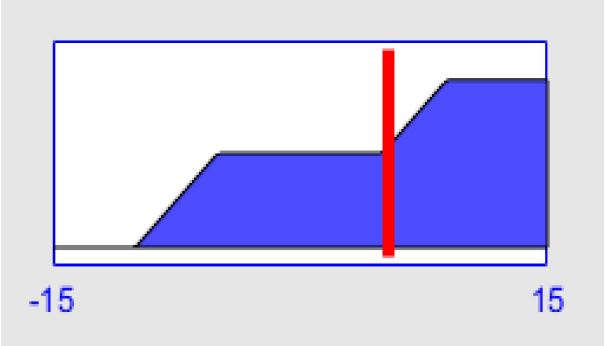


Figure B.12: Defuzzified results for inputs (80 , 135).

The total fuzzy system is shown in Figure 7.

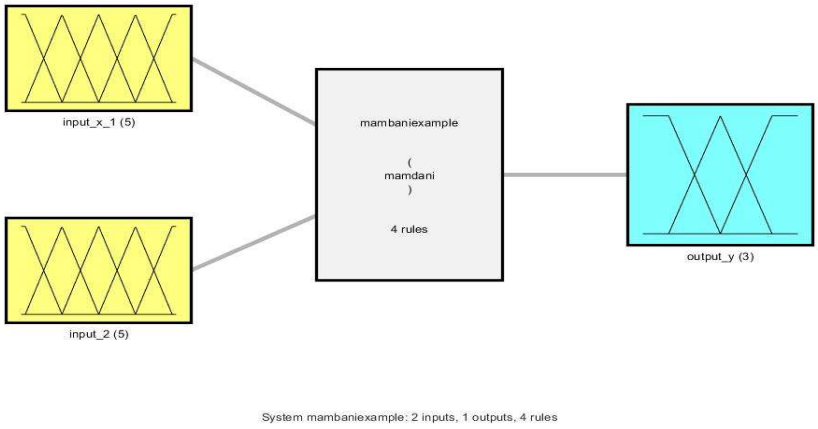


Figure B.13: Mamdani system for problem statement.

B.5 Results

The 3D surface results for this simulation are accessed through the *Surface* tab under *View*. The following Figure shows the 3D surface view for this simulation.

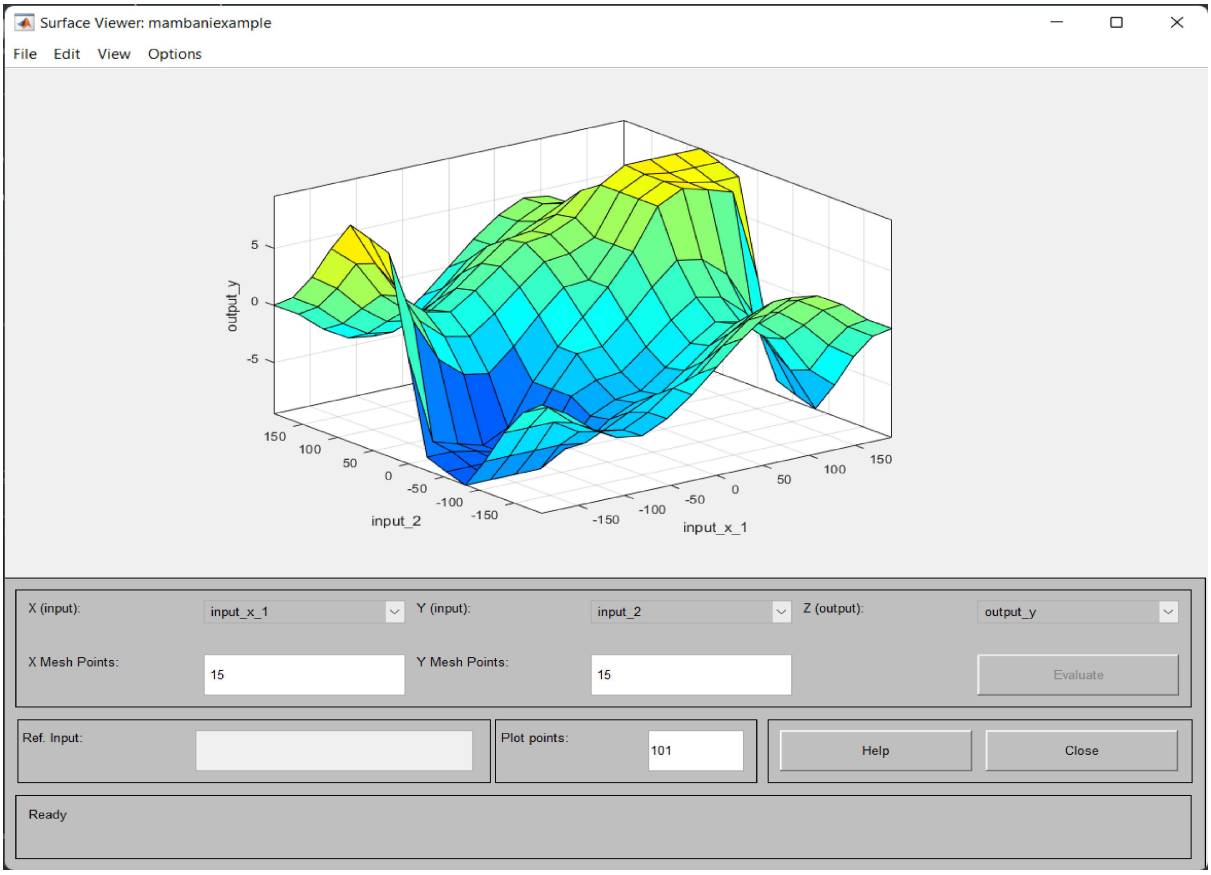


Figure B.14: 3D surface view.

To get a better idea of how the function $y = 10 \sin x_1$ is represented through this fuzzy logic simulation, we will take the inputs [-180 -135 -45 45 135 180] and examine the solution plot (Figure B.15). Note that there were two sets of inputs used to generate the fuzzy logic simulation through the Matlab Fuzzy Logic Designer, to generate the following plot through the Matlab Workspace the following matrix of inputs was used: *inputs = [-180, -180;-135, -135; -45, -45; 45, 45;135, 135; 180, 180].*

The fuzzy logic solution resembles a sine function, which comes to a surprise since

there where only five membership functions used to generate the solution curve. It is also fascinating that even though the *sine* function was not used in the making of the input membership functions or the output membership functions, the fuzzy logic toolbox was still able to generate a plot similar to what we would expect when plotting the answer for the sine trig function.

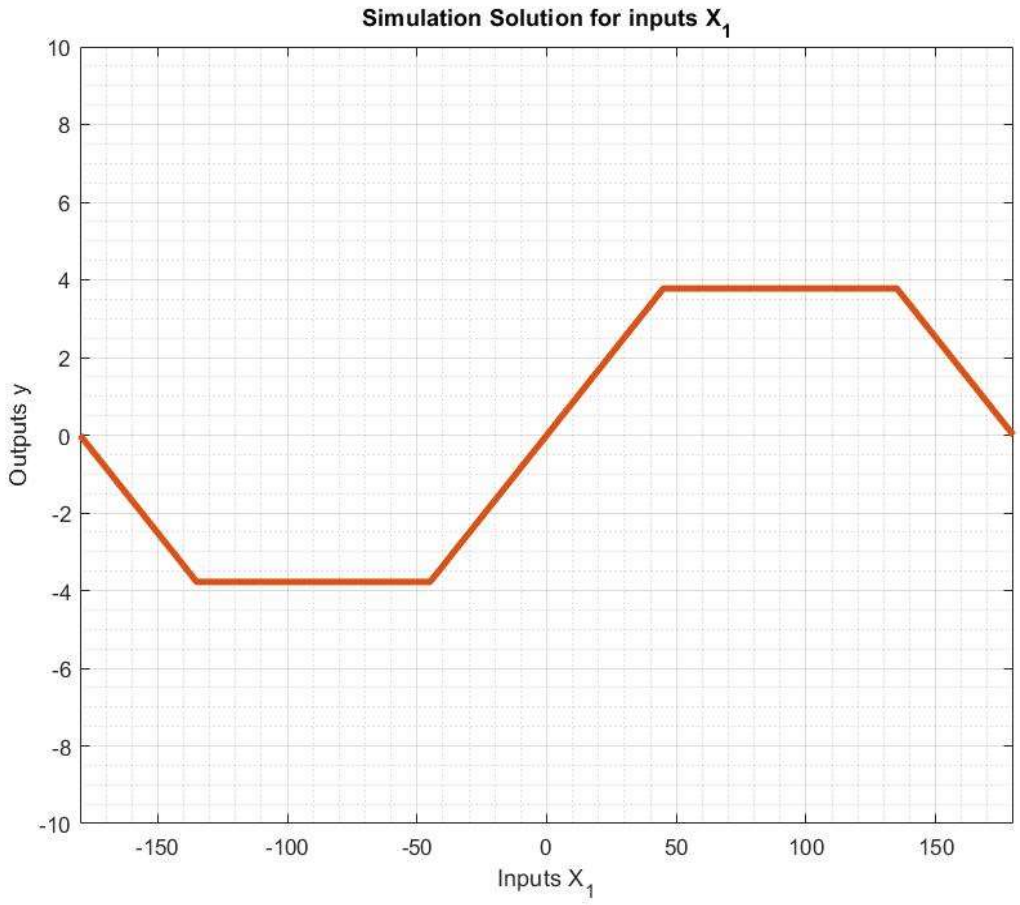


Figure B.15: Output for input values x1.

The next question question to be examined is, what happens when the rules for this system are increased? It would be logical to conclude that since the fuzzy logic controller is being fed more information in the form of membership functions and rules, that the outcome would be more refined. As an example, take the following plot (Figure B.16),

notice how the plot in green resembles a sine wave closer than to that of the red plot. Therefore it is concluded that increasing the amount of information that is fed into fuzzy systems translates to more accurate results.

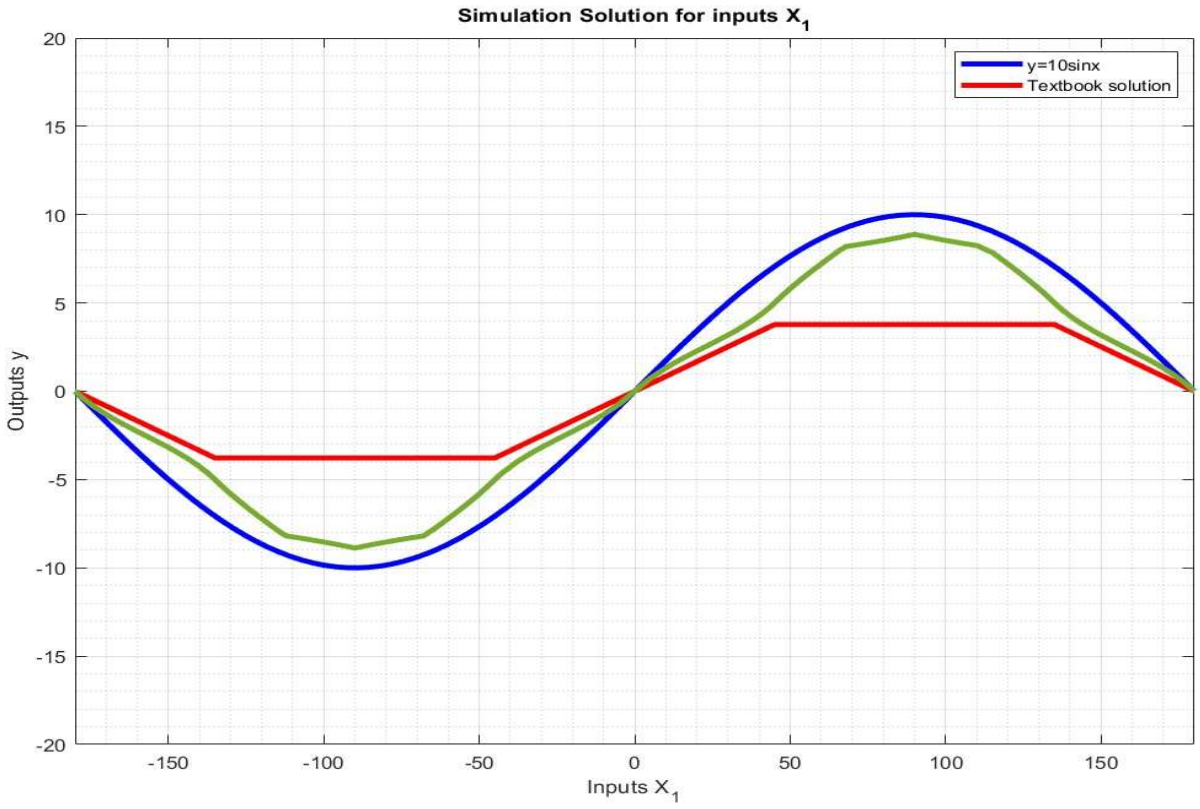


Figure B.16: Comparison of plots.

B.6 Appendix

Figure B.17 shows the rules that where added to the original fuzzy system to plot a graph that more closely resembles $y = 10 \sin x_1$.

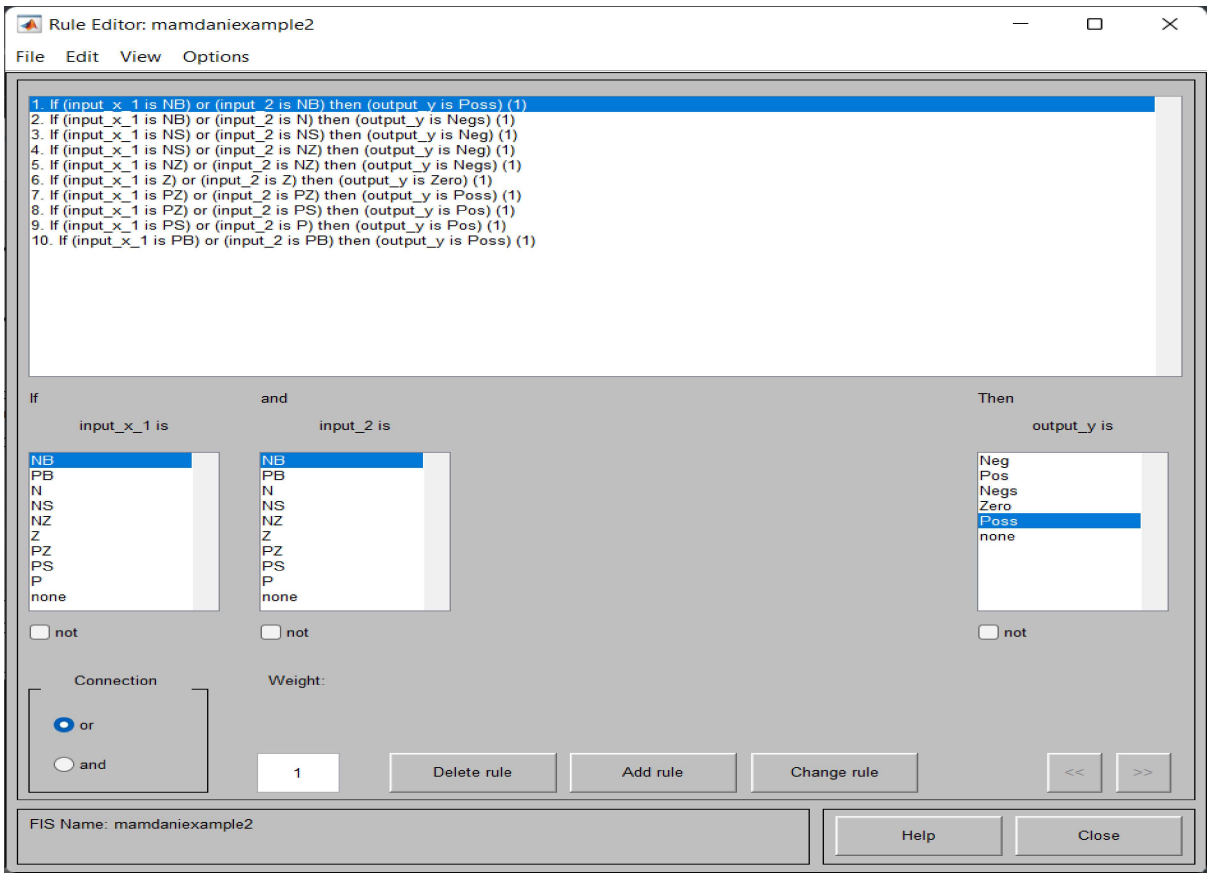


Figure B.17: Added rules.

Appendix C

FUZZY LOGIC EXAMPLE OF HEAT EXCHANGER MODELING

This appendix provides details of the fuzzy logic modeling process of a heat exchanger. This example has been taken from the *Fuzzy Logic with Engineering Applications* by Timothy J. Ross [57].

C.1 Abstract

The objective of this example was to use a fuzzy logic model to determine the size of a heat exchanger in which benzine is to be heated. Solving this problem required the use of three fuzzy logic inference methods: Mamdani, Sugeno, and Tsukamoto. The same three rules were used for each of these models and the final computed sizes where compared. It was found that using Mamdani graphical method resulted in the largest heat exchanger size, $AU = 7500$ kW/K, where as the Suegeno method of inference gave the lowest result $AU = 5282.58$ kW/K.

C.2 Problem Introduction

This example problem introduces fuzzy logic as a means to design a heat exchanger. The heat exchanger design equation $Q = AU\Delta T_{lm}$, where the subscript "ln" stands for the log mean value of the temperature difference, which is used to solve for A (area) and U (heat transfer coefficient). The heat exchanger presented in this problem statement is to heat Benzine using saturated pressure at 68.96 kPa and at a temperature of 362.7K. The initial temperature of the Benzine is set to 17°C and the following model is used to determine its size:

$$AU = wc_p \ln\left(\frac{T_s - T_l}{\Delta T}\right),$$

where the heat capacity of Benzine is given as $c_p = 1.7543$ kJ/kg K and $T_s - T_1 = 72.55$ K.

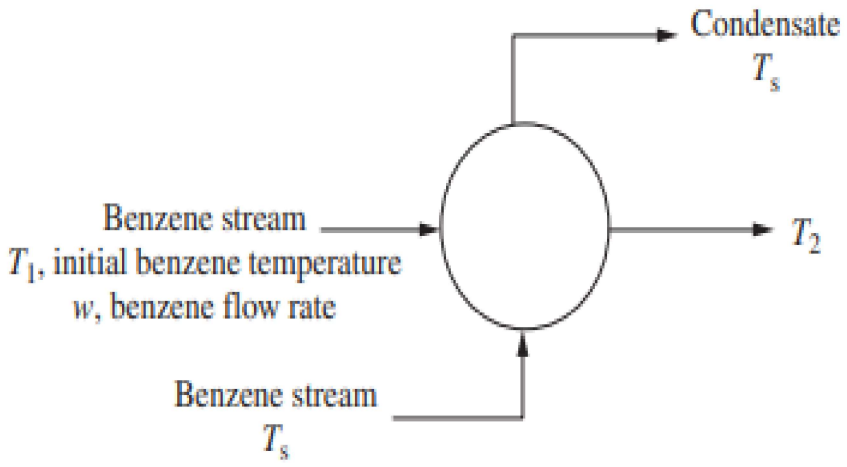


Figure C.1: Heat exchanger design [57].

C.3 Analytical Solution

The following rules where used to describe the relationship between the size of the heat exchanger, AU, to the flow rate, w, and the temperature, ΔT, of the Benzine:

(1) If w is $\underset{\sim}{A}_1^1$ (large flow rate) **AND** ΔT_{app} is $\underset{\sim}{A}_1^2$(small approach)

THEN AU is $\underset{\sim}{A}_1^1$ (large heat exchanger)

(2) If w is $\underset{\sim}{A}_2^1$ (small flow rate) **OR** ΔT_{app} is $\underset{\sim}{A}_2^2$(large approach)

THEN AU is $\underset{\sim}{B}^2$ (small heat exchanger)

(3) If w is $\underset{\sim}{A}_2^1$ (small flow rate) **AND** ΔT_{app} is $\underset{\sim}{A}_2^1$(small approach)

THEN AU is $\underset{\sim}{B}^1$ (large heat exchanger)

where $w = 1300$ kg/s and $\Delta T_{app} = 6.5$ K.

C.3.1 Mamdani Method

The Mamdani method of inference states that:

$$\mu_{\underset{\sim}{B}^k}(AU) = \max_k(min[\mu_{A_1^k}(w), \mu_{A_2^k}(\Delta T_{app})]), k = 1, 2, 3$$

Or when expressed in the rule based form:

(1) $\mu_w \cap_{\Delta T_{app}} (AU) = min[\mu_w(1300 \text{ kg/s}), \mu_{\Delta T_{app}}(6.5 \text{ K})]$

(2) $\mu_w \cap_{\Delta T_{app}} (AU) = max[\mu_w(1300 \text{ kg/s}), \mu_{\Delta T_{app}}(6.5 \text{ K})]$

(3) $\mu_w \cap_{\Delta T_{app}} (AU) = min[\mu_w(1300 \text{ kg/s}), \mu_{\Delta T_{app}}(6.5 \text{ K})]$

where A_1^k and A_2^k correspond to the first and second antecedents of the rules 1-3 and B^k refers to the consequent of A_1^k and A_2^k.

The disjunction "OR", which is defined by the maximum of a membership function, states that only one of the antecedents has to satisfy the rule base. The conjunction "AND", defined by the minimum of a membership function, requires that both antecedents have to satisfy the rule in question.

It is seen from Figure C.2 that the consequent of Rule 1 is 0.25. When looking closer at Figure C.2, it is apparent that the membership of $\Delta T = 6.5$ K within $\mu(\Delta T_{app})$ is greater than that of w=1300 kg/s within $\mu(w)$, but since we are taking the minimum consequent of Rule 1, we pay no attention to the larger degree of membership of ΔT because of the conjunction "AND" that defines Rule 1. The same goes for the consequent of Rule 3, this time the membership of ΔT is used because it has less of a degree of membership

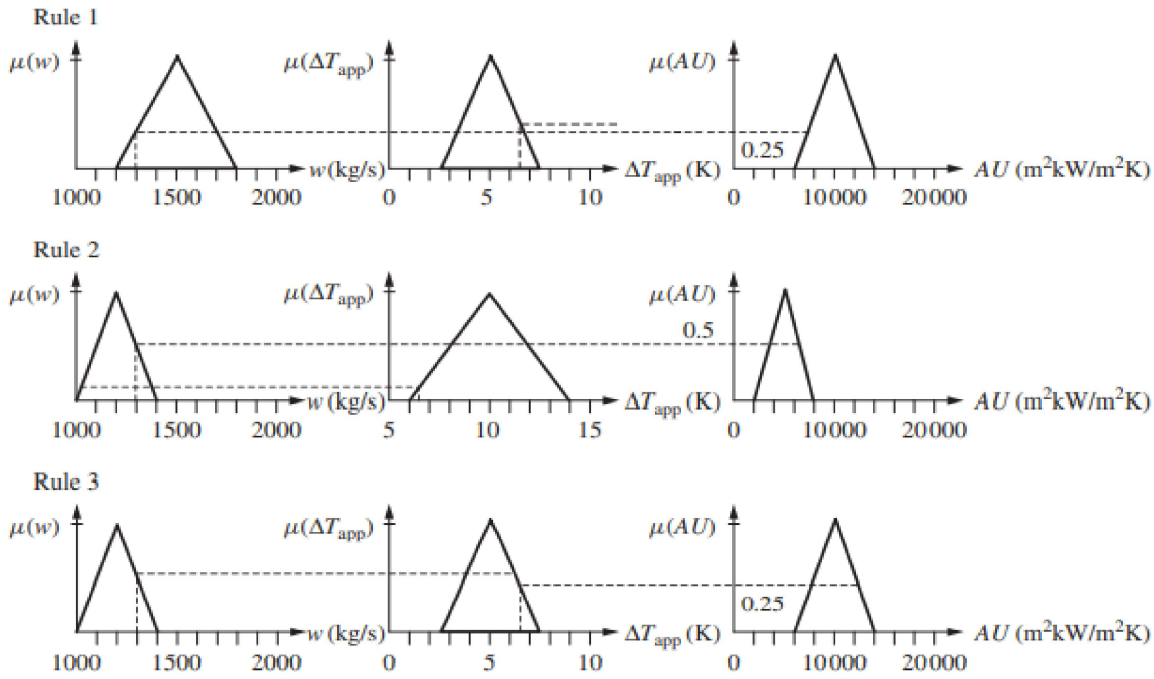


Figure C.2: Mamdani graphical inference [57].

within its antecedent than that of the flow rate w. Rule 3, however, is defined by the disjunction "OR" and therefore the maximum degree of membership is used to find the corresponding consequent.

The process of defuzzification yields crisp outputs from fuzzy sets and rule-based membership functions. It can be seen from Figure C.3 that all the inferences of the rules (the last column of Figure C.2) are plotted together. There are numerous ways to defuzzify fuzzy sets, such as: the max membership principle, centroid method, weighted average method, and the mean max membership [57].

For this example we will be demonstrating the centroid, the weighted average, and the mean max methods of defuzzification. We can dive deeper into what each of these defuzzification methods entail through a thorough analysis of Figure C.3.

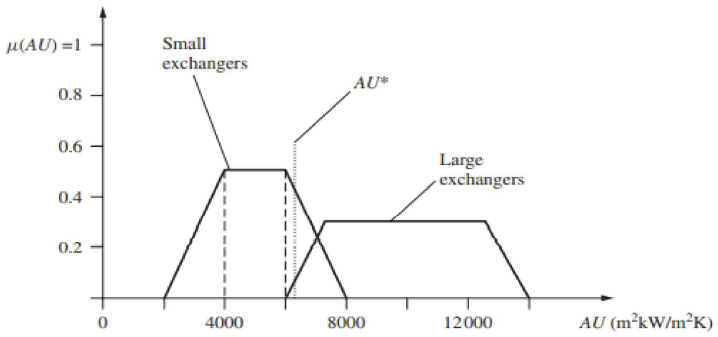


Figure C.3: Defuzzification of Mamdani inference method [57].

Centroid Method

The centroid method of defuzzification is defined as:

$$z^* = \frac{\int \mu_{\underset{\sim}{C}}(z) z dz}{\int \mu_{\underset{\sim}{C}}}(z) dz \tag{C.1}$$

where z^* refers to the crisp output of AU and $\mu_{\underset{\sim}{C}}(z)$ is the membership of z within the union of inferences of the membership functions such that $\underset{\sim}{C} = \underset{\sim}{C}_1 \cup \underset{\sim}{C}_2$. Defining $\underset{\sim}{C}_1$ as the trapezoid representing the small heat exchangers and $\underset{\sim}{C}_2$ as the trapezoid representing the large heat exchangers within Figure C.3.

To employ the centroid method of defuzzification we will need to find the area of the trapezoids that make up the inferences of the membership functions for this system.

Using Figure C.4 as a reference, the areas of each respective shape are:

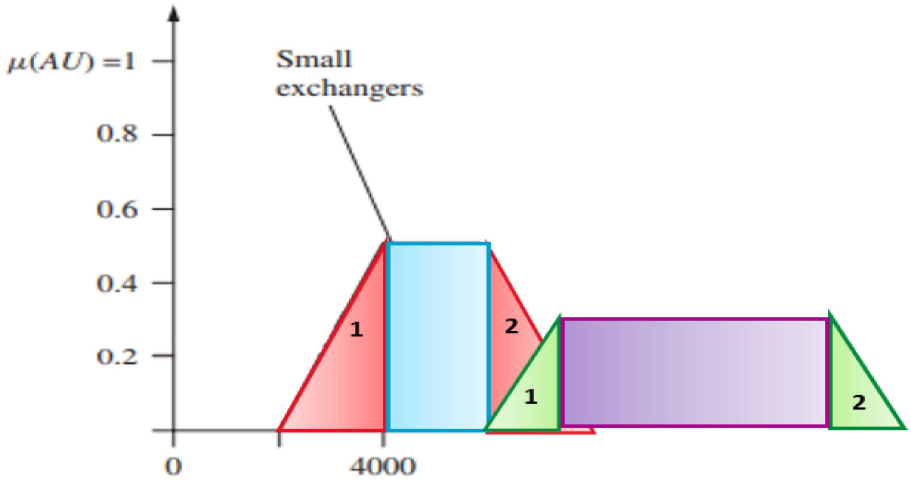


Figure C.4: Shape break down for centroid method of defuzzification.

$$\text{Area of First Red Triangle} = \frac{1}{2}bh = \frac{1}{2}(4000 - 2000)(0.5) = 500$$

$$\text{Area of Blue Rectangle} = bh = (2000)(0.5) = 1000$$

$$\text{Area of Second Red Triangle} = \frac{1}{2}bh = \frac{1}{2}(8000 - 6000)(0.5) = 500$$

$$\text{Area of First Green Triangle} = \frac{1}{2}bh = \frac{1}{2}(7000 - 6000)(0.25) = 125$$

$$\text{Area of Purple Rectangle} = bh = (12500 - 7000)(0.25) = 1375$$

$$\text{Area of Second Green Triangle} = \frac{1}{2}bh = \frac{1}{2}(14000 - 12500)(0.25) = 187.5$$

and the centroid of each area is:

$$\text{Centroid of Red Triangle} = \frac{2000 + 4000 + 4000}{3} = 3333.33$$

$$\text{Centroid of Blue Rectangle} = \frac{4000 + 6000}{2} = 5000$$

$$\text{Centroid of Second Red Triangle} = \frac{6000 + 6000 + 8000}{3} = 6666.67$$

$$\text{Centroid of First Green Triangle} = \frac{6000 + 7000 + 7000}{3} = 6666.67$$

$$\text{Centroid of Purple Rectangle} = \frac{7000 + 12500}{2} = 9750$$

$$\text{Centroid of Second Green Triangle} = \frac{12500 + 12500 + 14000}{3} = 13000$$

Table C.1: Table for centroid method of defuzzification.

	Shape	$\int \mu_Q(z)dz$	z	$\int \mu_Q(z)zdz$
Small Exchanger	Red Triangle 1	500	3333.33	1666665
	Blue Rectangle	1000	5000	3333335
	Red Triangle 2	5000	6666.67	5000000
Large Exchanger	Green Triangle 1	125	6666.67	833333.75
	Purple Rectangle	1375	9750	2437500
	Green Triangle 2	187.5	13000	13406250

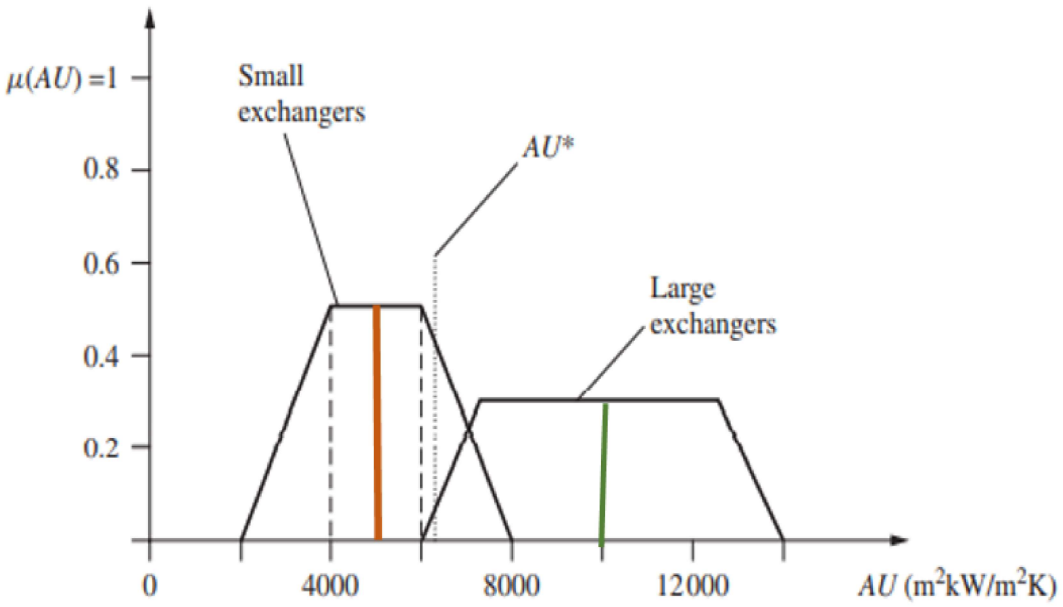


Figure C.5: Weighted average defuzzification procedure.

Following C.1,

$$AU^* = \frac{1666665 + 3333335 + 5000000 + 833333.75 + 2437500 + 13406250}{500 + 500 + 1000 + 125 + 187.5 + 1375} = 7234.46$$

Therefore using the centroid method of defuzzification, $AU = 7234.46$ kW/K

Weighted Average Method

The weighted average method of defuzzification is defined as:

$$z^* = \frac{\sum \mu_{\underset{\sim}{C}}(\overline{z})\overline{z}}{\int \mu_{\underset{\sim}{C}}}(\overline{z}) \tag{C.2}$$

where $\overline{z}$ is the mean of each symmetric membership function [57].

In Figure C.5, the orange line represents the mean for the small heat exchangers and

Table C.2: Table for weighted average method of defuzzification.

Rule	$\int \mu_{\mathcal{Q}}(\overline{z})$	$\overline{z}$	$\int \mu_{\mathcal{Q}}(\overline{z})\overline{z}$
1	0.25	10000	2500
2	0.50	5000	2500
3	0.25	10000	2500

the green line represents the mean for the large heat exchangers.

Following equation 2,

$$\frac{2500 + 2500 + 2500}{0.25 + 0.50 + 0.25} = 7500$$

Therefore by using the weighted average method of defuzzification, $AU = 7500$ kW/K

Mean Max Method

The mean max method of defuzzification is defined as:

$$z^* = \frac{a + b}{2} \tag{C.3}$$

From Figure C.3 and from Table C.2, we can say that a= 4000 and b = 6000. so,

$$\frac{4000 + 6000}{2} = 5000$$

Therefore by the mean max method of defuzzification, $AU = 5000$ kW/K.

C.3.2 Sugeno

The Sugeno inference method is similar to the Mamdani inference method except that the for the Sugeno type output membership functions are either constant or linear. A typical IF-THEN Sugeno rule is such that:

IF x is $\underset{\sim}{A}$ and y is $\underset{\sim}{B}$, THEN z is $z = f(x, y)$

where x and y are inputs, z is an output, and $z = f(x, y)$ is a crisp function of the consequent [57].

In this heat exchanger model, we will use the polynomial expressions given on page 150 of [57] to solve for AU through the Sugeno inference method.

Given polynomial equations:

$$AU_{small} = 3.4765w - 210.5\Delta T_{app} + 2103 \tag{C.4}$$

$$AU_{large} = 4.6925w - 526.2\Delta T_{app} + 2631 \tag{C.5}$$

and taking the memberships of rules 1-3 from the Mamdani inference method:

(1) $\mu(AU) = 0.25$

(2) $\mu(AU) = 0.50$

(3) $\mu(AU) = 0.25$

We then proceed to substitute $w = 1300$ kg/s and $\Delta T_{app} = 6.5$ K into equations C.4 and C.5 to get the following results.

$$AU_{small} = 5254.2$$

$$AU_{large} = 5310.95$$

Next, we will use the weighted average method to find the crisp value for heat exchanger size. plugging in the values computed above into C.2:

$$AU^* = \frac{(5310.95)(0.25) + (5256)(0.50) + (5310.95)(0.25)}{0.25 + 0.50 + 0.25} = 5282.58$$

where in this case, we use the values given by the polynomial equations C.4 and C.5 as the $\overline{z}$ value.

Therefore the crisp value for heat exchanger size AU is 5282.58 kW/K through the use of the Sugeno method of inference.

C.3.3 Tsukamoto

The Tsukamoto method of inference is similar to that of the Mamdani method in that they require the use of the same membership functions for their inputs. However, the Tsukamoto output membership functions requires what is refered to as "shoulders", therefore yield the Tsukamoto method flexible to systems with limited data.

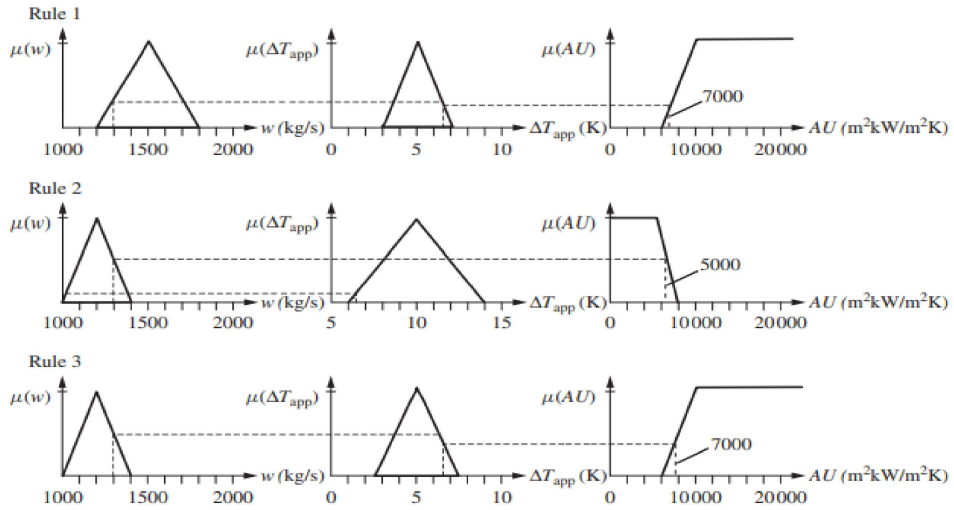


Figure C.6: Tsukamoto inference method [57].

Using Figure C.6 and C.2:

$$AU^* = \frac{(7000)(0.25) + (5000)(0.50) + (7000)(0.25)}{0.25 + 0.50 + 0.25} = 6000$$

Therefore by the Tsukamoto inference method of defuzzification, $AU = 6000$ kW/K.

C.4 Simulated Results

The simulated results for this example were generated through Matlab's Fuzzy Logic Toolbox. To start, we selected the Mamdani method of inference and added two inputs and one output: flow rate, temperature change, and AU.

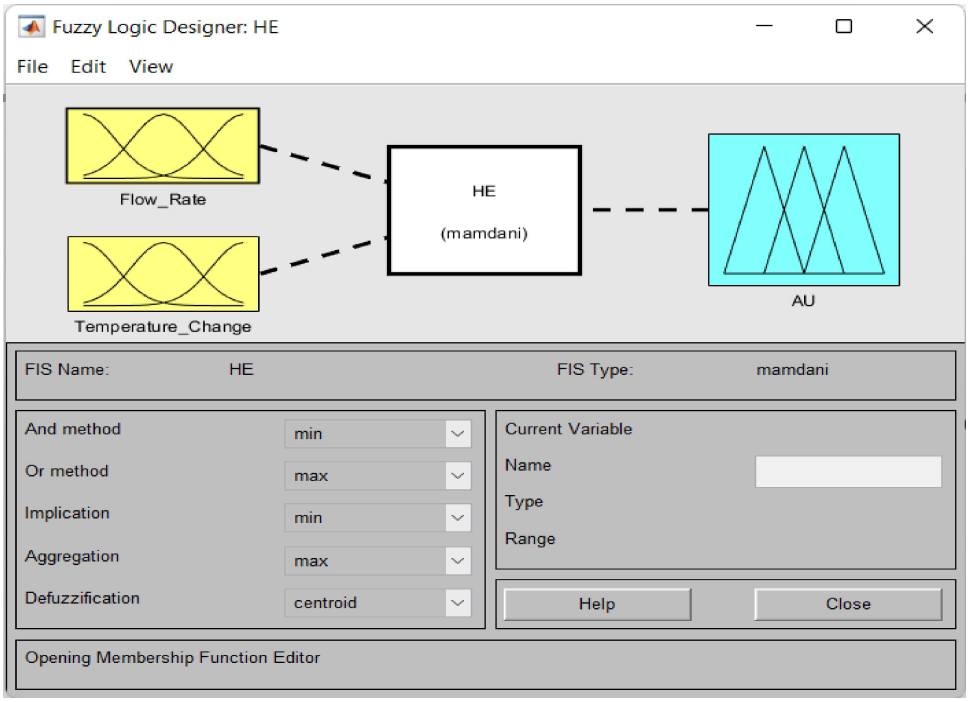


Figure C.7: Heat exchanger fuzzy system.

Setting up the flow rate membership functions first:

where

Similarly, the membership functions for temperature change are defined as:

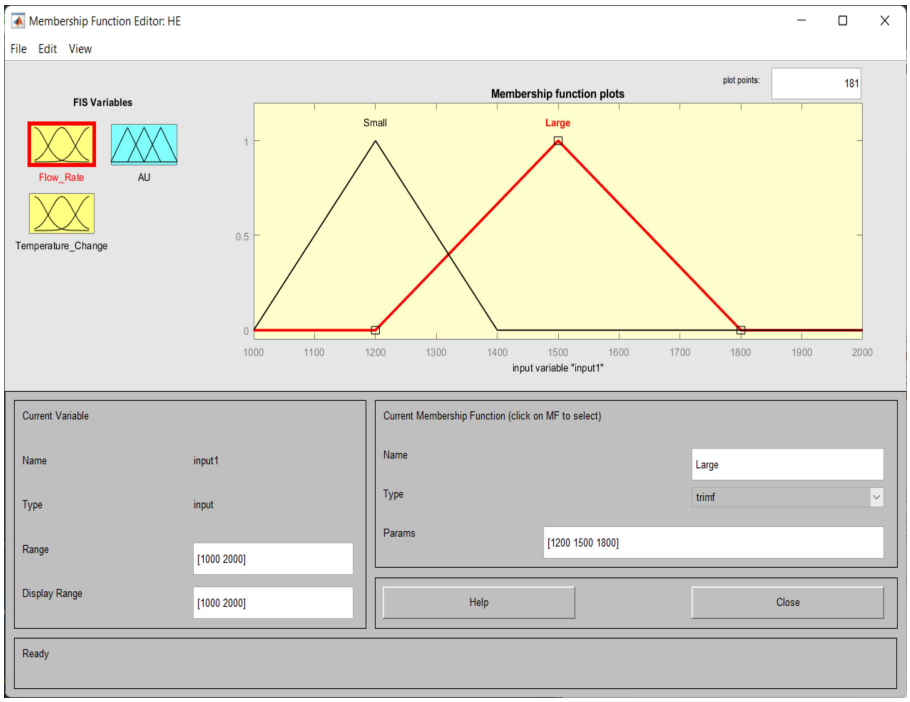


Figure C.8: Flow rate membership functions.

Table C.3: Membership of w in sets Small and Large.

MF Name	**Membership within MF**
Small	$\mu_{\underset{\sim}{Small}^k}(w) \in$[1000 14000]
Large	$\mu_{\underset{\sim}{Large}^k}(w) \in$[12000 18000]

where

Table C.4: Membership of ΔT_{app} in sets $Small_{tempdiff}$ and $Large_{tempdiff}$.

MF Name	**Membership within MF**
$Small_{tempdiff}$	$\mu_{\underset{\sim}{Small_{tempdiff}}^k}(\Delta T_{app}) \in$[2.5 7.5]
$Large_{tempdiff}$	$\mu_{\underset{\sim}{Large_{tempdiff}}^k}(\Delta T_{app}) \in$[6 14]

The membership functions for the output AU are defined a follows:

where Figure C.11 shows the rules stated in Section B.3.

The resulting answer for $w = 1300$ kW/K and $\Delta T_{app} = 6.5$ K is $AU = 7810$ kW/K.

When looking at Figure C.12, notice how the aggregated consequent of the rules matches

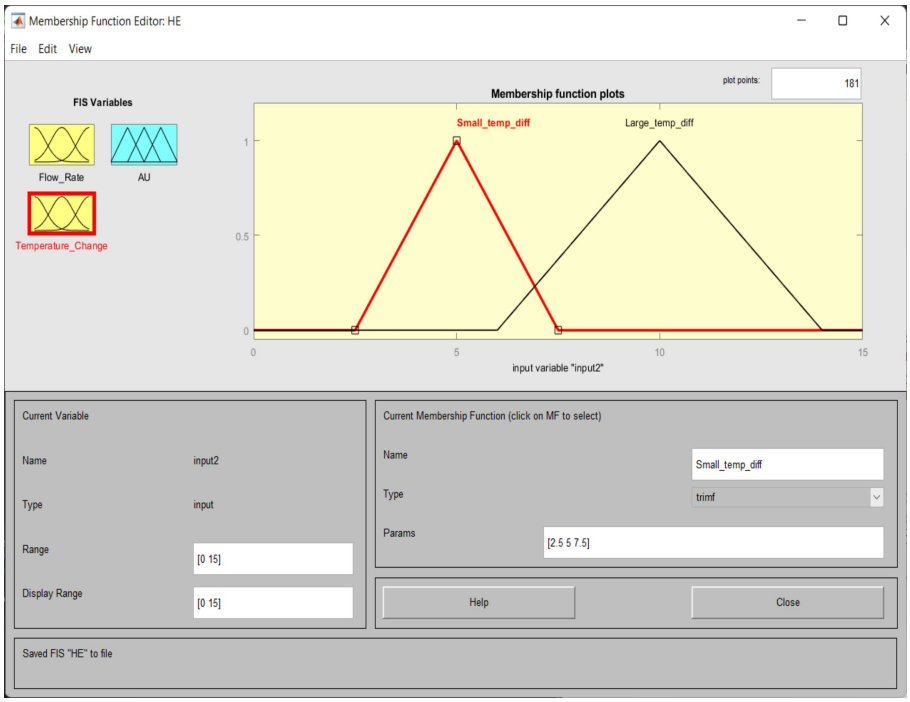


Figure C.9: Membership functions for temperatre change.

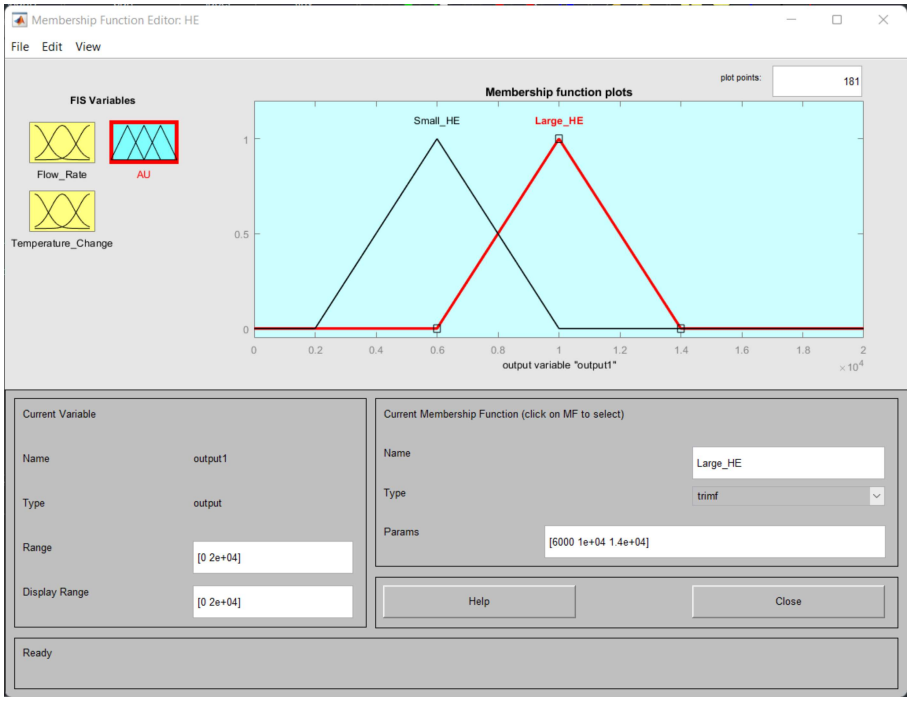


Figure C.10: Membership funcions for AU.

that of the consequent gathered from the Mamdani Inference method.

Table C.5: Membership of AU in sets $Small_{HE}$ and $Large_{HE}$.

MF Name	Membership within MF
$Small_{HE}$	$\mu^{k}_{\underbrace{Small_{HE}}}(\Delta AU) \in [2000\ 10000]$
$Large_{HE}$	$\mu^{k}_{\underbrace{Large_{HE}}}(\Delta AU) \in [6000\ 14000]$

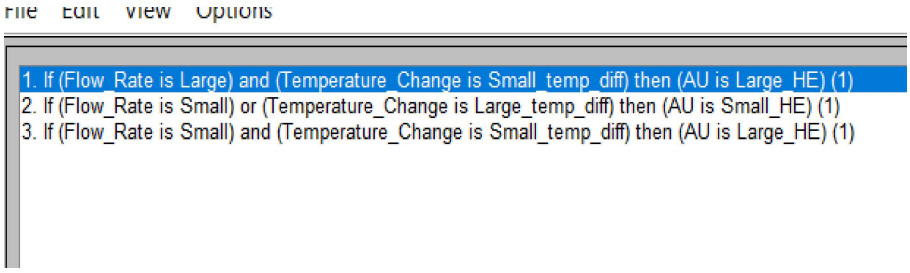


Figure C.11: Rules for heat exchanger system.



Figure C.12: Results for heat exchanger size simulation.

C.5 Conclusion

In conclusion, all three fuzzy logic inference methods gave extremely different results. When comparing the results for the Mamdani inference method, it can be seen that the mean max method of defuzzification yielded a number that is not as close as the numbers

Table C.6: Results for AU (kW/K).

Inference Method / Defuzzification Method	Mamdani	Sugeno	Tsukamoto	Simulation
Weighted Average	7500	5282.58	6000	
Centroid	7234.46			7810
Min-Max	5000			

yielded by the weighted average and centroid methods. This is due to the fact that only two data points are used for this method, and therefore it is safe to say that the mean max method is not an accurate mode of solving fuzzy systems.

On the other hand, both the weighted average and the centroid methods gave answers that did not differ by very much. Unlike the mean max method of inference, the weighted average and centroid methods made use of the implications defined by the conjunctions and disjunction of Rules 1-3.